THE EFFECTS OF FUEL EVAPORATION

ON ENGINE KNOCK

DEREK PAUL MORAN BSc(Mech Eng) Cape Town

April 1993

Submitted to the University of Cape Town in
fulfilment of the requirements for the degree of
Master of Science in Engineering

ACKNOWLEDGEMENTS

I am most grateful to my supervisor, Dr A D B Yates, for entrusting me with this most interesting and rewarding M.Sc. thesis topic, and for his encouragement and insightful suggestions throughout the course of the project.

I would like to thank Mr R J Nates for proof-reading a draft of this thesis. He also contributed to this investigation by being ever-willing to discuss any aspect of the project.

I thank the staff of the Mechanical Engineering workshop for their help and advice in the manufacture of the experimental equipment, and also for their tolerance of my experimentation.

This project was funded with a SASOL research contract, and this is gratefully acknowledged. The research effort also benefitted from interaction with SASOL personnel, especially Dr A B Taylor and Dr J J Botha, and their interest in this project is appreciated.

Associate Professor T T Dunne willingly spent much of his time performing the statistical analysis that helped to verify the findings of this project, and I am most appreciative of his help.

Mr A J Collins provided his super-computing facility to perform model testing; a facet of the investigation which would have been otherwise impossible, and his time spent in this regard is gratefully acknowledged.

SYNOPSIS

It has been known for a long time that alcohol-gasoline blended fuels exhibit an unexplained tendency to knock at high engine speeds; a characteristic that is not generally experienced with conventional gasoline. Early studies showed that the problem could be linked to an unusually high temperature sensitivity exhibited by the blended fuels, but the exact cause of this temperature sensitivity was not readily identified, and research efforts became diversified in attempts to make headway.

Initial studies in the field of high-speed knock were based on the assumption that a chemical-reaction sensitivity to temperature was the root cause. It is now suspected that the effect may be due to a thermal manifestation of the variation in evaporative cooling characteristics of different fuels at different engine speeds. Research findings leading up to the present project have indicated that the high-speed knock phenomenon could be explained by the influence on the overall mixture temperature of the thermal-evaporative behaviour of a fuel during the inlet process. The thermal-evaporative behaviour is very complex, however, and has been characterized only tentatively, as yet.

The present project was initiated to study the effect of engine speed on the fuel evaporation behaviour and on the complex heat transfer processes that occur within the intake manifold of a spark-ignition engine. The primary aim of the project was to establish the temperature of the air/fuel mixture after the inlet process has been completed, and to identify how this temperature responds to changes in engine speed and fuel composition. The fuels investigated included conventional gasoline and gasoline-alcohol blends. It was anticipated that the findings of the project would enable the fundamental hypothesis concerning the basic cause of high-speed knock to be evaluated.

A mathematical model of the fuel evaporation in the intake system of a spark ignition engine was formulated. A corresponding computer program was developed and was used to study the effects that various parameters have on fuel evaporation. The model allows for multi-component fuels, which are present in the manifold both as entrained liquid droplets and as wall films. Data are presented showing general intake manifold evaporation phenomena, as

well as data showing the effect on fuel evaporation of such parameters as fuel temperature, droplet size, air temperature, droplet velocity and fuel distribution. A sensitivity analysis was performed using the computer model to isolate important parameters that merited special attention in the research effort. The validity of some of the phenomena predicted by the model are compared with the empirical behaviour observed using a test-rig.

A test-rig was developed to study fuel evaporation under a range of conditions. These data were to provide the basis for analyzing existing results of engine tests. The test-rig was developed to simulate the conditions assumed by the model. The rig was equipped with a set of thermocouples to measure the temperatures of the various fluid streams in the manifold. Data were gathered covering a wide range of air-speeds, fuel compositions and initial fluid temperatures, and these were subjected to a statistical analysis which showed that the measured trends were highly significant. The output of the computer model also showed a remarkable concordance with the experimental results.

The results of this investigation were then used to anticipate the influence of evaporative cooling on Octane Number. These predictions were then compared with the results of well-documented engine-based fuel tests, and it was found that several significant trends could be explained in terms of evaporative cooling, including the Octane Number performance, and the 'spark advance' characteristics of alcohol-gasoline blend fuels and other fuel types. Consequently, it was found that inherent fuel evaporation behaviour could explain many of the disparities associated with the Octane Number tests.

It is concluded that the action of evaporative cooling is sufficient, in itself, to account not only for the Research Octane Number enhancement associated with alcohol blend fuels, but also for the phenomenon of high-speed knock.

Finally, as a consequence of this study, suggestions are made concerning both the elimination of high-speed knock and the improvement of engine performance, and it is recommended that follow-up research concentrate on these topics, as well as on engine tests to substantiate further the conclusions reached in this study.

TABLE OF CONTENTS

1. INTRODUCTION

This project follows the investigative work that has been carried out in the field of high-speed knock as part of the programme of abnormal-combustion research within the Mechanical Engineering Department at the University of Cape Town. The principal findings that contributed to the initiation of this project are reported below.

1.1 PREVIOUS INVESTIGATIONS

There is an abundance of literature concerning fuel performance, engine knock and general thermal-evaporative phenomena, but there have been very few reports specifically focused on the phenomenon of high-speed knock. In order to clarify the build-up to and motivation for this investigation, the scope of this chapter has been limited primarily to the research efforts that have been undertaken at the University of Cape Town, with a more complete encompassment of the background literature being undertaken in later chapters.

A preliminary study[1] of the high-speed knock (HSK) phenomenon, which was based on a simple knock model, revealed that the auto-ignition behaviour of a fuel could be adequately characterized in terms of pressure, temperature and time. Three fuel types were examined, viz. local Cape Town fuel (refined from crude oil), coal-derivative fuels (oil from coal process) and coal-derivative fuels blended with alcohol. The fuels were found to differ distinctly in their sensitivities to changes in temperature and pressure. In particular, the alcohol blend fuel was found to exhibit significantly disparate qualities from those of the other fuel types.

In the light of these differences, it was possible to explain why the high-speed condition was the preferred environment for knocking of the alcohol blended fuel, in terms of an exceptionally pronounced temperature sensitivity. This discovery allowed an important conclusion to be drawn regarding the nature of HSK. It had previously been thought that HSK was a fundamentally different phenomenon to the more usual low-speed knock. What was apparent now, was that knocking at high speeds was merely due to a fuel responding sensitively to the slightly increased combustion temperatures prevalent at higher speeds.

The path for subsequent research was clearly to isolate the reasons why the alcohol blended fuel exhibited this temperature sensitivity. The answer to this question has proved to be elusive, and the research direction was diversified by more recent indications that the apparent increased sensitivity may be an illusion arising from problems in the determination of temperatures within an internal combustion engine. It is now suspected that what was originally perceived as a chemical-reaction temperature sensitivity, may be nothing more than a thermal manifestation of the variation in evaporative cooling characteristics of different fuels at different engine speeds.

Research is presently being conducted into both the chemical-reaction and the thermal property approaches. The former approach is being entertained by such projects as a National Energy Council (of South Africa) sponsored chemical kinetic modelling project. For this kind of modelling it is imperative to determine the gas temperature very accurately; a difficult task for which a 'Coherent Anti-Stokes Raman Spectroscopy' (CARS) laser system is being used, which is being adapted to measure gas temperatures in an engine. Projects involved in the latter approach (of which this project is a member) concentrate on the premise that thermal properties (like the latent heat of evaporation) play a dominant role. There is considerable evidence to support the latter premise.

1.2 THESIS MOTIVATION

Several research investigations have been on-going within the Mechanical Engineering Department at the University of Cape Town, each of which was involved in the high-speed knock research effort, with each having had significance for the initiation of this project.

The knocking combustion of methanol was compared with that of gasoline using an elementary auto-ignition model[2]. The findings revealed that the auto-ignition reactions of methanol were an order of magnitude faster than those of gasoline, meaning that methanol should be easily capable of knocking at high speeds. The analysis of the data was confounded, however, by the uncertainty in determining the exact temperature of the air/fuel mixture at the point of auto-ignition (as mentioned before).

In order that the research effort might continue, a number of techniques to measure this temperature have been explored[3] (apart from the aforementioned CARS laser system). Initial work using acoustic techniques in a test chamber during 1989 established an accuracy of better than a few degrees Celsius[4]. Preliminary tests on an engine have been carried out, but this technique requires considerable development effort before it can be utilized for engine research.

One aspect of gas temperature within the engine warranted special consideration, namely the latent heat of evaporation property of the fuel. The latent heat of alcohols is considerably higher than that of gasoline, and alcohols consequently have the potential to lower the temperature of the fuel/air mixture drastically if they were to evaporate. This would cause knock suppression independent of any inherent knock-resisting chemical qualities that alcohols might exhibit.

A recent investigation[5], (which was the immediate predecessor to the present study), aimed at identifying the influence of evaporative cooling on the knock resistance of methanol by comparing the differences between liquid and vaporised methanol, and this study revealed some remarkable results that have significant implications. Liquid methanol is known to have a much higher knock resistance than the vaporised form, and this was found to be due to the lower temperature at the start of compression caused by evaporative cooling. In the test case with the inlet air preheated to 60°C, evaporation of 15% of the fuel was all that was required for the inlet mixture to be cooled to the ambient pressure equilibrium temperature of about 10°C. The remaining fuel was therefore compelled to gain its heat of evaporation by direct contact with the inlet tract and the cylinder walls.

Several interesting implications arise from the above findings:

1. It is well known that blending alcohol with regular gasoline produces a marked improvement in the Research Octane Number (RON) for low percentages of alcohol addition[6]. This ties in with the finding that the alcohol's knock resistance is derived by the evaporative cooling of the first 10% to 20% that evaporates. It is to be expected therefore, that after about 25% addition, minimal further improvement in RON value be experienced, and this is exactly what has been observed in practice.

2. The Motor Octane Number (MON) is known to be significantly lower than the RON for alcohol fuels and alcohol blends[6]. This can now be attributed to the fact that the MON ensures pre-evaporation by specifying a mixture temperature of 149°C, whereas the RON dictates only that the air temperature be 51.7°C. The RON test, by allowing fuel to cool the air by evaporation, enables alcohol fuels to manifest their high latent heats of evaporation resulting in lower inlet air temperatures and subsequent improved knock resistance. The MON test, on the other hand, by ensuring complete vaporization (149°C), removes the basis of the alcohol's relatively excellent knock resistance. The difference between the two tests could thus be explained in terms of evaporative cooling. The pertinent question remaining would be how to interpret the numbers obtained by the two tests.

3. The above inference (2) raises the possibility that at high engine speeds, and depending on the inlet system design, there may not be time for a blended fuel to attain equilibrium evaporation conditions. In such a situation, the fuel would tend to approach a knock performance indicated by the MON test, and knocking at high speeds would result. General operating experiences with alcohol-blended fuels would seem to support this inference (3).

This project was initiated as an extension to the above studies to investigate formally the influence that evaporative cooling exerts during the fuel inlet process, and to study the resultant effect in terms of explaining the high-speed knock condition.

1.3 PROJECT OUTLINE

The present project comprises an in-depth study of the inlet process of a spark ignition engine to understand the fuel evaporation process and its interaction with the complex heat transfer processes. The fuels investigated included local gasoline and gasoline-alcohol blends. The project was launched with a primary aim of establishing the temperature of the air/fuel mixture after the inlet process has been completed, and to identify how this temperature responds to changes in engine speed.

The approach to this research programme included studies of the evaporation process that lead to the development of a mathematical model. A test-rig was built to study fuel evaporation under a variety conditions using thermocouples, as an empirical check of the mathematical model. These data provided the basis for the analysis of engine tests. Finally, the fundamental hypothesis concerning the basic cause of high-speed knock was examined against the findings of this project.

The development of the computer model is discussed in the next chapter (chapter 2), and the model is used to perform a sensitivity analysis on the system (chapter 3). Chapter 4 describes both the test-rig and the procedure that was used to obtain experimental data. Chapter 5 outlines the analysis of the experimental data, and includes an appraisal of the performance of the mathematical model in its capability to predict the experimental readings. The implications of the evaporative cooling behaviour presented in chapter 5 are developed in chapter 6. Stemming from this study, certain insights into the RON and MON tests were gained, and these are discussed in chapter 7. The findings of this project are discussed, in chapter 8. Finally, conclusions regarding the thesis objectives are drawn, and recommendations for follow-up research are submitted.

2. THE MATHEMATICAL MODEL

The development of the computer model is described, firstly by discussing previous models, and secondly by detailing the workings of the present model, including the assumptions that were made. Several characteristics of flow and evaporation processes, that were elucidated using the model, are presented and discussed, including stream temperatures, velocities, fuel composition and evaporation histories for multi-component fuels.

2.1 LITERATURE SURVEY

Numerical models of manifold flows

Several computational studies have been carried out on fuel/air flows in inlet manifolds dealing with different aspects of inlet systems, and with differing analytical approaches. The earliest studies aimed at applying standard equations describing state, motion, and heat and mass transfer to the intake system. Yun et al.[7] and Lo and Lalas[8] were the first to attempt such an approach, the former studying the flow of iso-octane in a venturi; the latter a series of single-component fuels. The aspect of multi-component fuels was included in later models by Finlay et al.[9] and Boam and Finlay[10], whose models monitored the heat and mass transfer interactions of the gaseous, liquid droplet and liquid film bodies as they progressed along the manifold of a constant depression carburettor. The Boam and Finlay model formed the basis for several subsequent investigations (as mentioned below), but they made several noteworthy assumptions and simplifications:

1. System variables change only in the direction of flow.
2. The initial distributions of phase, concentration and temperature were taken to be uniform.
3. All liquid transferred from the droplets to the wall film (and vice versa) mixed perfectly with the surrounding liquid.
4. Uniform initial droplet sizes (75μm across speed spectrum).
5. A stationary fuel film which was uniformly distributed around the manifold.
6. Steady air flows and steady-state conditions existed.

This study[10] concentrated on the proportion of fuel evaporated as a consequence (i) of secondary droplet atomization due to a throttle plate, and (ii) of manifold heating. An important conclusion was that more evaporation occurs at lower speeds because "at lower speeds forced convection acts around the droplets for a greater time".

Subsequent research has yielded information to supplement the Boam and Finlay model. In an effort to study transient engine response, due to fuel film behaviour, Milton and Behnia[11] expanded the Boam and Finlay model to include a moving fuel film, which was assumed to be a Couette flow driven only by shear forces. This analysis produced data on film velocity and thickness. Various alcohol-gasoline blends were modelled to establish percentage evaporation.

The above analyses hinged on one-dimensional approximations of manifold flow phenomena. Bland et al.[12] formulated a two-dimensional model for use on a commercially available fluid dynamics package (Phoenics), with the intention of predicting the changes in intake specifications on mixture formation and engine performance under transient loads. This analysis is capable of modelling specific individual quantities, for example the progress of each of 1200 droplets (initial droplet size 90 μm) is monitored in each run. However, this analysis omitted the capability to model multi-component fuels. The proportion of fuel evaporated in the manifold was tested for two injector positions, and for various valve temperatures.

A three-dimensional approach was adopted by Servati and Yuen[13], who examined the equations of motion of a droplet in a flow field under aerodynamic drag and gravitational forces, and this allowed the proportion of fuel deposited to the film to be determined. Apart from modelling only single-component fuels, this analysis introduced two main simplifying assumptions, (i) all droplets have the same initial size, and (ii) zero initial droplet velocity. A significant finding of this study was that the system parameters were strongly dependent on (i) initial droplet size, and (ii) gas velocity. Another important finding was that "droplets smaller than 25μm will be totally evaporated".

Brown and Ladommatos[14] formulated a computer program to model fuel evaporation in a hot port-injected manifold operating at low load and low speed. The analysis featured a mono-size spray of a single component fuel. This model investigated injector aim, and the effect of manifold wall heating. The model hinged on an important assumption, that "fuel finds its way into the cylinder only as a result of vaporization and wall film flow". Consequently, the model comprised two programs, the 'droplet program', and the 'film program'. The 'droplet program' was used until "impingement occurred" when the 'droplet program' was stopped, and the 'film program' was started using the results produced by the droplet program. It was concluded that "heat loss of the air due to droplet evaporation was found to be too small to affect the air temperature significantly", and that "almost all of the fuel evaporation is from the fuel film". This can be attributed to the fact that the manifold was modelled to be 80°C (heat flux 7100 $W.m^{-2}$), which would provide latent heat for film evaporation, and this would dominate the system.

The above-mentioned investigations ignored the influence of cylinder induced pulsations, assuming steady flow for their analyses, and this provided the framework for their investigations. Low et al.[15] applied a method of characteristics to examine the effects of air flow pulsations on the fuel transportation process. Finally, Tanaka et al.[16] provided an experimental study of pulsation effects in a carburetted manifold. This type of analysis provided additional information over the steady state models, particularly in the case of single cylinder, carburetted engines, for which flow pulsations are particularly significant.

Fuel film investigations

The treatment of the wall film requires some innovation since no reliable documentation or experimental information exists to predict either the initial conditions or the droplet deposition rates. While both demand considerable further research, one traditional approach concerning the field of deposition rates, which is discussed in several papers, was developed by Friedlander and Johnstone[17]. This approach is based on von Kármán's extension of the Reynolds analogy, and although it was developed and investigated for solid particles[17], it was used in previous studies involving fuel droplets[10, 11] because of its simplicity. Subsequent exploratory computations performed both in this study and by previous researchers[10] showed that the predicted evaporation rates are relatively insensitive to the deposition rates.

The re-entrainment rate (mass flux of liquid fuel whipped off the wall film body to join the droplet body) suffers from the same lack of definition as the deposition rate, and is assumed for the present model to be a lagging function of the deposition rate. The model in this study was found to be relatively insensitive to changes in entrainment rate.

Several investigations have been undertaken aimed at identifying the nature and characteristics of wall films[17-32], some of which were experimentally based[17-25], while others incorporated various numerical models[24-32]. Hasson and Flint[18], in particular, investigated deposition and re-entrainment rates by measuring the quantity of fuel present in the wall film of a carburetted engine using a separator designed for the purpose. This investigation[18] provides the empirical data against which the theoretical predictions of Milton and Behnia[11], in particular, can be evaluated.

Fuel droplet investigations

The thermal-evaporative behaviour of suspended fuel droplets has been studied in great depth[33-59], varying from comprehensive droplet vaporization models[33-48] through spray calculations[45-54] to experimental analyses and studies of flow processes[55-59]. Certain generalizations have to be made in order to formulate 'universal' models such as those mentioned above[7-16]. The highly detailed analyses of some of the studies referenced above[33-59] would therefore be misplaced in the 'universal' models (cognizant of the fact that small inaccuracies in these generalizations probably would override any improvement in model performance due to a more detailed analysis of certain specific areas).

Droplet sizes

In a definitive work Ingebo[59] summed up droplet size and spray vaporization theories that were current in 1954, and compared them with information gained photographically using a specially-adapted rig. Relevant droplet size investigations[59-68] cover three principal areas (i) experimentally-based measurements and measurement techniques[59-64], (ii) fuel property correlations with droplet size, applied to regular and alternate fuel types[62-65], and (iii) atomization and spray descriptions as related to engine performance[65-68].

2.2 THE PRESENT ANALYSIS

The model developed here follows a conventional formulation similar to that used by previous researchers[10, 11], with the steady state equations for conservation of mass, momentum and energy as well as equations of state being solved. This type of analysis was chosen because of its relative simplicity and generality, but essentially because it is the only type of analysis that was found to incorporate the specifics of modelling multi-component fuels. This capability was imperative for the purposes of this investigation.

A set of thirteen ordinary differential equations have been developed to consider the gas stream, suspended fuel droplets and wall film, and these are included in Appendix A. These equations are solved using a fourth order Runge-Kutta numerical technique. The equations on which the model is based are discussed below. The nature and complexity of the model necessitated the use of a computer program, the primary documentation for which can be found in Appendix B.

Flow in the intake manifold of a carburetted engine is extremely complex involving highly turbulent pulsating two-phase flow (liquids and gases) with the liquid fuel present both as suspended droplets and as wall films. These complications are further exacerbated by geometrical considerations like area changes across the carburettor and throttle plate, as well as bends and branch points. The computational effort required for a rigorous analysis would clearly be prohibitive. However, with a few simplifying assumptions, the problem can be reduced to a manageable size without a significant sacrifice in validity. The assumptions made for this model are listed below, and incorporate many of the simplifications used by Boam and Finlay[10]:

1. All variables change only in the direction of flow.
2. The distributions of phase, concentration and temperature are taken to be uniform.
3. The liquid fuel is assumed be in the form of droplets (adopting a particular drop size) and a stationary wall film. Both droplet deposition onto the film and particle re-entrainment are considered.

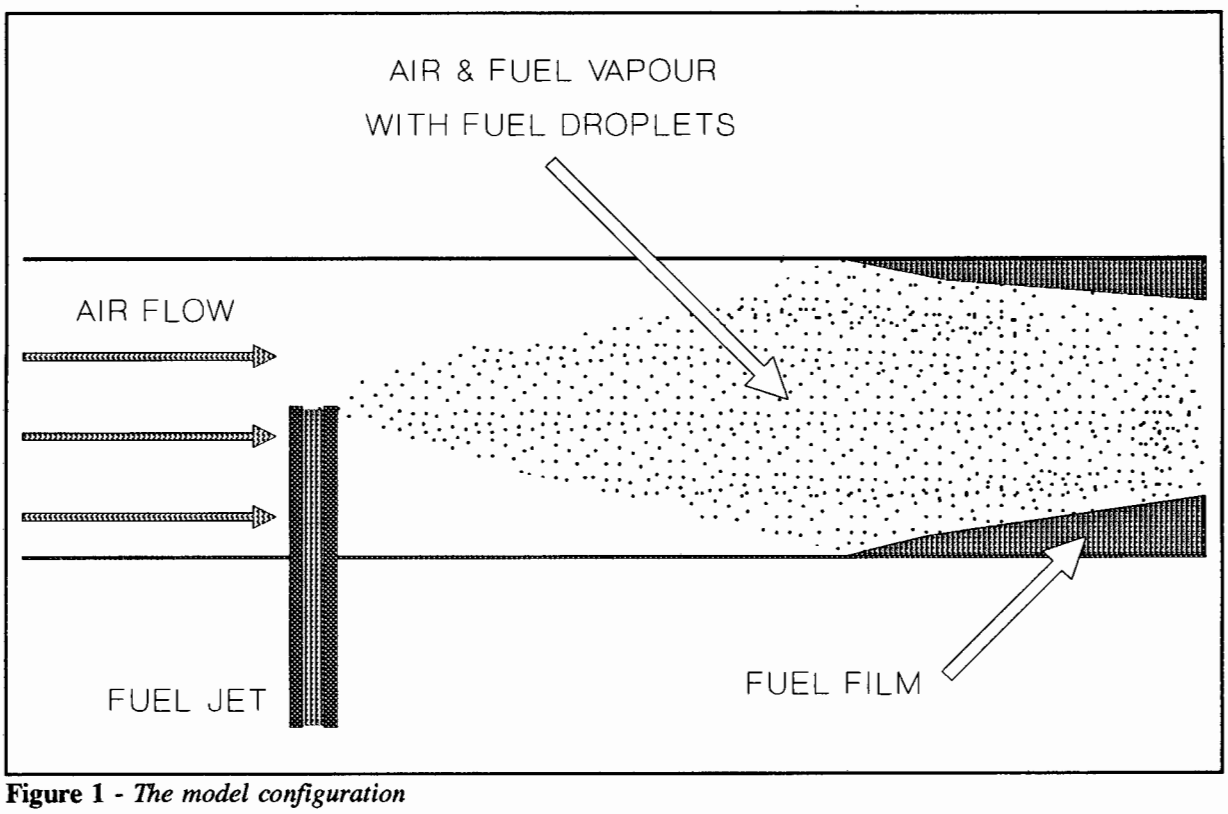

Figure 1 - *The model configuration*

4. The liquid fuel transferred to the film from the droplet body and vice versa is assumed to mix perfectly with the new body. There is no coalescence or shattering of droplets (although it would be relatively simple to include these factors were they thought to be important).
5. Steady state conditions exist.
6. The fuel is assumed to mix homogeneously with the airflow. This assumption is made for simplicity, a more realistic encompassment of the situation is depicted in Figure 1 which shows the fuel spreading out from a point source at the jet. (The model was later amended to include a spray-plume, but it was found that this did not make a significant difference to the temperatures present at the end of the inlet manifold).

Fuel composition

Regular gasolines are made up of approximately 36 or more different hydrocarbons[10], some of which are present only in very small proportions. The computational effort required can be reduced by lumping together these smaller quantities, to produce a gasoline simulation with only the more important components represented. This 'gasoline' approximation

faithfully reflects the vapour pressure/temperature relationship of conventional gasolines[10]. The 'gasoline' simulation used in the present model encompasses the seven components that comprise the largest proportions of regular automotive gasoline (see Appendix B), and it was anticipated that this simplified formulation would provide an adequate gasoline analogy.

The laws of conservation of mass, energy and momentum are applied to the liquid and gaseous bodies, and the resulting set of equations form the model. These equations are described, in essence, below. The full equations are recorded in Appendix A. All the differential equations are based on distance down the 'manifold' from the fuel inlet point.

Conservation of energy

These equations describe the temperatures of each fluid body (gas, droplet and film), and include enthalpy changes due to temperature variation and to mass transfer, as well as kinetic energy changes due to velocity changes and heat and mass transfer effects.

Conservation of mass

These equations simulate the increases and decreases in mass and the changes in composition of each stream due to evaporation and deposition/entrainment as appropriate.

Conservation of momentum

These equations monitor changes in velocity of the gas and droplet streams under the influence of pressure and drag forces as well as momentum changes due to mass transfer effects.

Interactive system equations

The whole system of equations include physical properties of the fuel components which have to be updated both for changes in temperature and for changes in mole concentration (as the components evaporate selectively).

One of the prime-movers initiating the formulation of a general model, was the capability to perform a wide sensitivity analysis so that the more important features may be identified and studied in depth (experimental as well as literature-based studies). This type of analysis was

performed using the model and is described in chapter 3. Some assumptions that were applied to the fuel droplets were consequently identified as being highly influential on the thermal-evaporative characteristics of the inlet process, and a special experimental investigation was launched to clarify these assumptions (section 4.3).

Thus the model was derived from previously described models, and was enhanced using further information gained from the literature. The computer program, that was devised to provide a working framework for the model, yielded many insights into aspects of the intake process, and some of these are presented in section 2.3 below.

2.3 FLOW AND EVAPORATION PROCESSES

The model revealed a host of valuable information about the fuel transportation processes existing within an inlet manifold. Information about the mixture temperatures is of particular interest to this study, and will be reported separately, in chapter 3. In order for the model to function, many ancillary features of the transport process had to be simulated, which in themselves elucidate the conditions present in an inlet manifold, and these are discussed in this section. The graphs presented here serve to illustrate the model's capabilities. All of the figures presented in this chapter were generated using data produced by the mathematical model developed in this study. In order not to complicate matters unnecessarily, the simplest of setups has been used for most of these simulations, for example a single-component fuel (specifically, pure methanol), where applicable.

General temperature profiles

Temperature correction processes start as soon as the liquid fuel is mixed with the air stream. In order to explain the temperature profiles observed, a specific case (illustrated in Figure 2) will be discussed (namely, a low air velocity, 40°C initial air temperature and pure methanol with an initial temperature of 20°C).

Forced convection heat transfer between the air and droplets (as well as between the air and the film) acts to bring the air temperature closer to that of the liquid streams. Evaporation

starts as soon as the liquid fuel is introduced into the air stream, and this causes dramatic cooling of the remaining liquid fuel, which has to provide the latent heat energy of evaporation. The gas stream is also cooled by newly evaporated vapour, which has to attain the gas stream temperature. The fuel film evaporates at a slower rate than the droplets (per unit mass) due mainly to the lower surface to volume ratio for the film body, and this is reflected by the film and droplet profiles in Figure 2. (For the same reasons, droplet reheating is faster than that of the film, as is the case for gasoline).

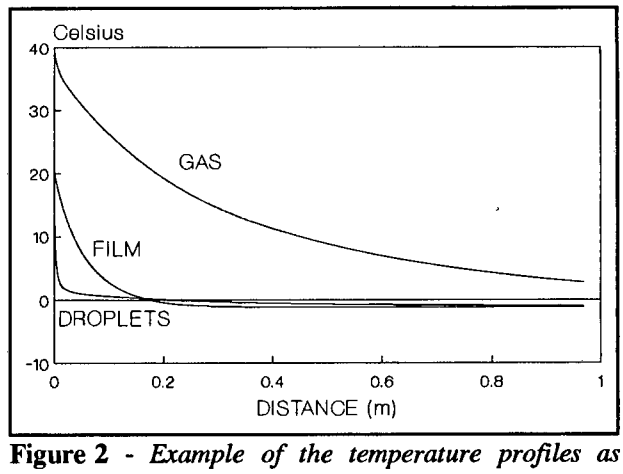

Figure 2 - *Example of the temperature profiles as predicted by the model*

(Note that the temperature profiles presented in Figure 2 represent a specific case. The profiles produced for other combinations of fuel types and air-speeds etc., can be radically different from these, as is evident in the sample graphics in chapter 5.)

It is worth noting that the temperatures at a distance of 0.2m downstream of the fuel inlet (the length of a typical automotive manifold) are still not close to equilibrium temperatures. Figure 2 shows temperature profiles for the chosen setup (specifically, pure methanol together with a low air-speed) which resulted in equilibrium temperatures after the shortest distance of any of the setups tested in this study . The manifold length required for equilibrium was found to be in the order of many metres (for many of the cases tested in this study). It is common in engine calculations to adopt the simplifying assumption that equilibrium evaporation has occurred in the inlet manifold. In the light of the above information, it is likely that this assumption could cause significant inaccuracies.

Velocity profiles

The fuel enters the air-stream with a minimal initial velocity (for a carburettor in this demonstration case). The fuel droplets are then accelerated up to the gas stream velocity, the smaller the droplets the sooner they attain this velocity.

The effect of a throttle plate was investigated in this and previous studies[10], and found to affect the manifold temperatures significantly. The inclusion of a throttle plate greatly enhances evaporation, partly due to increased forced convection and increased turbulence, but mainly due to secondary drop shattering, because drop size strongly influences evaporation rates (as discussed in section 3).

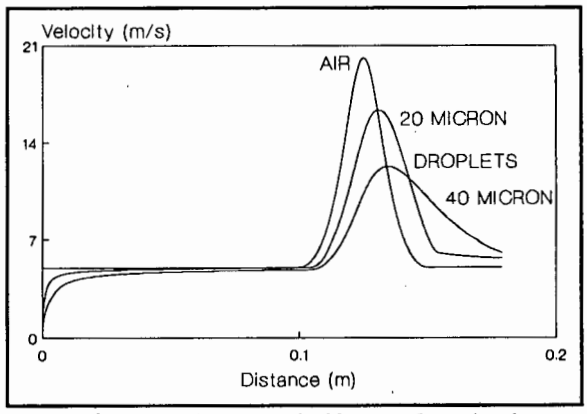

Figure 3 - *The effect of a half-open throttle plate on manifold velocities*

In Figure 3, the effect of a throttle plate on the manifold velocities of air and suspended droplets is illustrated. The flow diameter is halved in this example throttle plate setting. The droplet velocities lag the air stream due to their greater inertia opposing the accelerating air drag forces. For the remainder of this investigation, wide open throttle (no constrictions whatsoever) is the only condition that will be considered.

Fuel distribution

The fuel can be introduced into the manifold either as droplets or wall film, and, as is demonstrated both by theory and experiment, the relative distribution of the fuel has a very significant effect on evaporation (see chapter 3). Unfortunately, as with the droplet sizes, neither experimental data nor theoretical predictions exist whereby initial fuel distribution can be determined with adequate precision.

In previous studies[10, 11] it was assumed that all fuel entered in the droplet form, which then migrated to the wall by diffusion to create the film. Mass was exchanged between the droplet body and the film by entrainment from the film and by deposition of the droplets.

The present model allows the fuel distribution (proportion of fuel initially in the film, as opposed to droplets) to be specified, since experimental observation (Chapter 4) has shown that a significant proportion of the fuel can be introduced as film.

Proportion of fuel mixture evaporated

Figure 4 shows a graph of the proportion of fuel evaporated along the manifold for various speeds. The amount of fuel evaporated in the manifold is all important in determining the temperature of the mixture entering the cylinder. It is assumed, in most simple engine cycle models, that equilibrium evaporation conditions exist. This is clearly a false assumption (see Figures 4-6) even for slow speeds where evaporation is enhanced as compared with higher speeds (this is in agreement with the previously-mentioned findings of Boam and Finlay[10]).

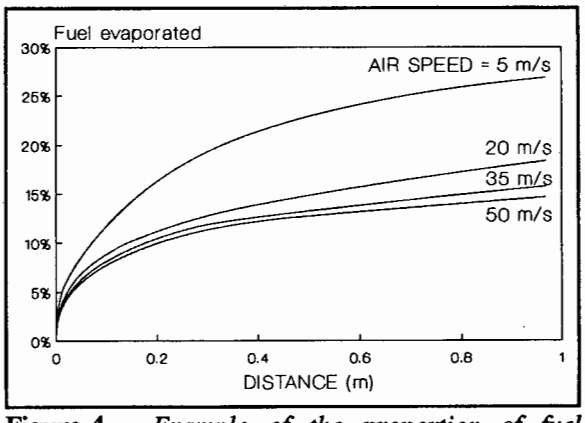

Figure 4 - *Example of the proportion of fuel evaporated versus distance for various speeds*

Proportion of each component evaporated

A graph showing the relative evaporated proportions of several components of a gasoline fuel is shown in Figure 5. These data were produced by the mathematical model, (this time specifically for the multi-component 'gasoline' fuel). As expected, the lighter fractions evaporate almost completely, and the heavier fractions hardly at all. Iso-octane, although not represented in the graph, follows the established trend exhibiting very low percentage evaporation. The data for Figures 5 and 6 were produced using the computer model, and it is noted that they agree with the similar observations of Milton and Behnia[11]. It is informative to note that the evaporation of the heavier components is suppressed while the lighter fractions evaporate preferentially.

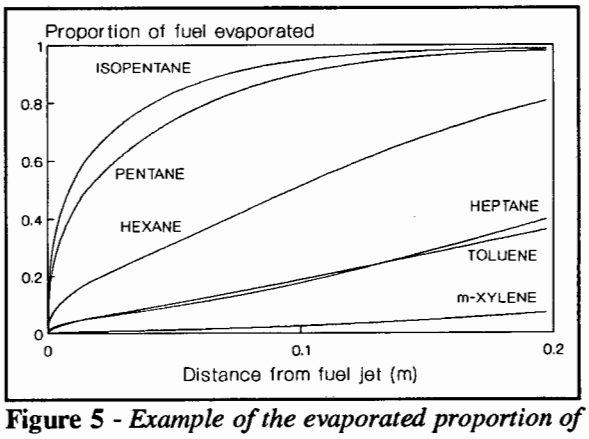

Figure 5 - *Example of the evaporated proportion of some gasoline components versus distance*

Proportion of fuel evaporated for various fuel blends

A graph of proportion of fuel evaporated as a function of distance from the fuel jet for some methanol-gasoline blends from pure gasoline to pure methanol is shown in Figure 6. Even though only 20% of the pure methanol evaporates (after 0.2m) compared with 50% for pure gasoline the cooling effect provided by the methanol is much greater due to a much higher latent heat (five times higher than the typical figure for gasoline) combined with a greater stoichiometric fuel/air ratio (over twice as high as the typical ratio gasoline).

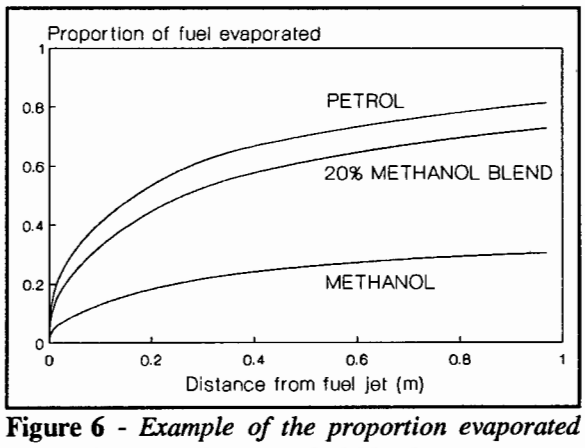

Figure 6 - *Example of the proportion evaporated versus distance of various fuel blends*

Finally, it must be reiterated that the graphs in this section (2.3) serve to represent trends, insofar as the profiles can be significantly affected by a host of variable conditions. The effects of the more important of these variables are discussed in chapter 3.

3. SENSITIVITY ANALYSIS

A sensitivity analysis is performed using the model, aimed at the identification of parameters that deserve attention both for the workings of the model itself, and for the experimental investigation. Droplet size and fuel distribution, inter alia, are readily identified as being highly important.

The sensitivity analysis was ultimately aimed at determining the effect of engine speed on the temperature of the fuel/air mixture entering the cylinder. Towards this goal, the effects of various parameters on the gas temperature were studied for a range of air speeds (broadly representative of the engine speed range 600 rpm to 6000 rpm). From this, the factors which affect the gas temperature could be identified.

The procedure was to use the computer model to predict the effect of varying a certain parameter. The influence of speed was monitored for manifold air-speeds of 5, 20, 35 and 50 metres per second in combination with each parameter to be investigated, and hence the four curves presented in each of the graphs below correspond to these speeds.

Effect of engine speed

The effect of speed on the gas temperatures within the manifold is shown graphically in Figure 7. The existing situation is clearly a trade-off between several factors, for example:

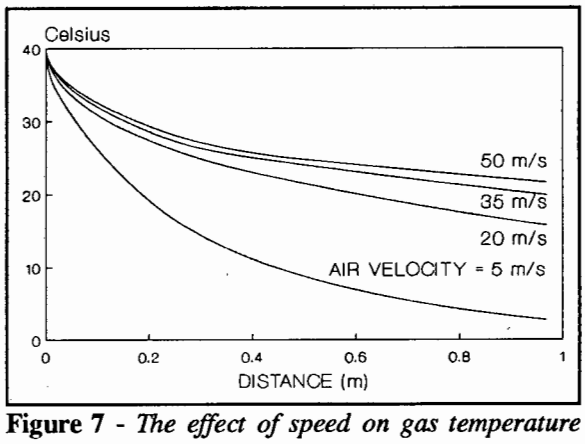

Figure 7 - *The effect of speed on gas temperature versus distance*

1. The higher the speed the faster the fuel is transported through the manifold thus lowering the residence time and therefore limiting evaporative cooling.

2. The higher the speed, the greater the turbulence and relative velocities between the fuel particles and the air, which would tend to increase heat and mass transfer rates thus encouraging evaporation and lowering the temperature of the mix.

From the computer model, the overall effect of raising the speed is that cooling is hindered, and the gas temperatures are not cooled as effectively at higher speeds (i.e. greater cooling occurs at lower engine speeds).

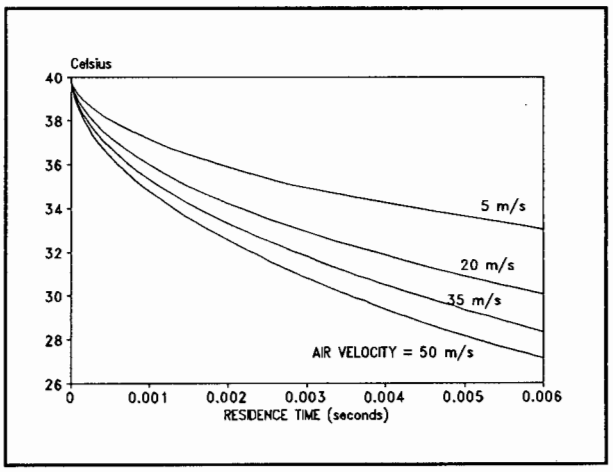

Figure 8 - *Gas temperatures versus residence time in the manifold for various air-speeds.*

Many of the factors affected by engine speed (for example turbulence, mass and heat transfer coefficients etc.) would tend to introduce the opposite trend to that observed above (i.e. they would tend towards greater cooling at higher speeds). Therefore, the lack of residence time of the fuel in the manifold (due to being carried off faster under the action of a higher air speed) would seem to be the dominant factor. If this were the case, it would be expected that better cooling per unit residence time would result for the higher speed conditions. This is confirmed when the temperatures are plotted against residence time as in Figure 8.

Model test procedure

The following technique was used to test the influence of other input parameters. A set of standard initial conditions formed the foundation for comparison, where only the parameter to be tested could be varied.

The test parameter (e.g. initial fuel temperature, fuel viscosity etc.) was varied through a range of values, and the gas (air and fuel vapour) temperature was monitored at a fixed distance of 0.2 metres downstream of the fuel jet. In order to gauge the effectiveness towards cooling the gas that varying a certain parameter had, the data were plotted relative to the initial gas temperature (which is all air initially). This is the difference between the initial gas temperature (fixed arbitrarily at 40°C for this purposes of this analysis) and the gas (air and fuel vapour) temperature at the arbitrary distance of 0.2 metres (0.2m is the length of a typical automotive inlet manifold).

Initial fuel temperature

The sensitivity of the system to variations in initial fuel temperature was investigated by checking the temperature of the gaseous (air/fuel vapour) mixture after it had travelled 0.2 metres down the manifold from the point where the fuel was introduced.

The initial air temperature was chosen to be 40° Celsius (for all the following demonstration cases) which was one of the temperatures used in the test-rig.

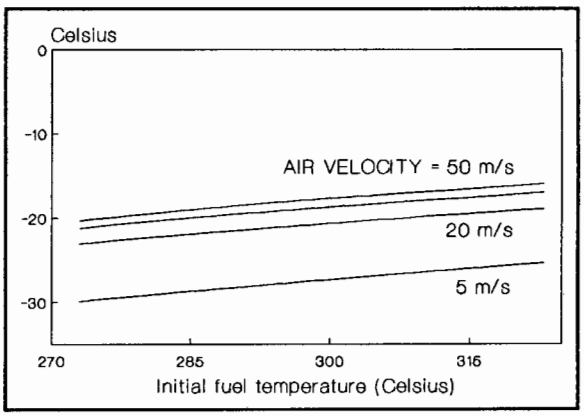

Figure 9 - *Temperature lost by gas for various air-speeds versus initial fuel temperature*

From Figure 9, it can be seen that a 10°C change in initial fuel temperature is reflected in approximately a 1°C difference in the gas temperature. Thus gas temperature (at this distance) is not very sensitive to changes in fuel temperature. This can be ascribed to the fact that, while significantly more fuel evaporates for higher initial fuel temperatures, the heat of evaporation is taken from the liquid. The energy the gas contributes is used to heat the vapour up to general gas temperature (much less energy required), and to heat up the liquid (which is a slow process). The effect of heating the fuel is, therefore, to improve evaporation without having an immediately noticeable effect on the gas temperatures. Boam and Finlay[10] noticed that the most energy efficient way to increase the proportion of fuel evaporated was to heat the liquid fuel. This method would not be expected to affect the gas temperatures significantly (see Figure 9).

Air speed

An interesting fact emerging from the study was that the effect of speed on gas temperature could be considered almost as an independent operator, as in Figure 9 where the various speed curves are almost exactly the same profile. The effect of speed on temperature lost can be isolated and is graphically illustrated in Figure 10.

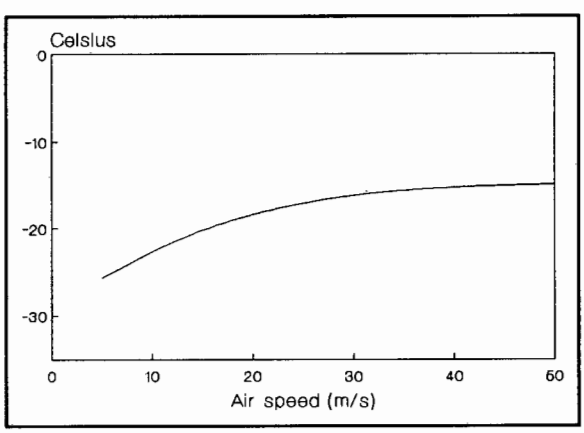

Figure 10 - *Gas temperature loss versus air-speed.*

A numerical curve fit was applied to the temperature lost as a function of speed and initial fuel temperature. Several equation forms were investigated where the terms for speed and temperature act combinatorially, for example

$f(S,T_i) = g(S) + h(T_i) + k(S,T_i)$ where S = Air speed, T_i = Initial fuel temperature

but the two variables were found to act almost independently (for this case and also for the other cases presented later in this section), and hence the best equation form was :

$$\textit{Temperature loss} = f(S,T_i) = g(S) + h(T_i)$$

where the effect of speed is simply to shift an established curve vertically without changing its shape appreciably.

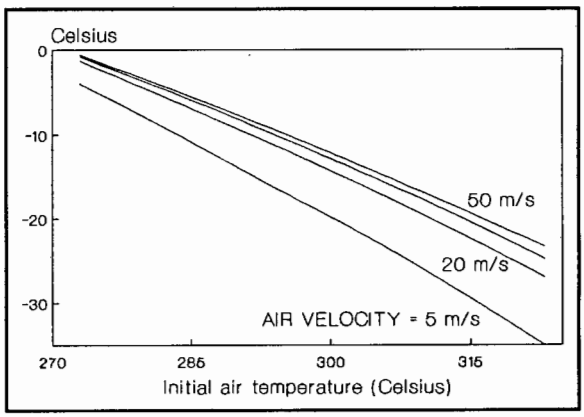

Figure 11 - *Temperature lost by gas versus initial air temperature.*

Initial air temperature

It can be seen, from Figure 11, that varying air temperature has an almost linear effect on the final air temperature. The better cooling offered by lower speeds is more pronounced for higher air inlet temperatures. The trend, therefore is for any differences in temperature caused by differences in air velocity to become exaggerated the higher the initial air temperature.

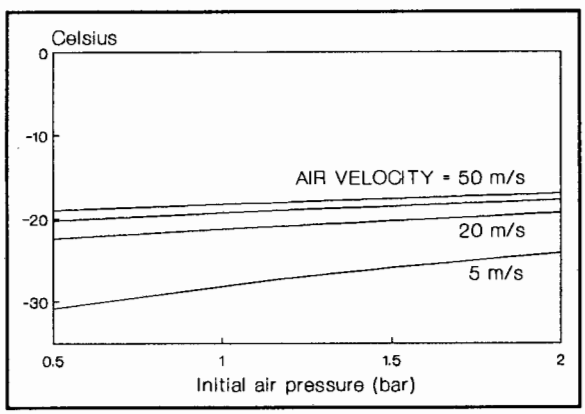

Figure 12 - *Temperature lost by gas versus initial air pressure.*

Initial air pressure

The effect of varying initial air pressure is shown in Figure 12. The effect of changes in pressure is more pronounced for the lower speeds, and less significant at higher speeds. The differences in the curve elevation (for each different speed) correlate very well with the 'effect of speed' as explained above (see Figure 10). (This analysis revealed that the magnitude of the changes in pressure associated with different air-speeds on the test-rig were not significant, and could thus be ignored.)

Initial droplet velocity

It was assumed that the initial droplet velocity was zero when using the carburettor setup. A study of the effect of varying the initial droplet speed showed that for higher initial droplet speeds the evaporative cooling effect diminished (Figure 13). This is to be expected as a result of both the reduced droplet residence time and the reduced relative velocity between the droplets and the air. It is anticipated that having a negative initial drop velocity (such as would be the case for reversed fuel injectors) would further encourage evaporation as well as diminish the relative effect of speed (i.e. equally good cooling would be provided for all speeds). This is a significant finding, the implications of which are discussed further in chapter 8.

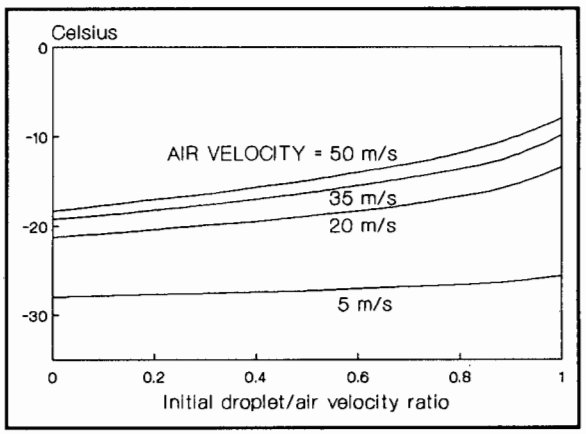

Figure 13 - *Temperature lost by gas versus initial droplet velocity.*

Initial fuel distribution

This parameter was found to be important for evaporative cooling both in theory and in practice. Figure 14 shows temperature loss versus fuel distribution (all fuel not initially in droplet form is assumed to enter the manifold as part of the wall film).

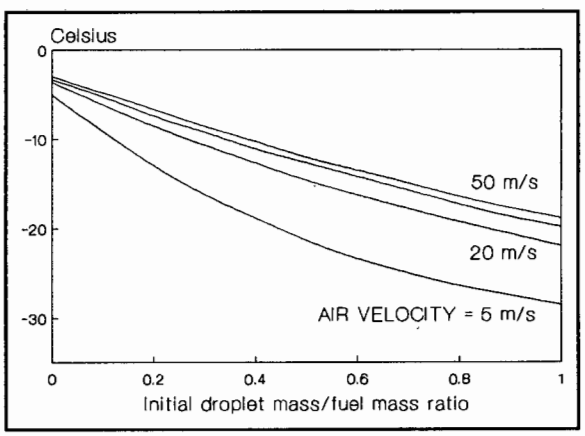

Figure 14 - *Temperature lost by gas versus initial fuel distribution.*

When most of the fuel is initially on the walls in films, there is very little evaporative cooling heat exchange between the air body and the fuel irrespective of speed. For the case when all of the fuel is initially in droplet form, the evaporative cooling effect is pronounced, and is sensitive to changes in speed. The implications of this trend are discussed in chapter 8.

Initial droplet size

The mathematical model assumes one initial drop size for all the droplets produced at the jet. In reality a range of drop sizes are produced. The assumed drop size attempts to represent a mean diameter of all the droplets. The single droplet size is intended to be the mathematical equivalent of having a range of sizes, and it is anticipated that the temperature profiles produced using this simplification would not vary significantly from those that would be produced using a range of droplet sizes. There is information available on the calculation of drop sizes from an array of fuel introduction systems, however experimental studies presented in the literature[59-64] have reported widely variant mean droplet diameters (20 to 2000 μm) dependent on the type of system being used. Moreover, many of the equations to calculate droplet sizes were derived using setups that are not akin to those used in typical automotive inlet systems. Figure 15 illustrates the importance of drop size. Clearly it is imperative to predict this parameter accurately, as it may vary significantly with changes in air-stream velocity and fuel composition (surface tension and velocities, which influence drop size, may therefore play a key role in the cooling dynamics of the system).

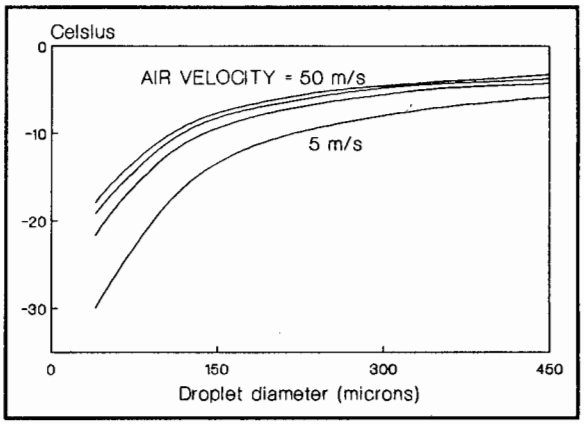

Figure 15 - *Temperature lost by gas versus initial droplet size.*

From the above investigations, some of the trends regarding the evaporative cooling effects of a range of parameters have been clarified. As a result of this general sensitivity analysis, the relative importance of a set of parameters has been evaluated, some of which have been identified to be most important (eg. droplet sizes), whereas others have been noted to be of lesser significance. This type of analysis was vital in the formative stages of this project to isolate those features worthy of attention in the theoretical and the experimental investigations. The model was subsequently refined in those areas of importance to produce a program that was capable of predicting the experimental results very accurately (see chapter 5). The experimental investigation also benefitted from the sensitivity analysis insofar as the equipment was designed and used with an understanding of the relevant features, and this facet of the project forms chapter 4.

4. THE EXPERIMENTAL INVESTIGATION

The physical test-rig, with which the experimental investigation was performed, is described, and the capabilities and limitations of the setup are discussed. The measurement techniques that were developed are also discussed including a critique of their relative effectiveness. The experimental procedure is described, and the chapter ends with a brief outline of the investigation into droplet sizes.

4.1 THE PHYSICAL APPARATUS

A test-rig was assembled (Figure 16) that allowed accurate measurement of the temperature of the various fluid streams as a function of the original air and fuel temperatures, air speeds and distance down the 'inlet manifold'.

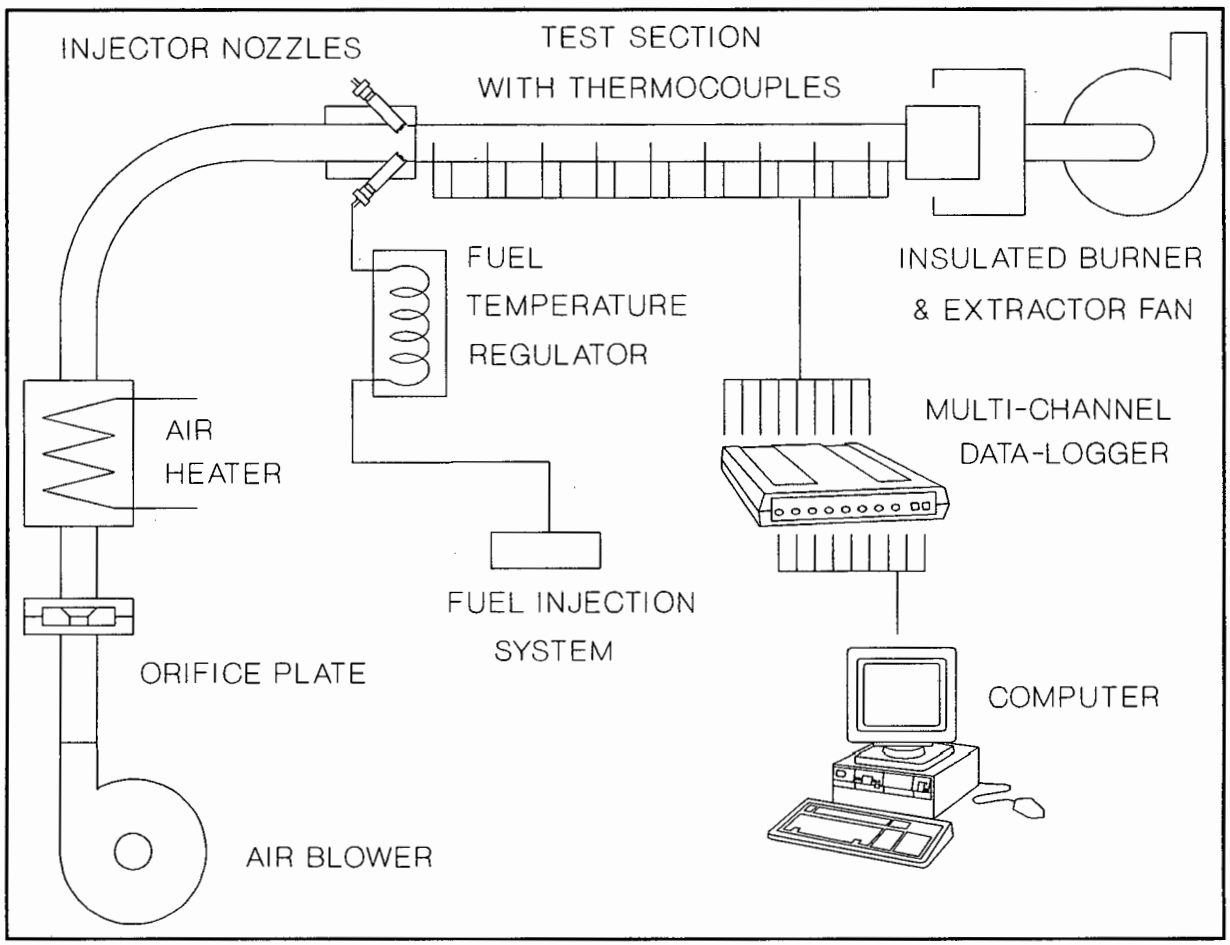

Figure 16 - *The test rig*

Air and fuel supply

A centrifugal fan was used to deliver air to the test section via an electrical heater. The fuel supply consisted of a Bosch K-Jetronic mechanical fuel injection system and a heat exchanger to regulate the fuel's temperature.

Table 1 (below) shows the range of supply parameters, and these could be set at any chosen point in the relevant range to the specified precision.

	Units	Min	Max	Precision
Fan air delivery	g/s	0	60	± 1 %
Initial air temperature	Celsius	40	80	± 0.25 *
Fuel flowrate	ml/s	0	7	± 2 %
Initial fuel temperature	Celsius	10	30	± 0.25 *

Table 1 - *The operating ranges of the test-rig*

* - thermocouple precision

Method of fuel introduction

Four K-Jetronic injector nozzles, positioned radially around the pipe, and angled at 30 degrees to the direction of flow, were used for the majority of the experiments.

The test section

A pyrex pipe equipped with J-type thermocouples formed the test section (Figure 17). Thermocouples placed in recesses in the pipe wall measured the fuel film temperatures, while others were placed in the centre of the pipe to measure the droplet temperatures (Figure 18).

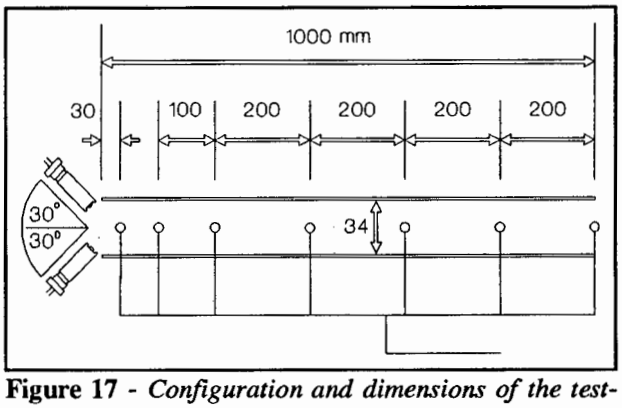

Figure 17 - *Configuration and dimensions of the test-section*

The data recording equipment

Temperature readings taken by thermocouples distributed at relevant locations around the rig were monitored continuously by a 12-channel data logger, which produced both analogue and digital temperature history data. The measurements from the various stations were integrated and recorded in a computer that concurrently calculated the physical conditions present (air density and velocity, air-fuel ratio etc.).

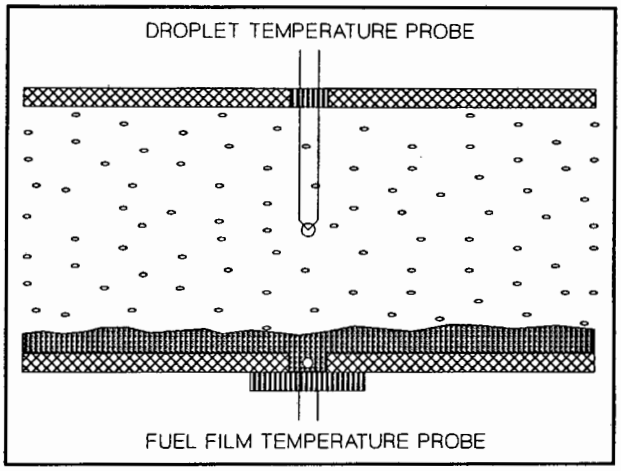

Figure 18 - *Positioning of the thermocouples in the test-section*

Effluent disposal

A combustible, highly explosive fuel/air mixture was tested in the rig, and this necessitated a scheme to dispose of the used fluid safely. The charge was neutralized by burning it off in an insulated chamber, and the hot gases were then extracted and vented.

The influence of the burner section

Due to space constraints in Figure 16 the insulated burner was not illustrated in full detail. The burner section was separated from the pyrex test-section by a 1.2m length of piping. This pipe together with a 'hose and hose-clamp' connection to the test-section ensured that the test-section was not influenced in the slightest by conductive heat transfer from the extremely hot burner section. Furthermore, although light from the burner section could be seen in the test-section (glistening off the film) it was assumed that radiation from the flame could be ignored.

The burner was cast out of Refcast 50 (high temperature insulating substance), forming a cylinder in which the combustible mixture was ignited. The main flame was thrown out of the initial burner into a large hob where the hot gas was diluted and cooled in contact with surplus fresh air. All this gas was drawn off and ducted to a ventilation tower. The flame was initiated by a pilot bunsen burner incorporated in the setup. After the flame was lighted, it was self-sustaining, and the bunsen gas supply could be shut off. This flame was

prevented from propagating back up the pipe by a wire gauze. This gauze blockage was a major contributor in raising the internal pressure of the test-section with increased air mass flow-rates.

Measurement of fluid temperatures

The purpose of the test rig was to monitor the temperature-distance relationship of the three fluid streams (gas, droplet and film) in the test-section. In fulfilling this objective, the probes firstly had to be non-intrusive, and secondly had to be able to measure the true stream temperatures. The former criterion means that the presence of upstream probes should not affect the readings of any downstream probes, while the latter concerns the accuracy of the measurement techniques.

One setup that was considered consisted of a set of traversing probes that could be moved up and down the length of the pipe, and while this method would have been less intrusive than the chosen method, it posed several practical problems. It was decided to equip the rig with fixed probes at several positions down the length of the pyrex pipe (see Figures 16-18), and the design and capabilities of each are discussed below.

Fuel film temperature probes

These thermocouples were placed in recesses in the pipe wall (see Figure 18), which was necessary to ensure the total submersion of the wall thermocouples for all conditions (the film was very thin at high speeds). This configuration worked well in practice, and yielded results that were considered to be accurate.

Droplet temperature probes

The measurement of the temperature of the suspended droplets in the highly turbulent air stream is a task requiring some deliberation. A probe's reading should not be influenced by the air temperature, nor should it be skewed by any evaporative cooling effects associated with a wet surface being blown dry. One particular prototype that was designed to minimize these effects covered the thermocouple tip with a felt swab, but this yielded exactly the same readings as a probe without the swab (a bare thermocouple), and so the latter design was

used throughout. This probe design was thought to measure the true droplet temperature accurately. (At the lowest speeds tested, droplets would tend to cling to the thermocouples, building-up before being blown off (every few seconds). The readings were not observed to vary significantly, however, and this effect was ignored.)

Gas temperature probe

The temperature of the gas (air and fuel vapours) was considered an important parameter for the determination of evaporation rates and later for the evaluation of engine tests (see chapters 5 and 6), and thus considerable effort went into the development of an appropriate probe. Previous researchers[10, 14] neglected to measure the gas temperatures, concentrating their efforts on measuring the film and droplet temperatures, and since they were attempting to validate their mathematical model simulations (similar to the one used in this study), the exclusion of any gas temperature measurements was an important omission.

The measurement of the gas temperature in a highly turbulent air stream, in which a fine mist of liquid droplets is entrained, is a difficult task. An obstruction of this sort, placed in a flowing stream usually generates a turbulent wake, which would tend to throw back liquid particles onto the measuring probe, and this would corrupt the readings. These liquid particles also coalesce to form blockages in the throat of the shroud, isolating the probe from the gas stream, and this necessitated the use of a liquid-removal device. A probe was eventually designed that worked for extensive periods under high speed conditions without any visible probe wetting or blockages occurring. The features of the final gas temperature probe are illustrated in Figure 19.

The principle employed in this design was that the momentum of most droplets would carry them past the probe, and any liquid carried into the mouth of the probe would be deposited on the inner walls, and subsequently would be removed by tiny needles connected to a vacuum pump. The tip of the thermocouple would thus encounter only 'dry' air, giving a representative temperature reading.

This probe was the last in a progression of designs, most of which clearly failed to measure the desired temperature, because the thermocouple tips were seen to be completely wetted

(all the probes were transparent). The final design (complete with liquid-extracting needles) could be used indefinitely without the thermocouple displaying any visible signs of wetting, and this type of probe yielded temperatures that were significantly different from the droplet temperatures. These readings, however, were noticeably lower than the corresponding model predictions, and since droplets as small as five microns in diameter were known to be present in the air-stream (see Appendix D), it is considered likely that these invisible droplets were inevitably reaching the thermocouple, thus corrupting the measurements. Other factors likely to be prejudicial to the accuracy of the probe include, inter alia, (i) the time from when some gas enters the probe's throat until it comes into contact with the thermocouple tip will correspond with when the original gas body is significantly displaced downstream, and (ii) the film which forms on the outer surface of the shroud may exert a cooling influence (although this was not considered to be a major source of inaccuracy).

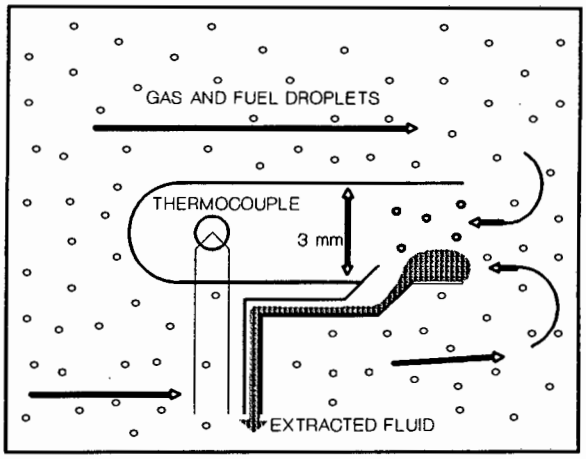

Figure 19 - *Schematic diagram of the gas temperature probe*

It was concluded finally, that it is presently not possible to measure accurately the true gas temperature by means of an intrusive physical probe of this sort. The probe was therefore useful only to verify that the gas temperatures were significantly higher than the temperatures of both the liquid streams, and that therefore equilibrium temperatures had indeed not been reached.

The test-rig setup

Film and droplet temperatures along the length of the 'manifold' were the relevant measurements that the rig provided, and these made up the set of response variables. It was also capable of generating a range of input conditions under which the response variables could be measured, and this provided the framework for the experimental procedure, which is discussed in section 4.2 below.

4.2 EXPERIMENTAL PROCEDURE

This section outlines the procedure employed whilst using the test rig, and explains any assumptions made. A complete documentation of the specific tests that were conducted is included in Appendix C.

Selection and blending of fuels

Three nominal types of fuel were used:

1. 100G:- 100% regular leaded pump gasoline (97 RON), widely available in South Africa at sea level, typically comprising 13.3% LSR (Light Straight Run), 50.2% Light and Heavy Platformate and 36.5% LCN (Light Cracked Naphtha),
2. 10M90G:- 10% blend (by volume) of chemical grade (anhydrous) methanol with 90% 100G gasoline,
3. 20M80G:- 20% methanol (as above) with 80% 100G gasoline.

The fuels of each type were assumed to be chemically identical, with no 'batch effects' (due to different consignments of 200ℓ base fuel barrels), and any effects associated with a fuel standing for a length of time in a barrel (slight vaporization for example) were ignored.

To produce any fuel-methanol blend, two or four litres (as appropriate) of methanol were accurately measured into a 20ℓ container, which was then topped up with gasoline. It was estimated that the blends would be accurate to within 0.4% of the desired concentrations. (The method of mixing is of relevance because, due to mixing irregularities, adding 18ℓ of gasoline to 2ℓ of methanol will not result in exactly 20ℓ of blend).

Fuel supply

A chosen flow could be selected using the fuel-injection mechanism, and this flow was then verified by timing the use of a fixed volume (150 mℓ). The flow supplied for a given setting varied, however, from day to day and with different fuel blends, necessitating the volumetric measurement for every new setting selected.

The mass-flow was calculated by assuming a gross density of 720 $g.\ell^{-1}$ for all fuel-types. (It was important to eliminate as many differences in dynamics between the reference fuels as possible, and therefore it was decided to ignore any small differences in density that would result from blending).

The initial temperature of the fuel was measured just upstream of a nozzle, and it was assumed firstly that this temperature was the same for all the nozzles, and secondly that it did not change significantly across the nozzles. (The latter assumption could well be a source of error).

Air supply

A butterfly valve was calibrated so that air mass-flows of 10, 20, 30, 40 and 50 $g.s^{-1}$ could be selected, and these constituted the five available 'air-speeds' that were used throughout the experiments. The supply air was assumed to be free of any petrochemical vapours that may inhibit the evaporation of any of the constituents in the test fuels. Moreover, the day-to-day atmospheric variations (humidity, pressure etc.) were assumed to have had no significant effect on the properties of the air, and to have had no concomitant effect on the fuel evaporation process (the sensitivity analysis using the model indicated that these factors were insignificant).

Fuel/air equivalence ratio

The equivalence ratio was obtained by associating the mean of a set of fuel mass-flow readings with a particular air mass-flow reading, typically resulting in an uncertainty of $\pm 2\%$.

The test section

The length of pyrex pipe was assumed to be thermally insulated from the surroundings, and although the surrounding ambient temperatures were monitored throughout testing, it was decided to ignore any heat loss/gain through the pipe.

The test-rig described in this chapter was used to produce an extensive set of results (see Appendix C), and the next chapter comprises the analysis and interpretation of these results.

4.3 DROPLET SIZE INVESTIGATION

One aspect of the investigation that was thought to warrant special consideration was that of droplet size, since the model sensitivity analysis (see chapter 3) revealed this parameter to be very important, to the extent that some of the predicted trends would be affected, even reversed, were the droplet size to change in concert with other parameters (eg. velocity or fuel composition). Consequently, the existing trends might be masked by the powerful secondary effect of changing droplet sizes.

A wealth of literature exists that deals with droplet sizes, but these studies involve mainly air-blast atomizers and other setups that were not akin to the setup used in this study, and hence applicable estimates were neither well documented nor easily measurable (as noted by previous researchers[11]). Due to the importance attached to droplet sizes, doubts were raised concerning whether the literature-based reports could be used in this investigation. Consequently, a comprehensive investigation into droplet sizes was initiated, and this encompassed photographic as well as laser-diffraction techniques.

Visual data from a high-speed video camera (10 000 frames per second) was sent to an image-capturing computer program, but the resolution of the video tape proved to be insufficient, and this method was scrapped. Laser diffraction techniques successfully measured the small droplet sizes produced by fuel injector nozzles, but was not used to measure the range of larger sizes associated with carburettors, for which photographic techniques were used.

Droplets produced by fuel injectors

A Malvern particle sizer employing laser diffraction techniques was used to produce a spatial profile of the droplet sizes produced by a single fuel injector nozzle operating for various air speeds (see Figure 20). Several fuel types were tested, including leaded pump gasoline (100G) and

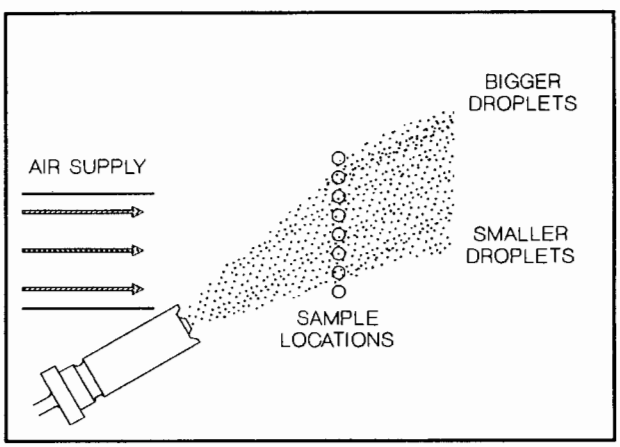

Figure 20 - *Particle sizing using laser diffraction techniques*

the standard 10M90G methanol blend, as well as pure methanol and an 'unleaded' gasoline which comprised most of the constituents of 100G gasoline before lead addition. This investigation yielded information regarding the spatial distribution of various droplet size realms for different air-speeds.

Size of droplets produced by carburettors

The Malvern particle sizer was not used to measure the larger droplets associated with carburettors, and therefore a photographic study was initiated[63], in order to cover the full range of droplets produced by carburettors across the speed range. In this study[63] the measured droplet sizes were correlated with air speeds and fluid properties. Appendix D encompasses a more complete description of both of these investigations, and their results.

This chapter has provided an account of the test-rig and the experiments that were performed. A comprehensive set of results were accumulated using the rig (see Appendix C), and in the next chapter the analysis and interpretation of these results is described.

5. EVAPORATIVE COOLING AND INLET TEMPERATURE

The format of the experimental data is described, together with the results of a statistical analysis of these data. The statistical analysis showed that the experimental results are well described by the input variables, and that the mathematical model is successful in predicting these experimental values. An appraisal of the model performance is undertaken, and the model predictions are evaluated against the corresponding experimental data points. With the robustness of the model considered to have been proven, some definitive model simulations are presented for a range of air-speeds and fuel compositions, awaiting further analysis in the following chapter.

5.1 ANALYSIS OF THE EXPERIMENTAL RESULTS

Statistical analysis of the experimental data was undertaken to establish the significance of the apparent trends. This analysis was initiated for the following reasons:

1. To determine whether the experimentation had yielded statistically significant trends.
2. To ascertain whether model predictions corresponded well with the experimental results.
3. To demonstrate the robustness of the model (2) in order to lend credibility for ensuing analyses.
4. To verify the model's sensitivity predictions (on the test-rig, it was impossible to vary one specific parameter in isolation, and the model was intended to facilitate this kind of study).

A multivariate analysis of variance was chosen as being the appropriate vehicle to test the fidelity of the experimental results.

Description of the data

Each sample comprised the data gathered for the nine thermocouples along the length of the test-section of the rig, coupled with the corresponding set of five initial conditions (see Figure 21).

For each test, one particular combination of initial conditions was selected, and the steady state thermocouple readings were monitored for a fixed time period (150 seconds, after equilibrium had been established), yielding mean and range data for each station based on the thirty data points accrued for each station in that time. Statistical analyses of variance could then be performed with the data in this form, the primary documentation of which can be found in Appendix E.

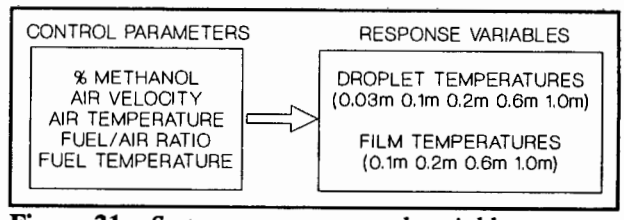

Figure 21 - *System parameters and variables*

A comprehensive multivariate analysis was performed using commercially available software (on the local VAX network). Although specific details of this aspect of the study are beyond the ambit of this section, the study had several significant conclusions, and these are worth noting here:

1. The response variables were correlated significantly with the control parameters. This means that the variations in control parameters were, in themselves, sufficient to explain the variations the measured response variables.
2. As a consequence of (1), it was also concluded that no significant factors affecting the behaviour of the measured response variables had been left out of the set of control parameters.
3. The computer model (which was fed only the values of the control parameters) managed to predict the values of all the response variables with accuracy; the connection between the measured and predicted quantities was found to be highly significant.

The above conclusion (3) is important because it verifies that the computer model is successful in simulating the physical situation across the wide range of conditions that were tested. The performance of the computer model is discussed in more detail in section 5.2.

5.2 COMPUTER MODEL PERFORMANCE

Despite the concentrated efforts made to clarify the important and influential facets of the computer model simulations, many factors could be only broadly approximated (for example the surface area of the film, or the droplet deposition rate). It was decided to estimate the behaviour of these features with the following method, and with the stipulated constraints:

1. The range of realistic values for any parameter in question was identified, and all estimates were confined to this range.
2. A parameter could then be refined (within the appropriate realistic range) to produce improved computer model simulations. If improved correlations with the experimental results were observed across the board, then this refinement was adopted.

(If the latter method seems akin to a 'self-fulfilling prophecy', bear in mind that, in general, an improvement in one case would contradictorily correspond with worsened simulations for several other cases. This behaviour prevented any 'fitting of the theory to the data'. A cursory effort was made to hone the model performance using this method, but no noteworthy improvements over the initial runs were achieved, and hence these first runs were adopted for this investigation. The model was limited by some rather primitive assumptions, for example, no effort was made to investigate the film shape beyond the initial crude description. Appendix B details these factors.)

All the experimental data points were compared with the corresponding computer model predictions (generated using the identical control parameter set) in order to evaluate the model's power and versatility. The graphs which comprise Figures 22-29 serve to illustrate the robustness of the mathematical model in following the experimental trends accurately for the wide range of initial conditions presented. They also show a remarkable concordance of the model predictions and the experimental data.

Table 2 provides the key to Figures 22-29, in which open squares represent the experimental droplet temperatures, and asterisks represent experimental film temperatures. The curves were generated using the computer model. The runs depicted in Figures 22-29 were chosen

specifically to represent the extremes of all the experimental conditions (very hot initial temperatures with high velocities, through to very cool initial temperatures in combination with lowest velocities). Only in Figure 23 is the model shown to deviate significantly from the experimental values (and this is probably due to inadequate film-shape description - see Appendix B), and it is noted that the model generally performed very well when compared with the empirical data. In the light of the fact that very little time was spent clarifying poorly defined aspects of the model (eg. film shape and behaviour), it is anticipated that the model could be improved further, to produce a very robust tool.

Figure No.	Fuel type	Run No. *	Air flowrate [g/s]	Initial fuel temperature [°C]	Initial air temperature [°C]
22	100G	501	10	27	60
23	100G	531	10	28	80
24	100G	517	50	38	60
25	100G	540	50	33	80
26	20M80G	1072	10	19	40
27	20M80G	752	10	14	60
28	20M80G	1091	50	23	50
29	20M80G	1175	50	22	80

Table 2 - *Key to the initial conditions of the demonstration graphs*
* Run number corresponds with a particular set of experimental data (see Appendix C).

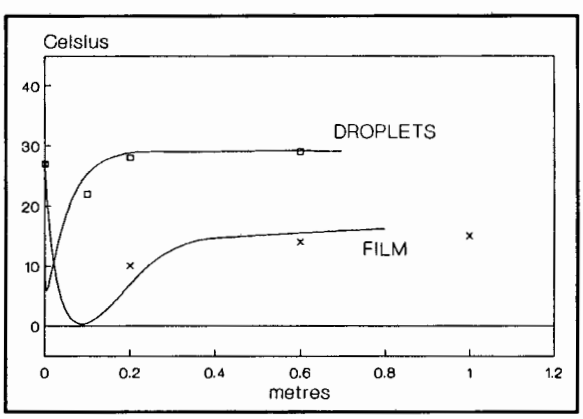

Figure 22

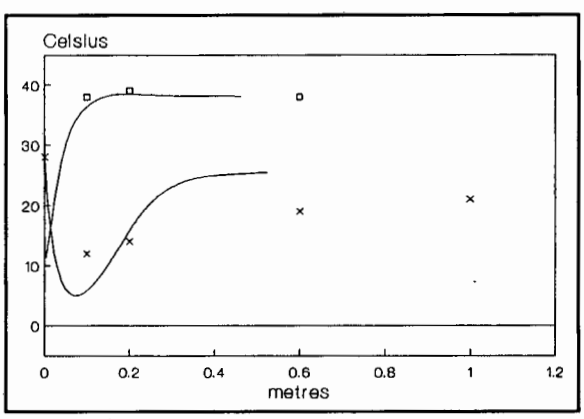

Figure 23

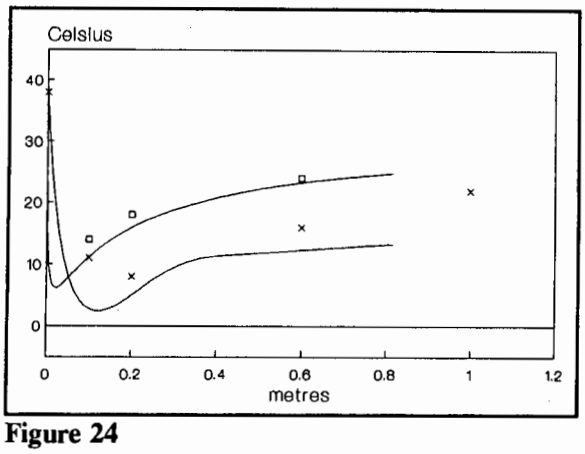

Figure 24

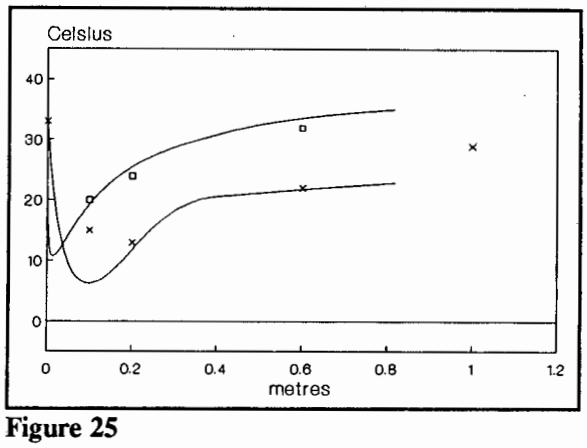

Figure 25

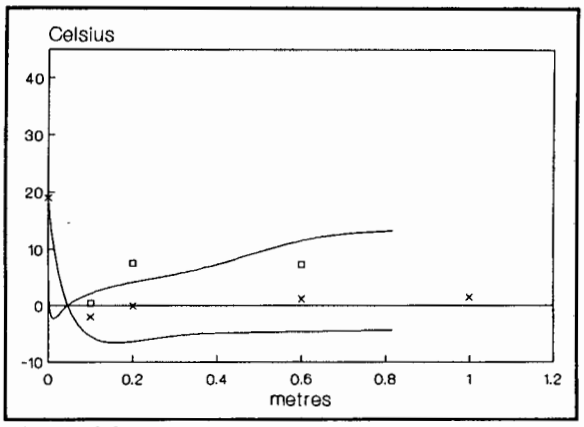

Figure 26

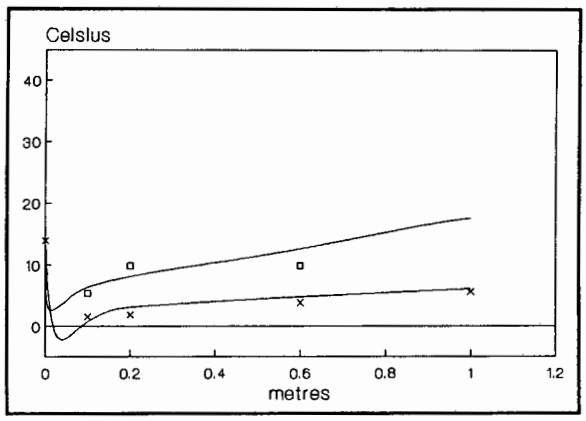

Figure 27

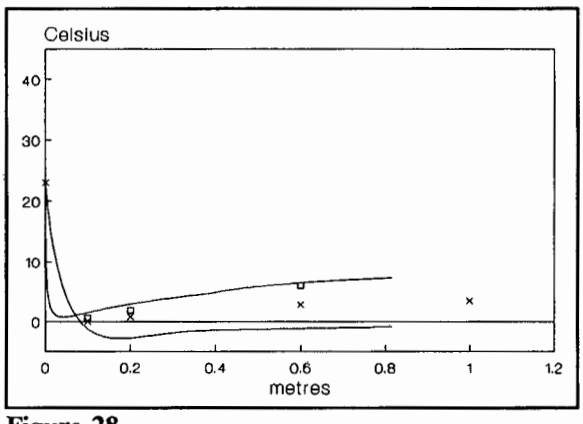

Figure 28

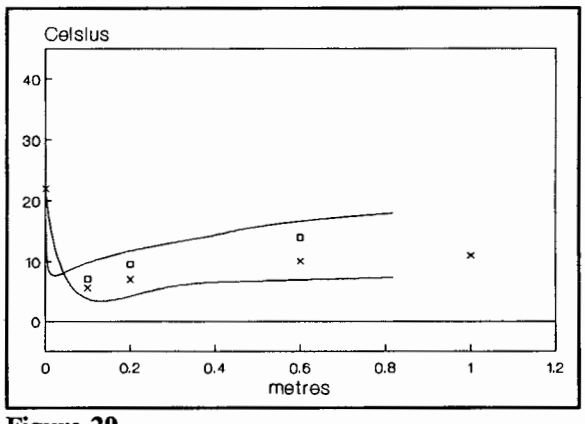

Figure 29

Since the model performed well both against previous models (see chapter 2) and against the wide range of experimental results obtained in this study, it was considered sufficiently reliable to generate data to be used as a basis whereby the fundamental hypotheses of this thesis could be evaluated. These data are presented in the next section.

5.3 EFFECTS OF SPEED AND METHANOL CONTENT ON EVAPORATIVE COOLING OF FUEL

The computer model was used to produce a set of idealised curves that represent the effect of varying one particular parameter, in isolation. The temperature profiles presented in Figures 30-35 (overleaf) show the results of these computer runs, for varying percentages of methanol and for two air-speeds. Appropriate empirical data echo the fidelity of these simulations. (In these figures, the '% methanol in blend' is the mass percentage, and the fuel/air mass ratio is stoichiometric. The stoichiometric mass ratio is a linear interpolation between the values for pure gasoline (0.07 [kg/kg]) and pure methanol (0.15 [kg/kg]), based on the mass proportion of methanol in the blend.)

From Figures 30-35 it can be seen that:

1. Adding even small proportions of methanol to the gasoline results in dramatic cooling of the air-fuel mix. This is due to the relatively high latent heat of vaporization of the methanol fractions that evaporate.

2. The extra cooling accrued by adding more methanol to the blend becomes less dramatic the higher the methanol content of the fuel. This can be ascribed to the vapour pressure of evaporated methanol limiting further methanol evaporation.

3. The temperature profiles are altered radically by changes in engine speed. This effect has been attributed to the lower residence time at higher speeds (see chapter 3).

4. The temperature differences between the various blends is a function of distance down the 'manifold', as is the relative effect of engine speed.

5. The liquid fuel is initially cooled by the quick evaporation of all components, especially the lighter fractions. The resulting lower liquid temperatures, attendant with higher vapour pressures (due to the already vaporized fuel) act to inhibit further evaporation. Therefore liquid reheating tends to dominate, but is tempered in turn by increased evaporation associated with higher liquid temperatures.

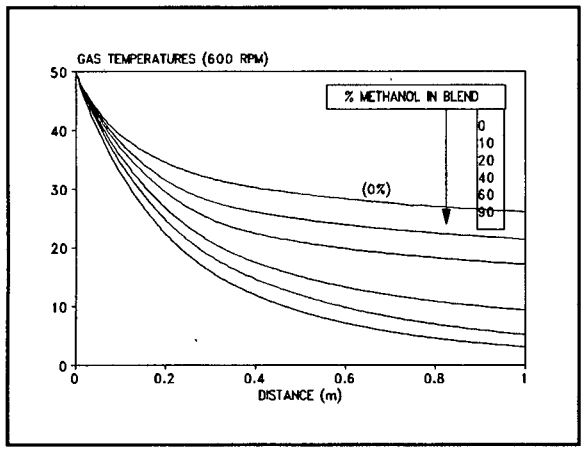

Figure 30

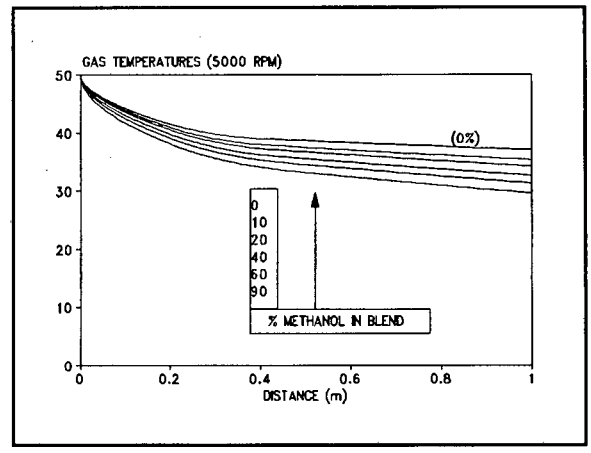

Figure 31

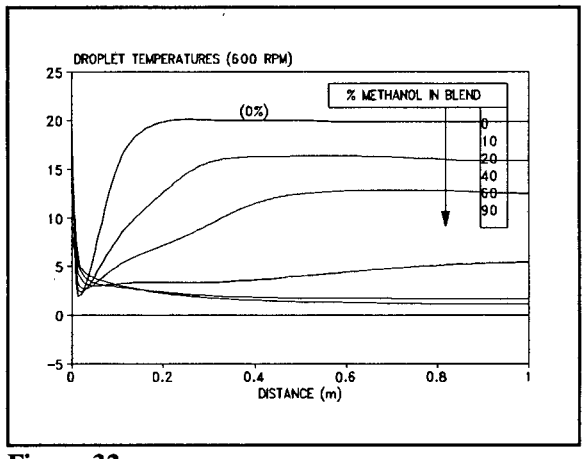

Figure 32

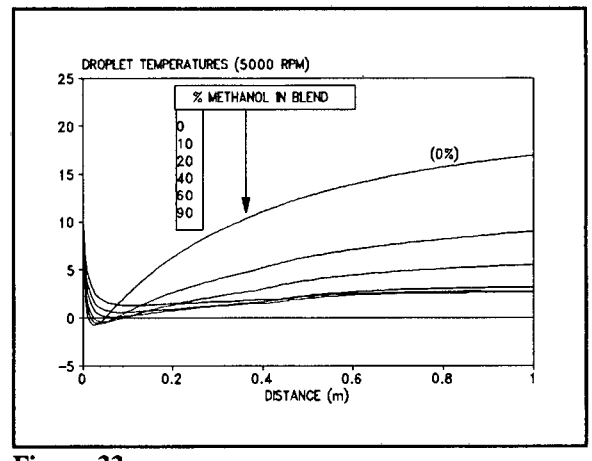

Figure 33

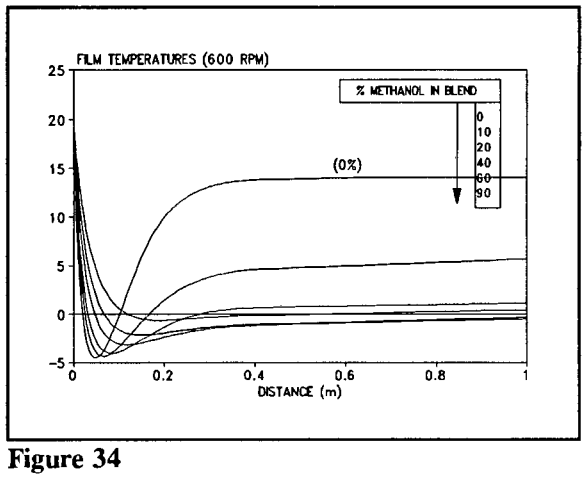

Figure 34

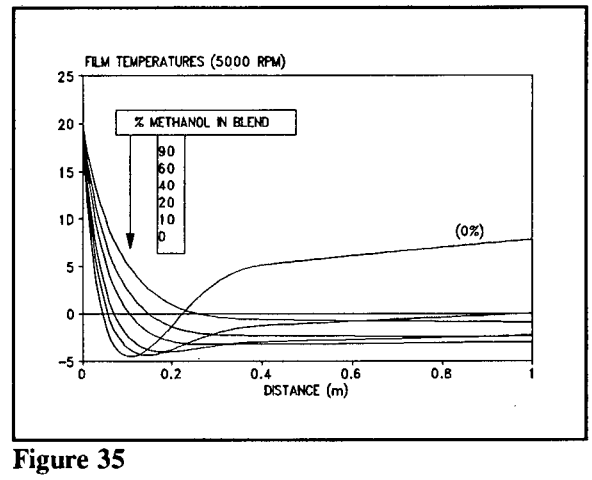

Figure 35

Figures 30-35 - *Graphs of temperature versus distance for the 3 fluid streams : gas (Figures 30&31), droplets (Figures 32&33) and film (Figures 34&35). The graphs plot the temperatures of pure gasoline, and of several methanol-gasoline blends. Graphs 30,32 and 34 are for low-speed conditions, while 31, 33 and 35 correspond to a high-speed situation.*

5. The higher the methanol content of the fuel the slower the initial liquid cooling, and correspondingly, the slower the reheat rate. This can be explained primarily by the fact that there is more liquid mass with the higher methanol content (stoichiometric fuel/air mass ratio means that there is approximately twice as much fuel mass present for pure methanol as compared with gasoline), and this additional mass acts to provide thermal inertia.

6. The subtle 'undulating' appearance of some liquid temperature profiles (Figures 32 and 33) can be attributed to the preferential evaporation of certain fuel components at certain stages (the lighter fractions are likely to evaporate very rapidly at first, thus limiting the vaporization of other components.

7. A pseudo-equilibrium liquid temperature is reached for some of the situations shown, but it is noted that both evaporation and heating are still taking place, albeit more slowly than at first.

From the statistical analyses of variance the model has been shown to be sufficiently robust to reflect the heat transfer processes accurately across the range of conditions tested. It is clear from the computer predictions that changes in fuel composition and in air-speed can affect the mixture temperatures drastically, but how this all relates to a particular fuel's engine performance is less obvious, and this question is addressed in chapter 6.

6. EVAPORATIVE COOLING AND ANTI-KNOCK PERFORMANCE

A procedure is developed to evaluate the effect that a fuel's evaporative cooling exerts on Research Octane Number (RON). Using this process to interpret model generated data, predictions are made concerning the expected enhancement in RON of adding methanol to gasoline, due purely to evaporative cooling. These predictions are then compared with actual RON test data, and consequently it is concluded that the RON behaviour of methanol-gasoline blends is influenced significantly by evaporative cooling. A similar analysis is applied to a high-speed condition, and the spark advance versus speed behaviour of a methanol-gasoline blend is projected. The spark-advance behaviour of the blend is anticipated to be significantly affected by the changing evaporative cooling environments prevalent at different engine speeds.

6.1 EVAPORATIVE COOLING AND OCTANE NUMBER

Relating the effects of evaporative cooling to a change in Octane Number (ON) can be attempted at best tentatively, since several tenuous assumptions must be used and some links must be made to span this indirect relationship (Figure 36). The process devised to evaluate the effect that inlet temperature has on ON is outlined very briefly in this section, so as not to interrupt the flow of the text. A much more rigorous explanation of the process with justifications of the assumptions made are to be found in Appendix F.

Compression ratio (CR)

It is assumed that almost all of the evaporation that takes place does so in the inlet manifold, and that therefore the compression temperatures can be estimated as a function of the temperatures of the inlet streams (see Appendix F). Also it is assumed that the mixture compression can be modelled grossly as being the compression of the gases only. Using these assumptions, any change in the inlet temperatures (caused by different evaporative cooling conditions for

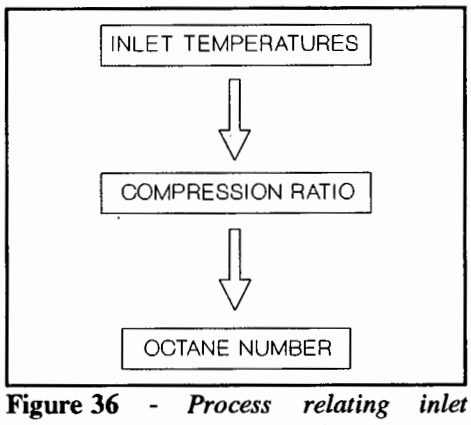

Figure 36 - *Process relating inlet temperature to Octane Number*

example) could be compensated for by a corresponding change in the compression ratio (CR) to result in unchanged final temperatures (at the end of the compression stroke). Inlet temperature changes (caused by evaporative cooling differences) may thus be connected to a change in compression ratio by this logic.

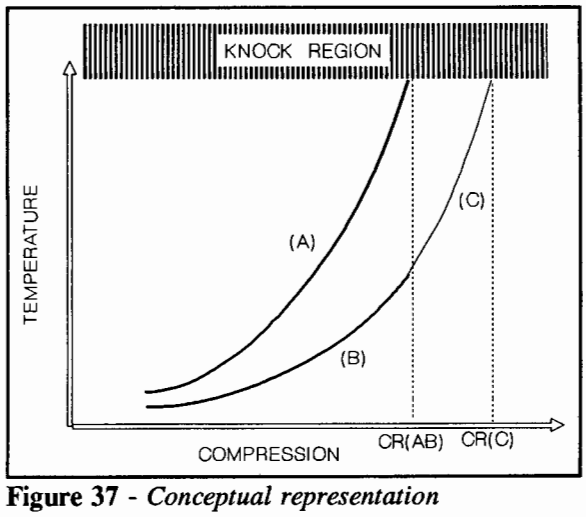

Figure 37 - *Conceptual representation*

In Figure 37, which is a graphical representation of this concept, lines 'A' and 'B' are the compression/temperature relationship for the gas at a particular CR (CR_{AB}). The difference between the lines' profiles arises from their individual temperatures at the start of compression, and it is instructive to note that, by the nature of compression, any small difference in starting temperature is necessarily magnified through compression. Line 'C' represents the further compression the gas in line B to a higher CR ($CR_C > CR_{AB}$), forcing the gas to a much higher temperature. For some particular CR_C, the top of compression temperature of the gas of line 'C' will give rise to 'similar' conditions that would arise from the conditions of line 'A' (and CR_{AB}). Therefore the effect of a change in inlet temperature (caused by evaporative cooling) can be connected quantitatively to a change in CR (to result in similar top of compression conditions).

Octane Number

Using the experimentally derived relationship between compression ratio and 'Octane requirement (RON test)' described in the literature[69-75], the effect of any change in compression ratio may be translated into a change in RON (see Figure 38). In short, for a particular fuel in a RON test, a different inlet temperature would necessitate an altered compression ratio in order to achieve a similar knocking situation, which would modify the indicated ON, and in this way it is possible to isolate and evaluate the influence that evaporative cooling exerts on the RON.

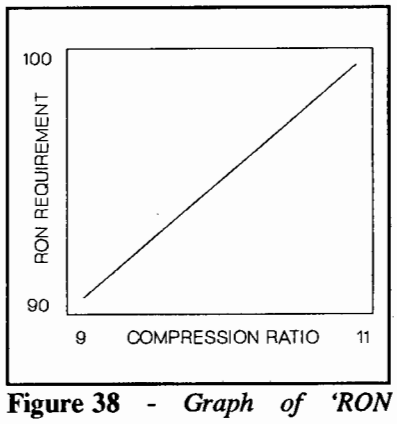

Figure 38 - *Graph of 'RON requirement' versus CR*

6.2 OCTANE NUMBER PERFORMANCE OF METHANOL-GASOLINE BLENDS

The influence that evaporative cooling exerts on the RON behaviour of methanol-gasoline blends may be determined utilizing this process, and this would be due to thermal effects only, and independent of any chemical-reaction/combustion differences associated with the various blends. Figures 39 and 40 show the results of such an analysis applied to some blends with pure gasoline as the reference fuel. For the purposes of this example the gasoline has been assumed to have an RON of 96, and this fuel is used as the datum in Figures 39 and 40. The 'RON' of the other blends have been predicted, using the procedure developed in section 6.1, from the relative gas temperature with respect to the gas temperature of the reference gasoline.

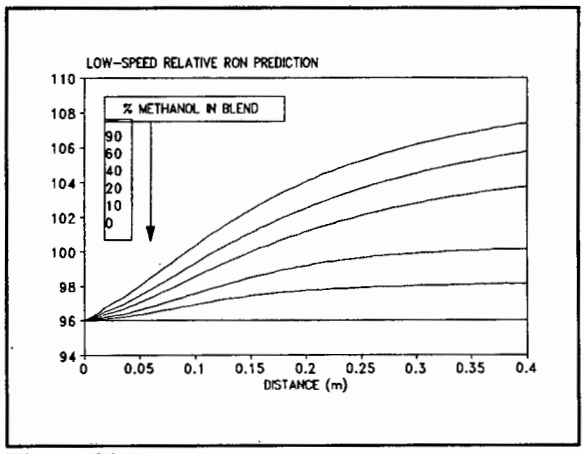

Figure 39

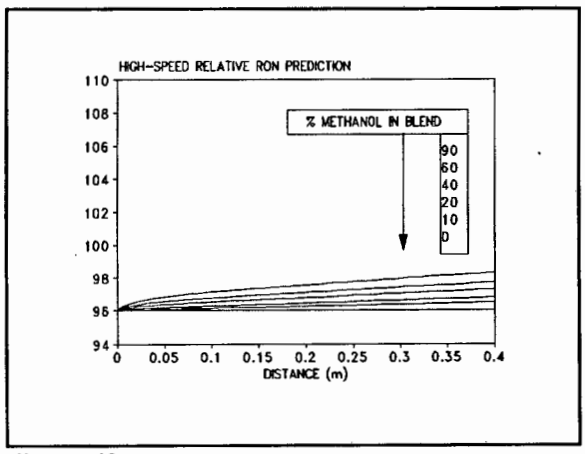

Figure 40

Figures 39 and 40 - *Expected RON predicted by the evaporative cooling of several methanol-gasoline blends relative to the behaviour of pure gasoline for (a) low-speed (Figure 39), and (b) high-speed conditions (Figure 40).*

All these gas temperatures were predicted using the data generated by the model (and presented as Figures 30-35), and several assumptions had to be made in attempting to simulate the conditions of the RON test (Figure 39):

1. An initial air speed of 2.5 m/s was used, which corresponds with an engine speed of 600 rpm.
2. Stoichiometric mixtures were assumed. (The actual test is usually run with a higher fuel/air than stoichiometric, which would tend to exaggerate the differences between the blends).

3. The manifold flow processes were assumed to be the same as those that were studied using the test rig, and for which the model's robustness had been proven. The effects of bends in the real RON test engine manifold were ignored.
4. An inlet manifold length of 0.4m was assumed to be an 'equivalent length' of the RON test engine manifold. (This manifold is notably long, when compared with a typical automotive inlet manifold length of 0.2m).

The last criterion (4) has a somewhat vague foundation, since the effects of bends etc. of the real manifold may cause cooling equivalent to a very long straight manifold. The result of assuming slightly longer 'effective lengths' are shown in Figure 41, which is merely the translation of the data presented in Figure 39 read at the specified 'distance' down the manifold.

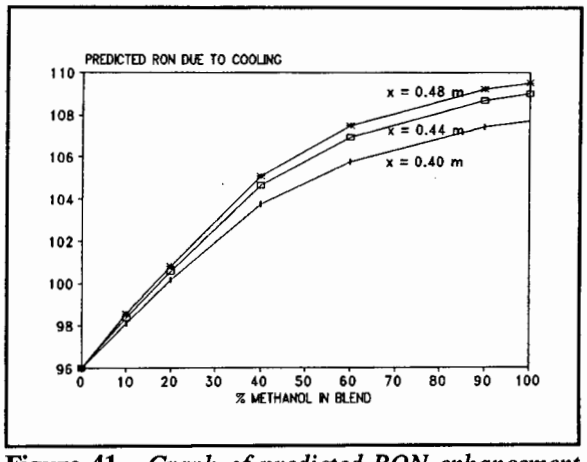

Figure 41 - *Graph of predicted RON enhancement due to evaporative cooling for varying percentages of methanol in gasoline blends*

In order to assess the extent to which differences in ON can be ascribed to evaporative cooling in isolation from chemical effects, it is useful to compare the results of tests where evaporative cooling clearly plays no role with tests wherein evaporative cooling effects do play a role, and the differences between the MON and RON tests are ideal for such an analysis.

It is essential here to understand the salient differences between the two ON tests. The MON test is performed with a mixture temperature of 149°C, at which temperature methanol, having a boiling point of 64.7°C, can be assumed to have been completely pre-evaporated, and thus any evaporative cooling effects associated with blends of varying proportions of methanol can be considered to have been eliminated. The RON test, on the other hand, specifies an initial air temperature of 51.9°C, and thus the mixture temperatures in the manifold can, and will be affected by fuel evaporation.

For the purposes of this discussion, therefore, any difference in MON exhibited by different methanol-gasoline blends are assumed to be due to chemical differences only, and not at all due to thermal effects. The RON test, on the other hand, is assumed to be influenced by both the chemical and the thermal properties of the fuel. The magnitude of the effect on RON of thermal properties can thus be estimated, by examining the comparative performance of a fuel on the RON and MON tests. Using this logic, the difference in the RONs of two fuels which have identical MONs can be attributed to thermal effects.

Johnson and Riley[6] performed a series of RON and MON tests using methanol-gasoline blends, ranging from 2% to 100% methanol by volume. Figure 42 presents the results of one of these experiments that is pertinent to this discussion (top line in Figure 42), and this is plotted against the predictions of the analysis developed in this study.

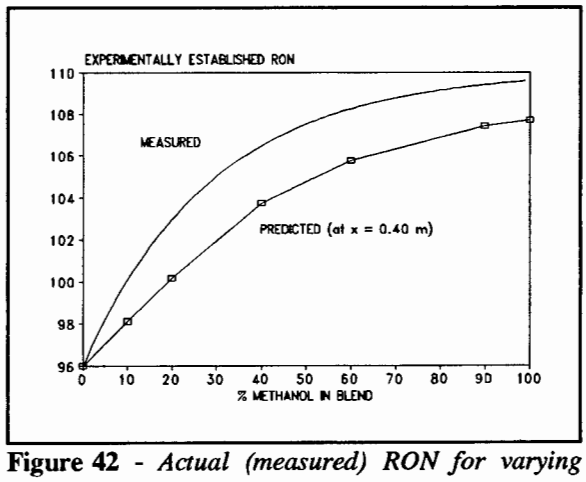

Figure 42 - *Actual (measured) RON for varying percentages of methanol in gasoline blends*

It is important to state that, for the particular base gasoline that was used in Johnson and Riley's experiment that is reported here, the MON was seen to remain almost constant across the range of methanol blends, while the RON exhibited a significant sensitivity to the blend concentration of methanol. (Adding methanol to a base fuel with a MON different to that of methanol will obviously result in a MON sensitivity to the percentage of methanol present. The salient feature of the Johnson and Riley experiment is that it was chosen for this discussion specifically because the base fuel had an identical MON to that of pure methanol. While there is no reason to suppose that the MON of blends of these two fuels should remain the same as that of the base fuels, this was the case for these fuel blends[6]. The RON behaviour of blends of these two fuels can therefore be ascribed to effects other than those of chemical origin.)

A good correlation is observed between the 'RON due to cooling' and the 'experimentally established RON'. It must be pointed out that the cooling predictions were based on a setup that is not akin to the actual RON test engine manifold. There will clearly be inaccuracies

internal to the model/experimental setup, and in addition there will be sources of error as a result of applying the model to simulate the test-engine. These inaccuracies and sources of error are likely to introduce both overestimation and underestimation (for example, the bends of the actual manifold may cause high re-entrainment rates and a longer effective length manifold, whereas, on the other hand, the larger droplets associated with carburettors are likely to provide lower cooling rates than was evident in the experimental rig). In addition the effect of pulsations, which are pronounced in the real RON test, have been ignored in the present analysis.

It is clear, however, from this analysis, that the evaporative cooling mechanism is sufficient to explain the RON enhancements associated with methanol-gasoline blends both in the magnitude and in the overall trend of the effect. These observations, more than the absolute predictions of the analysis, serve to corroborate the underlying hypothesis.

This analysis was based on several approximations (and these are discussed in chapter 8, the specifics appearing in Appendices B and F), but it has served to demonstrate that the action of evaporative cooling is sufficient, in itself, to explain the enhancement in RON experienced when adding methanol to certain base fuels.

6.3 EVAPORATIVE COOLING AND SPARK ADVANCE

An estimate of the spark advance (SA) curves for several fuels over a range of speeds can be made, linked to the analyses already developed in this chapter. Using the data shown above (Figures 39 and 40), the SA performance of a 10% methanol-gasoline blend, for example, can be predicted relative to established data for pure gasoline for example. This analysis requires a translation from Octane Number to SA, and Figure 43 provides a summary of such information derived experimentally[73-75]. The data presented in Figure 43 show the general SA improvement per unit ON increase, measured for a range of fuels and engine speeds (the area between the lines corresponds to variations associated with the range of engines and fuel types tested).

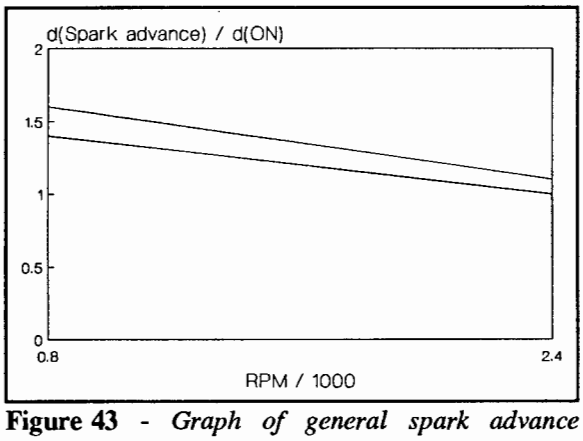

Figure 43 - *Graph of general spark advance increase per Octane Number increase*

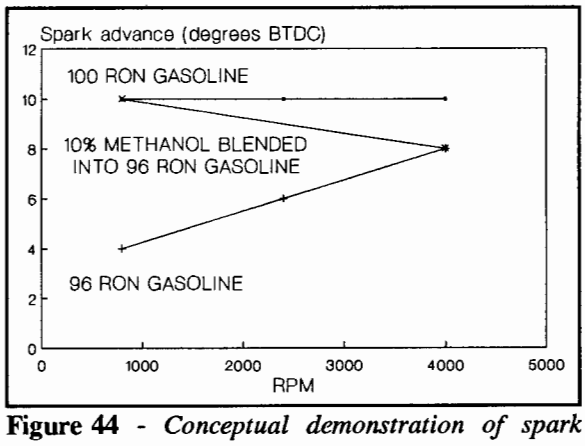

Figure 44 - *Conceptual demonstration of spark advance behaviour of two fuels plotted relative to a that of 100 RON gasoline.*

Figure 44 uses this information to anticipate the performance of two fuel types (96 RON gasoline and 10% methanol blended with 90% 96 RON gasoline) relative to a reference fuel (100 RON gasoline). The SA performance of the reference fuel was chosen arbitrarily, with the other SA curves being calculated relative this line.

A more realistic SA curve for the 100 RON fuel, based on well documented SA data, is shown in Figure 45, with the performance of the other two fuels being calculated relative to this datum, as in Figure 44. The resulting trend for the SA curve for the methanol blend fuel is of great importance, because it corresponds exactly with results of engine tests (as yet unpublished). The disparities known to exist in the SA curves of methanol-gasoline blends

can thus be explained in terms of evaporative cooling, and this relationship is discussed further in chapter 8.2.

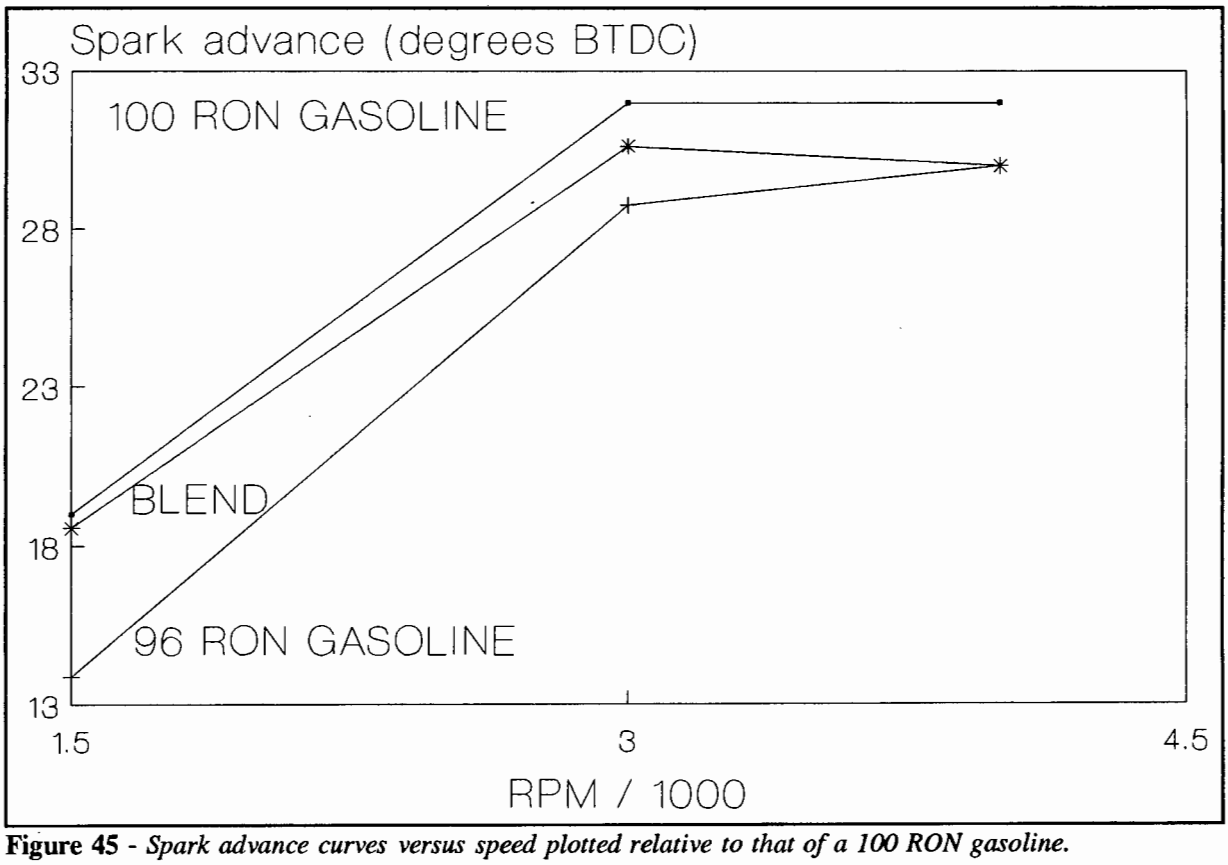

Figure 45 - *Spark advance curves versus speed plotted relative to that of a 100 RON gasoline.*

A method whereby the influence of evaporative cooling on Octane Number may be evaluated has been developed in this chapter. The results of the analyses presented in this chapter have shown that the RONs of methanol-gasoline blends are significantly affected by the action of evaporative cooling. This important finding raises the possibility that the RONs of other fuel types could similarly be affected by evaporative cooling, and, moreover, the possibility is raised that the action of evaporative cooling dictates the difference between the RON and the MON tests. Chapter 7 is devoted to the investigation of these possibilities.

7. EVAPORATIVE COOLING AND THE RON AND MON TESTS

A hypothesis is tested in this section : that evaporative cooling is the dominant underlying factor explaining why some fuels perform relatively well on one ON test but poorly on the other test. All fuels (including the two reference fuels) exert some evaporative cooling effect on the RON test, and this is quantified using the approach developed in the previous chapter. A simple relationship is developed where a fuel's RON can be projected using its MON coupled with the cooling it provides (or vice versa). This indicates that the hypothesis is correct, and the relationship is strengthened further by examination of the underlying structure of the ON tests, which involves compression ratios.

7.1 CONCEPTUAL COMPARISON OF THE RON AND MON TESTS IN TERMS OF EVAPORATIVE COOLING

Knowing that the evaporative cooling qualities of a fuel will influence that fuel's performance on the RON test, and that therefore some of the underlying structure of the RON test is based on thermal as opposed to chemical properties, it may be possible to explain why some fuels perform well on the RON test and poorly on the MON test, purely in terms of thermal behaviour.

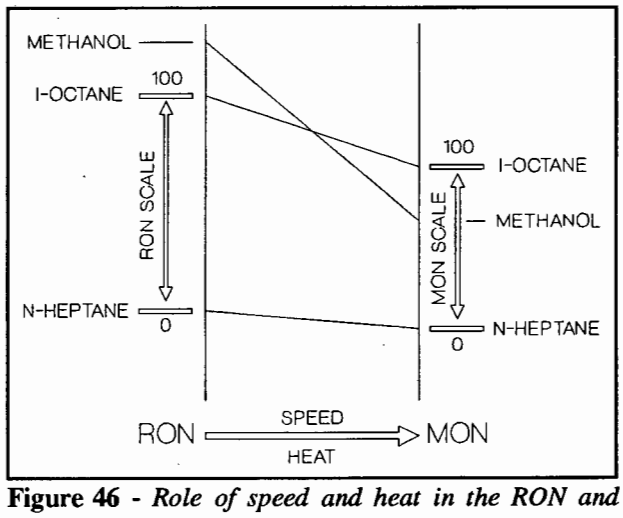

Figure 46 - *Role of speed and heat in the RON and MON tests*

Since the two ON tests are based on arbitrary scales relative to the performance of two standard fuel types, these two scales may not be comparable due to the fact that the RON test allows evaporative cooling of fuels including the standard fuels, whereas the MON test completely eliminates this effect (in most cases), being performed at a temperature at which most fuels would be pre-evaporated. Thus a test fuel that has a certain RON is unlikely to reproduce the same number under the MON test not only because its own thermal conditions are different (no cooling manifested), but also because the standard fuels against which the performance of the

test fuel is being judged have also been subject to altered conditions. The situation is further warped by changes in speed and heat input, and it would therefore be expected that some fuels may perform better on one ON test than on the other. This concept is illustrated in Figure 46. It is likely that evaporative cooling differences could explain many of the discrepancies between the numbers produced using the two ON tests.

The justification for Figure 46 arises from the fact that the more cooling provided by a fuel on the RON test, the higher its RON number will be, owing simply to improved cooling. Expanding the same concept further, two components of the transition from RON to MON exist, the first being the relative effect of evaporative cooling, and the second being the effect of speed and heating on evaporated fuels. Figure 47 serves to illustrate how, due to individual cooling characteristics (peculiar to each fuel type), the differences in the RON and MON numbers of any particular fuel may be explained.

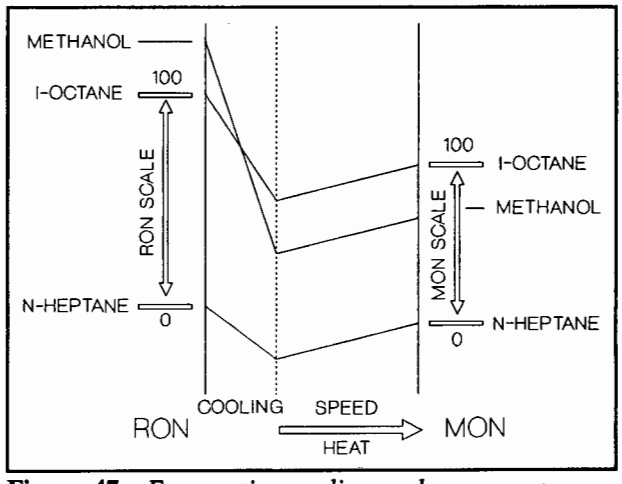

Figure 47 - *Evaporative cooling realm*

A link between RON and MON tests

For purposes of a simple comparison, it is useful to view the MON test as being based on fuels' inherent chemical differences, whereas the RON test is affected both by different evaporative cooling characteristics as well as by chemical considerations. To test the applicability of this concept a simple method to link the RON to the MON test via evaporative cooling was developed. In short, the computer model was used to simulate the evaporative cooling of certain fuels (including the two reference fuels). The same 'relative Octane Number' process as was developed in section 6.1, was used with respect to an imaginary fuel that provided

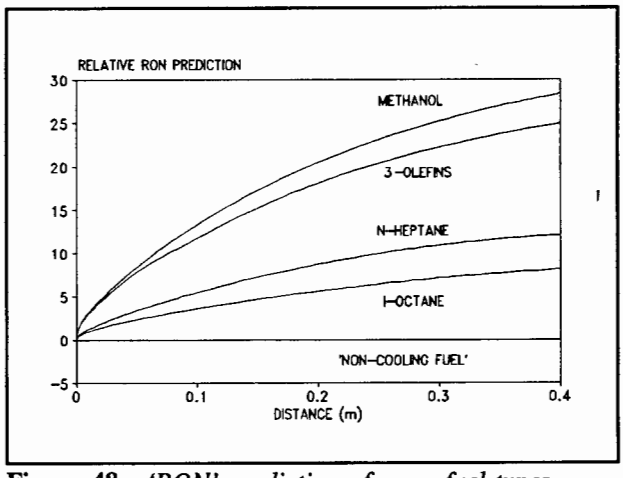

Figure 48 - *'RON' prediction of some fuel types*

no evaporative cooling to the system. Figure 48 shows the results of such an analysis, and Table 3 summarizes these results.

	MON	ON(cooling)	Projected RON	Actual RON
i-Octane	100	+8	100 (Ref)	100
n-Heptane	0	+12	0 (Ref)	0
n-Hexane	28	+12	29.2	29
3-Olefins (*)	75	+22	88.5	90
Methanol	86	+29	107.3	109

Table 3 - *RON linked to MON via evaporative cooling*

(*) (3-Olefins is a mix comprising mainly Pentene, with Hexene and Heptene)

$$Projected\ RON = 100 \times (MON + ON_{cooling} - 12) / (100 + 8 - 12)$$

'Projected RON' is a simple linear projection to force the reference fuels (i-Octane and n-Heptane) back to their designated RON numbers. It is worth noting that because i-Octane offers less effective evaporative cooling than n-Heptane, a fuel with a high MON will accrue a higher 'predicted RON' value than a fuel with a low MON, if each provided identical evaporative cooling. (Notice that this procedure can be applied just as effectively in reverse i.e. predict a 'MON' from RON).

This method provides a rather coarse means whereby the hypothesis that evaporative cooling is linked to the ONs may be tested, and it was included here in order to introduce the concept. A more 'scientific basis' for the same comparison is discussed below.

7.2 COMPRESSION RATIOS, EVAPORATIVE COOLING AND THE RON AND MON TESTS

The ON scales are generated in an arbitrary manner, insofar as the performance of any test fuel is judged relative to the two reference fuels (i-Octane's performance is defined to be 100, and n-Heptane to be 0). A fuel's 'performance' relates to the compression ratio at a standard knock intensity, and this is affected by the temperature of the gases at the beginning of compression (as explained in section 6.1 and further in Appendix F).

The transition from MON to RON may be explained in terms of evaporative cooling, remembering that the analysis is linked to the gas temperature in the test. Starting at the MON test conditions, the gross effect of slowing the engine and cooling the gases, as the RON conditions are approached, will be very much the same irrespective of which specific fuel vapour is diluting the air. It is postulated that if no fuel provided evaporative cooling to the gas, then the RON test would yield very similar results to those achieved using the MON test. The crucial difference between the tests would then be that, in reality, each fuel type provides a certain degree of further gas cooling. The lower the initial gas temperature of a fuel, the higher the compression ratio will have to be before the onset of knock. This higher compression ratio will be interpreted as a higher ON.

Following the same thought process that was applied in chapter 6, the change in compression ratio necessitated by a fuel's cooling, may be calculated in order to achieve the same top of compression gas temperature as would exist if there were no cooling. This translates to a compression ratio change 'due to evaporative cooling' and, since the basis of ON is relative compression ratio, this results in a different RON value than would have been achieved had there been no evaporative cooling.

Table 4 shows the results of such an analysis applied to certain fuels. 'CR' is the compression ratio of a fuel in the RON test (inclusive of the influence of evaporative cooling). 'CR Change' is the enhancement in compression ratio caused purely by the action of evaporative cooling (cooling the gas from the designated 51.7°C). 'CR 51.7°C' is the anticipated compression ratio if no cooling were to take place.

	RON[76]	CR[76]	CR Change	CR 51.7°C
Octane	100	7.8	1.27	6.53
Heptane	0	5	1.20	3.80
50Tol-50nH *	65.2	5.7	1.25	4.45
3-Olefins	90	6.7	2.0	4.7

Table 4 - *Compression ratios used to compare RON and MON*

* (50Tol-50nH is a 50-50 mix by mass of Toluene and n-Heptane)

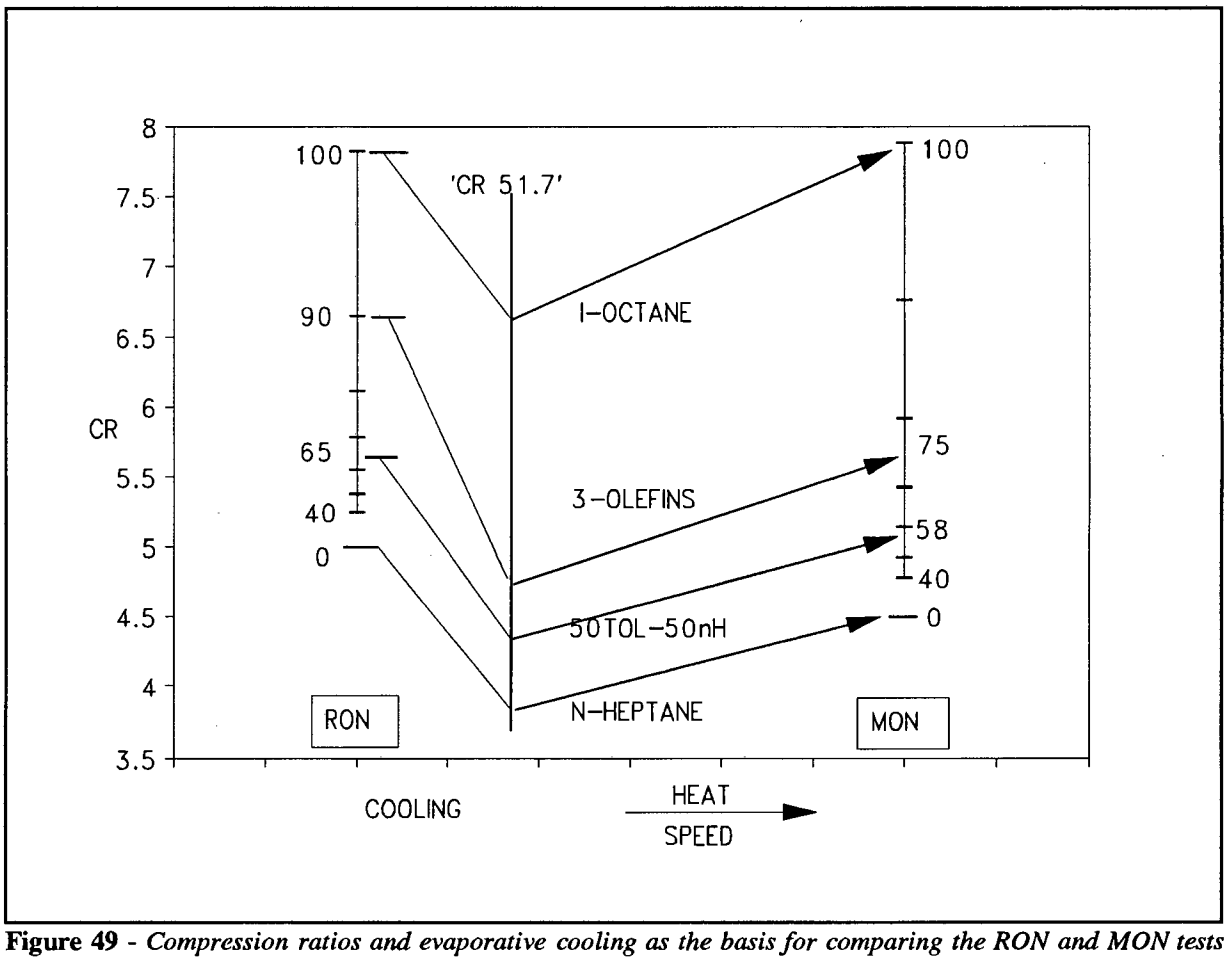

Figure 49 - *Compression ratios and evaporative cooling as the basis for comparing the RON and MON tests*

Figure 49 diagrammatically summarizes the information presented in Table 4. The RON and MON scales are plotted against the compression ratios from which they stem[76]. In Figure 49, the curve for a particular fuel is plotted from the known RON[76], to the 'CR 51.7°C'

predicted point, and from there to the known MON[76]. The MON test is performed at an inlet air temperature and an engine speed 149°C and 900 rpm (right hand scale in Figure 49). The corresponding RON test conditions are 51.7°C (before cooling) and 600 rpm, and this point is represented in Figure 49 as the central thick vertical line ('CR 51.7°C'). The fact that the lines between these two points are all similar serves to corroborate, tentatively, the propositions that gave rise to this section. (The thick line for iso-octane is the steepest of the four, with that of n-heptane having the shallowest slope. The apparent steady increase in gradient with CR does not weaken the hypothesis, as it would be an over-simplification to expect these lines to be parallel.) It must be reiterated as a caveat that these results presented in this chapter stem from analyses that are at best preliminary, and do not represent the findings of a rigorous investigation, which would have to encompass the action of many fuels.

In this chapter the hypothesis that evaporative cooling may be the underlying difference between ONs produced using the RON and the MON methods has been developed. The hypothesis has been supported, in principle, by initial quantitative testing. This implies that the dynamics affecting evaporative heat transfer will also influence the RON test, and these are discussed briefly in the next chapter.

8. DISCUSSION

The findings presented in the previous two chapters are discussed, and certain reservations concerning the method of analysis are expressed. Implications of these findings are explained, including insights into the cause of HSK in terms of 'Octane requirement' and spark advance. Tentative suggestions as to the elimination of the phenomenon of HSK are made, arising from understandings gained in this study. Finally, a brief criticism is levelled at the RON test in terms of the measurements performed in the test.

8.1 THE OCTANE NUMBER PERFORMANCE OF METHANOL-GASOLINE BLENDS

The ON enhancement experienced by adding methanol to certain base fuels has been correlated with evaporative cooling effects. Certain assumptions and generalizations had to be incorporated into the analysis, however, and although these do not invalidate the conclusions reached, they are worth discussing briefly here.

Certain assumptions will result in underestimates of the cooling provided (for example the assumption of stoichiometric fuel air ratios, or modelling the eccentric RON test engine manifold as being straight and flat), while others may exaggerate the effect (for example the droplet size range used in the experimental verification of the model is likely to be smaller than the range produced in the real RON test engine).

It is possible, however, that these conflicting influences could be compensatory, and the nett estimate could be reasonably accurate. The results of the analysis, therefore, should be interpreted not as being absolute, but rather as a strong indication that the action of evaporative cooling, in itself, is capable of producing ON enhancement of sufficient magnitude to explain the ON behaviour of methanol-blend fuels.

8.2 THE PHENOMENON OF HIGH-SPEED KNOCK

One of the objectives of this thesis was to investigate the interaction between speed and evaporative cooling in order to evaluate their role in the phenomenon of high-speed knock. It was speculated from the outset, firstly, that the main reason that adding methanol to gasoline caused RON enhancement was due to evaporative cooling effects (and this has been shown to be true in chapter 6), and secondly, that at higher speeds than the relatively slow 600 rpm of the RON test, that most of this evaporative cooling benefit would be lost allowing knocking to occur.

'High-speed Octane Number'

In trying to assess the magnitude of the effect that evaporative cooling exerts, it is useful to examine the fuels' performance in terms of a modified 'Octane Number' for the fuels operating at high speeds; a 'high-speed ON'. Applying the same method of analysis that was used in the previous sections, the benefit accrued by cooling can be evaluated with reference to the temperatures produced using the base gasoline, and Figures 39 and 40 represent the results of this analysis. It is clear by comparing the 'relative RONs' Figure 39 (low speed) and Figure 40 (high speed) that any 'relative RON' boost that was provided with alcohol by cooling for slow speeds is almost completely lost at higher speeds.

The conditions of the actual RON test are low speed (600 rpm) with a manifold length of approximately 0.4m. This means that the 'relative RON' data of Figure 39 applies (low speed), and should be read off the graph at the appropriate length (0.4m) for the RON test, and it has already been shown that the measured RON data corresponds well with this method of analysis. For an engine run at low speeds, with a manifold length of 0.2m (the length of a typical automotive manifold), 'relative RON' data should be read off Figure 39 at 0.2m. For the same engine running at a high speed, Figure 40 should be read at 0.2m.

The crucial difference between the low-speed and the high-speed conditions (Figures 39 and 40 respectively) is that any 'relative RON' enhancement due to evaporative cooling that was prevalent at low speeds is lost at higher speeds. This means that the root cause of the enhanced RON of the alcohol-blend fuels (relatively good evaporative cooling), is lost for

high-speed operation, and alcohol-gasoline blend fuel will behave like lower RON fuels, at high speeds.

The phenomenon of HSK can now be explained in terms of the 'Octane Requirement' (OR) of engines, and is perhaps best explained using an example. If a particular engine, that requires at least 100 RON fuel (for example) to avoid knocking, is run with a lower ON fuel, then knocking will unavoidably occur, and this is exactly what is known to happen with alcohol-blend fuels (for example a 10 percent methanol blend in a 97 RON base fuel). At low speeds, the alcohols manifest their high latent heats of evaporation to allow the blend to perform like a 100 RON fuel, but at higher speeds the alcohols lose this relative evaporative cooling advantage, and the blend will begin to behave increasingly more like a 97 RON fuel. This 'lowering' of ON at high speeds beyond the engine specification, together with the capability of alcohol-blend fuels to auto-ignite extremely rapidly[2], would not only enable knocking, but also facilitate it, and high-speed knock would result.

Spark advance

The HSK phenomenon associated with alcohol-blend fuels can also be explained in terms of the anticipated spark advance (SA) behaviour of these fuels. In general, an engine's performance (power and efficiency) is enhanced by advancing the timing of the spark. The degree of advance is limited, in turn, by the onset of knock, which is a broad function of the grade of fuel used (ON). Optimally, therefore, an engine should closely follow the advance limitations of the particular fuel that it uses, and this is precisely what engines are designed to do.

Figure 50 shows the spark advance curve for a typical engine designed to use 100 RON fuel. If a lower grade fuel were to be used, such as 96 RON (the lowest curve in Figure 45), knocking would certainly occur, because the engines SA curve would exceed the capabilities of that fuel grade.

The predicted behaviour of the alcohol-gasoline blend fuel (see Figure 50) would suggest that this fuel would not knock at low speeds (for the engine in question). However, this would not be the case for higher speeds, since the fuel's SA capabilities are not capable of matching

the engine's SA characteristics. Knocking for high-speed operation is therefore the expected behaviour for the alcohol-blend fuel, as a direct consequence of its evaporative cooling characteristics.

Thus it is possible to explain the phenomenon of high-speed knock in terms of evaporative cooling differences, and it is most probable that these differences are the primary underlying cause of the high-speed knock that is associated with alcohol-blend fuels. Given that these tests are insufficient to describe a fuel's performance across the range of speeds and engine designs that are currently in use, the reasons for the occurrence of HSK have been identified. The question remaining concerns how, if at all, might it be possible to eradicate HSK, and this question is addressed in section 8.3 below.

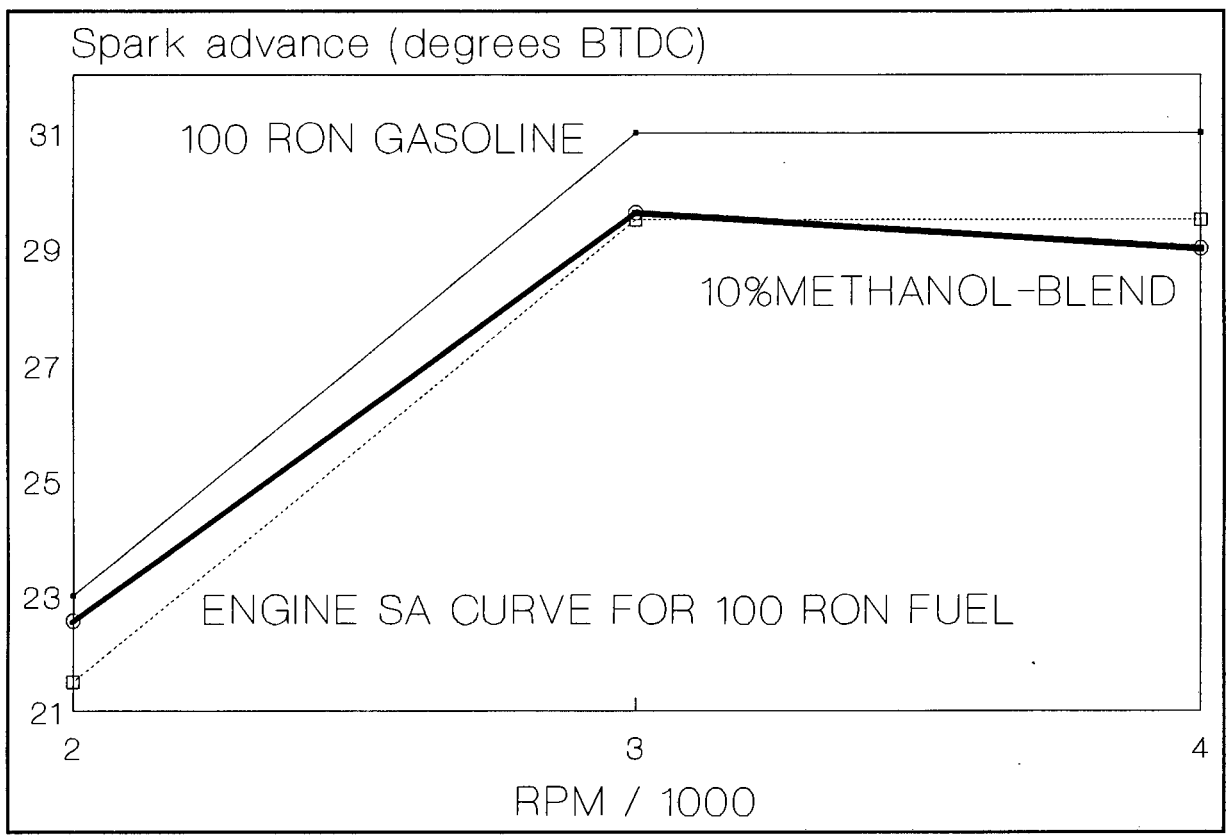

Figure 50 - *Graph comparing the anticipated SA performance of a 10% methanol to 90% gasoline blend (bold), with a typical engine SA curve (dotted)*

8.3 SUGGESTIONS CONCERNING THE ELIMINATION OF HSK

Since 'Octane Number' is meant to provide a basis whereby a fuel's resistance to knock may be estimated, and since it is clear that HSK occurs as a result of the inadequacy of this estimate for higher speed operation, it may be possible to eliminate HSK experienced with alcohol-blend fuels by ensuring that the beneficial conditions prevalent in the 'RON' test are not lost at higher speeds, with conventional inlet manifold designs. Two possibilities exist, namely inlet system design and fuel property modification, and these are both discussed below.

Inlet system designs

It has been established in this study that the cause of HSK is the loss, at high speeds, of evaporative cooling benefit that exists for the alcohol-blend fuels for lower speeds. The best method to combat this phenomenon would be to ensure that better evaporative cooling occurs at the high speed conditions, and one immediately obvious solution would be to design the inlet manifold for this purpose.

The object of an anti-HSK design would be firstly to improve evaporative cooling of all fuels across the speed range (which would benefit the performance of every fuel), and secondly to improve the rates of evaporative cooling at the higher speeds so that the cooling advantages prevalent at lower speeds are not lost at higher speeds.

The suggestion of specific changes to inlet manifold systems would be beyond the ambit of this study, especially since these may be in conflict with other performance requirements, and also since the design of such a system would require an in-depth study. The computer model, however, has highlighted certain trends upon which such a design may be based, and these are mentioned here.

It is important to have as much of the fuel in droplet form as possible, and for these droplets to be as small as possible (see Figure 15). These factors improve both the evaporation rate and the heat transfer rate, which combine to provide distinctly greater cooling.

Another interesting possibility involves the relative speed of the droplets to air-stream. Greater relative speeds, provide dramatically higher heat and mass transfer rates, which facilitate more effective cooling, but the captivating feature of this idea concerns that fact that these cooling rates need not dissipate with higher air-speeds. Examination of the relationship between relative velocities and associated cooling (Figure 13) illustrates the effect that raising the relative velocities might have. This could be achieved by pointing injector nozzles backwards (facing into the air-stream), for example. In theory, this would provide high cooling rates both for the lower speeds, as well as for higher speed operation, due firstly to the increased relative velocities, and secondly due to the improved atomization associated with higher relative velocities. In practice, the principle could result in improved efficiencies (due to the improved cooling across the speed range), and also combat the onset of HSK by providing adequate cooling even at high speeds. Smaller droplets are generally associated with higher relative velocities between the air and the fuel, and this would further encourage evaporation at high speeds.

It must be mentioned as a caveat, that these ideas arise from a theoretical analysis, and are focused purely on thermal considerations, in an attempt to facilitate better cooling conditions (especially at high speeds), and it is acknowledged that these methods may present practical problems associated with other related manifold phenomena (for example the last method may be problematical because of transient lags). For situations where engine response lags are not an important consideration, as in generators, for example, these methods hold promise for performance enhancement by increased compression ratios. A generator being run at a constant speed with an exceptionally long manifold might be an appropriate possibility.

Fuel property modification possibilities

Although this study was not launched with the aim of identifying specific changes to fuel properties that would limit HSK, certain generic suggestions can be made in this regard. The underlying principle would involve encouraging fuel evaporation for the high-speed conditions (and also for low speeds). Some tentative suggestions are put forward below.

Better evaporation rates are facilitated by smaller droplets, and methods to decrease the average droplet size would benefit evaporation across the speed spectrum. Some fuel

8.4 INSIGHTS INTO THE RON AND MON TESTS

As a result of this study, some insights have been gained into the physical processes that prevail in the inlet manifold of the ON test engine. These are likely to influence the test, and the intention of this sub-section is to level a brief criticism at the ON tests without restating well documented reservations[2, 70, 77, 78].

Measurements made in the ON tests

A critique can be levelled at the ON tests as to what is and what is not measured, insofar as certain parameters are not controlled, and others may not be registering the correct quantities.

The MON test stipulates a mixture temperature of 149°C. Bearing in mind it was found in this study that the three streams (gas, droplets and films) usually assume three very different temperatures, together with the fact that regular gasoline, having a final vaporisation temperature of approximately 220°C, will still be present in the liquid form at the 149°C of this test, the question must be raised as to what exactly this 'mixture temperature' is. It was stated in chapter 4, firstly, that it is considered almost impossible to measure the true gas temperature using an intrusive physical probe (if there are droplets present), and secondly that an unshielded probe in the gas-droplet stream will measure almost exclusively the droplet temperature. Therefore, the thermometer setup used in the MON test will, in all likelihood, be measuring the temperature of any fuel droplets present in the stream.

This has profound implications for the interpretation of the MON test. The 'mixture temperature' of a fuel that has completely evaporated at 149°C will be the true gas temperature, whereas if there is still liquid fuel present at this temperature, the 'mixture temperature' will be closer to that of the droplets, with the gas temperature likely to be very much higher. It is possible that the results of MON tests with high final boiling temperature fuels could be significantly distorted in this manner, by yielding a lower MON value than if the gas temperature were 149°C.

Evaporative cooling: insights into the RON test

In chapter 3, factors which affect the thermal behaviour of the mixture (such as fuel/air mass ratio, fuel inlet temperature, inlet manifold temperature etc.) have been identified as being important moderators of the overall gas and liquid stream temperatures. Since the above analysis has shown these temperatures to be able to affect RON significantly, the fact that these parameters are not specified would seem to be an inadequacy of the RON test.

A significant proportion of the evaporative cooling offered by methanol (as discussed in chapter 6) is due to the increased fuel/air ratio of the stoichiometric mixture (0.15 kg methanol required per kg of air compared with 0.07 kg of gasoline required per kg air), which causes improved cooling in itself. The combinatorial effect of the increasingly higher fuel/air mass ratios of methanol-gasoline blends, attendant with higher latent heats of vaporization act to provide the dramatically improved cooling associated with these blends. This contributes to the enhancement in RON associated with adding methanol to gasoline.

As a conclusion to this section, it must be reiterated that because thermal factors affect the RON test these ought to be considered, and standardization of other parameters such as the fuel inlet temperature would help stabilize the test conditions. Apart from well documented criticisms of the ON tests which concern the inapplicability of the test conditions to a real engine's running conditions[2, 70, 77, 78], from an evaporative cooling point of view, the test engine's unusually long manifold together with the low speeds used, both facilitate greater evaporative cooling than perhaps would occur in typical automotive engines in working conditions, even at low engine speeds (around 1000 rpm).

Since there has been much previous criticism of the ON tests[2, 70, 77, 78], which has now been extended to include thermal effects, it is apparent that a more complete characterisation of a fuel's behaviour is necessary to describe its performance. It is suggested, as a consequence of this study, that the ON tests should be extended to include tests at higher speeds, and that the relationship between manifold geometry (length, shape etc.) and fuel performance be investigated in depth. It has also been suggested[1-2] that fuels should be characterised in terms of more general combustion qualities (ignition delay and pressures), which would provide a less tenuous basis upon which the relative merits of fuels may be judged.

9. CONCLUSIONS AND RECOMMENDATIONS

Conclusions

This project was initiated to investigate the evaporation processes existing in spark-ignition engine intake manifolds, as part of a greater research effort into the phenomenon of high-speed knock. Specific conclusions relating to the projects objectives are drawn below.

The computer model that was developed for this purpose, was found to compare well with similar models reported in the literature[10, 11]. None of these previous investigations, however, was involved with predicting the engine performance of fuels (as was the case in this study), focusing rather on fuel distribution problems in intake manifolds. This project, therefore, concerned a novel application of the established analysis.

The experimental investigation was aimed at corroborating the model predictions for a wide range of conditions and fuels, and also at providing practical insights into the inlet process. This investigation provided vital insights into some of the assumptions that had to be made for the model, enabling a clearer definition of certain parameters that had been identified as being most important.

Statistical analysis showed that the model corresponded well with the experimental data over the wide range of conditions tested. The experimental investigation undertaken in this study was more extensive than any of those previously described in the literature, and, in addition, the correlation between the model and the practical tests was significantly better than any that are known to have been reported to date.

With the robustness of the model considered to have been proven for a wide range of conditions, predictions within this range could be made using the model. These predictions formed the basis for the ensuing analysis, which yielded several findings, each of which would seem to represent a significant advance:

1. The enhancement of RON experienced for various methanol-gasoline blends, is explained quantitatively and conclusively in terms of evaporative cooling. This

relationship has been suggested in the literature[2, 5, 78], but has not been followed up before.

2. The phenomenon of HSK associated with alcohol-gasoline blends was attributed to the less efficient evaporative cooling conditions prevalent at higher speeds not allowing the alcohols to manifest their higher latent heats of evaporation as effectively as they would for lower speeds.

3. In order to quantify the predicted HSK trends as caused by evaporative cooling, the analysis was extended to anticipate the spark-advance curves exhibited by certain fuels, and these were found to agree with the observed behaviour. This connection between evaporative cooling and fuel behaviour is an important understanding, and serves to focus the previously diversified HSK research efforts away from a chemical-property emphasis, and firmly into the realm of physical properties of fuels.

4. An underlying feature separating the RON and MON test conditions concerns thermal factors, and it has been shown in this study that the action of evaporative cooling is, in itself, sufficient to explain many of the disparities between the numbers yielded using the two tests. This was attributed to the widely disparate evaporative cooling environments of the two testing methods. This conclusion raises important questions as to how the results of these tests translate to the performance of fuels in the vast array of engines currently in use, which all will induce thermal conditions peculiar to their design.

In summary, it can be stated that the project objectives have been fulfilled, and that the fundamental hypothesis that motivated this work has proved to be correct.

Recommendations for follow-up research

Several interesting possibilities were raised as a result of the findings and conclusions of this study, some of which are recommended for follow-up research:

1. There is a need for a device to provide an accurate measure of the gas temperature in a multi-phase stream. This device would be of considerable use to engine research in general, and would have to be non-intrusive in order to achieve a true gas temperature measurement.

2. It is anticipated that evaporative cooling could be the key to understanding many of the disparities in the performance of fuels on the Octane Number tests. This study concentrated on the behaviour of methanol-gasoline blends, and touched on other fuels, and it is recommended that further research be performed to investigate the relationship between evaporative cooling effects and RON test performance of many fuel types. This research should involve engine tests.

3. Several avenues for future research have been identified in this study that could lead to improved engine performance across the speed range (particularly for alcohol-gasoline blend fuels). The most promising of these include changes to inlet manifold design to encourage evaporation and droplet atomization, as well as changes to the fuel itself, and it is recommended that these are investigated fully.

4. The applicability to road engine conditions of the traditional fuel rating methods (RON and MON tests) have long been criticized. In the light of this study, that has shown that the results of these test are not sufficient to describe a fuel's performance at high engine speeds, it is clear that there is an urgent need for a more descriptive rating system. The improved system should incorporate data covering a range of engine speeds, and, in addition, should involve the use of a more typical automotive inlet manifold than is currently in use on the test engine.

REFERENCES AND BIBLIOGRAPHY

INTRODUCTION

1. Yates, A.D.B., and Bennett, K.F., "An introductory investigation into the phenomenon of high speed knock", Report No. CON 033, ERI, University of Cape Town, October 1987.

2. Yates, A.D.B., "Abnormal combustion - methanol versus gasoline", Ph.D. Thesis Dissertation, University of Cape Town, April, 1988.

3. Yates, A.D.B., and Bennett, K.F., "High speed knock research", Department of Mechanical Engineering, University of Cape Town, December 1988.

4. Stuck, D., "The development of a technique to measure the gas temperature in a spark-ignition engine", Undergraduate thesis, Mechanical Engineering Department, University of Cape Town, 1989.

5. van Binsbergen, P.J., "Knock-limited performance - liquid versus evaporated methanol", Undergraduate thesis, Mechanical Engineering Department, University of Cape Town, 1989.

6. Johnson, R.T., and Riley, R.K., "Single cylinder spark ignition engine study of the Octane, emissions, and fuel economy characteristics of methanol-gasoline blends", SAE Paper 760377, 1976.

THE COMPUTER MODEL

7. Yun, H.J., Lo, R.S. and Na, T.Y., "Theoretical Studies of Fuel Evaporation and Transportation in a Carburettor Venturi" SAE Paper 760289, 1976.

8. Lo, R.S. and Lalas, D.P., "Parametric study of fuel-droplet flow in an idealized automotive system", SAE Paper 770645, 1977.

9. Finlay, I.C., Boam, D.J., and Bannel, J.L.K., "Computer model of fuel evaporation in air valve carburettors", Automotive Eng., pp.51-56, Dec. 1979.

10. Boam, D.J., and Finlay, I.C., "A Computer Model of Fuel Evaporation in the Intake System of a Carburetted Petrol Engines", Conference on FUEL ECONOMY AND EMISSIONS OF LEAN BURN ENGINES, London, June 12-14, 1979, paper C89/79, Institution of Mechanical Engineers, 1979.

11. Milton, B.E., and Behnia, M.A., "A Numerical Study of the Interchanging Vapor, Droplet and Film Flows in a Gasoline Engine Manifold", in HEAT AND MASS TRANSFER IN GASOLINE AND DIESEL ENGINES (Eds. D.B. Spalding and N.H. Afgan), 1989 (Hemisphere, New York).

12. Bland, R.J., Saunders, R.J. and Ma, T.H., "Modelling of Two Phase Mixture Flow and Vaporization in Spark Ignition Engine Intake Systems", CONFERENCE PAPER C433/005, Institution of Mechanical Engineers, London, 12-14 January 1991.

13. Servati, H.B., and Yuen, W.W., "Deposition of Fuel Droplets in Horizontal Intake Manifolds and the Behaviour of Fuel Film Flows on its Walls", SAE Paper 840239.

14. Brown, C.N., and Ladommatos, N., "A numerical study of fuel evaporation and transport in the intake manifold of a port-injected spark-ignition engine", Proc. Instn Mech. Engrs, 1991, 205(D), 161-175.

15. Low, S.C., Baruah, P.C., and Winterbone, D.E., "Transportation of Liquid Fuel Droplets in the Pulsative air flow within the S.I. Engine Intake Manifold", SAE Paper 810497.

16. Munenebo Tanaka, Tadanori Sato, and Kenzo Watanabe, "Pulsation Effects on the Air Fuel Ratio of Carburettor Engines", SAE Paper 861241, 1986.

FUEL FILMS

17. Friedlander, S.K., and Johnstone, H.F., "Deposition of Suspended Particles from a Turbulent Gas Stream", Ind. Eng. Chem, Vol. 45, no. 7, pp. 1151-1156, 1957.

18. Hasson, D.A., and Flint, W.L., "An investigation of liquid petrol wall film in the manifold of a carburetted spark-ignition engine: effect of carburettor and manifold geometry on wall quantities, engine performance and emissions", Proc. Instn Mech. Engrs, 1989, 203(D), 77-89.

19. Gardiner, D.P., and Bardon, M.F., "Mixture Maldistribution Due to Manifold Films in a Methanol Fuelled S.I. Engine", SAE Paper 860234, 1986.

20. Nagaishi, H. et al., "An Analysis of Wall Flow and Behaviour of Fuel in Induction Systems of Gasoline Engines", SAE Paper 890837, 1989.

21. Yan, W.M., Lin, T.F., and Tsay, Y.L., "Evaporative cooling of liquid film through interfacial heat and mass transfer in a vertical channel - I. Experimental study", Int. J. Heat Mass Transfer. Vol.34, No.4, pp.1105-1111, 1991.

22. Hayashi, S., and Sawa, N., "Measurement of fuel liquid-film flow in intake pipe of two-stroke motorcycle engine using conductive probe", SAE Paper 840554, 1984.

23. Parken, W.H., et al., "Heat transfer through falling film evaporation and boiling on horizontal tubes", ASME Transactions Vol.112, pp.744-751, Aug. 1990.

24. Shmerler, J.A., and Mudawwar, I., "Local evaporative heat transfer coefficient in turbulent free-falling liquid films", Int. J. Heat Mass Transfer. Vol.31, No.4, pp.731-742, 1988.

25. Iwano, H., et al., "An analysis of induction port fuel behaviour", SAE Paper 912348, 1991.

26. Bardon, M.F., Rao, V.K., and Gardiner, D.P., "Intake manifold fuel film transient dynamics", SAE Paper 870569.

27. Yan, W.M., and Lin, T.F., "Combined heat and mass transfer in natural convection between vertical plates with film evaporation", Int. J. Heat Mass Transfer. Vol.33, No.3, pp.529-541, 1990.

28. Bannwart, A.C., and Bontemps, A., "Condensation of a vapour with incondensibles: an improved gas phase film model accounting for the effect of mass transfer on film thickness", Int. J. Heat Mass Transfer. Vol.33, No.7, pp.1465-1473, July 1990.

29. Baumann, W.W., and Thiele, F., "Heat and mass transfer in evaporating two-component film flow", Int. J. Heat Mass Transfer. Vol.33, No.2, pp.267-273, 1990.

30. Nguyen, T.K., and Avedisian, C.T., "Numerical solution for film evaporation of a spherical liquid droplet on an isothermal and adiabatic surface", Int. J. Heat Mass Transfer. Vol.30, No.7, pp.1497-1509, 1987.

31. Brouwers, H.J.H., and Chesters, A.K., "Film models for transport phenomena with fog formation : the classical film model", Int. J. Heat Mass Transfer. Vol.35, No.1, pp.1-11, 1992.

32. Brouwers, H.J.H., "Film models for transport phenomena with fog formation : the fog film model", Int. J. Heat Mass Transfer. Vol.35, No.1, pp.13-28, 1992.

FUEL DROPLETS AND DROPLET VAPORIZATION THEORY

33. Tong, Albert Y., and Sirignano, William A., "Multicomponent transient droplet vaporization with internal circulation: integral equation formulation and approximate solution", Numer. Heat Transfer, Vol.10, pp.253-278, 1986.

34. Law, C.K., Xiong, T.Y., and Wang, C.H., "Alcohol droplet vaporization in humid air", Intl Jnl Heat Mass Transfer, v 30, n 7, July 1987, pp 1435-1443.

35. Tong, A.Y., and Sirignano, W.A., "Multicomponent droplet gasification in a high temperature gas", Combust Flame Vol.66, pp.221-235, 1986.

36. Aggarwal, S.K., Chen, G., Jackson, T.A., and Switzer, G.L., "Vaporization behaviour of fuel droplets in a hot air stream", Int. J. Heat Mass Transfer. Vol.34, No.10, pp.2669-2673, 1991.

37. Gakkhar, R.P., and Prakash, S., "Unsteady vaporization of fuel droplets in a convective environment with varying ambient conditions", Int. J. Heat Mass Transfer. Vol.33, No.5, pp.1003-1012, 1990.

38. Shaw, B.D., and Williams, F.A., "Theory of a low volatility, soluble impurity on spherically-symmetric fuel droplets", Int. J. Heat Mass Transfer. Vol.33, No.2, pp.301-317, 1990.

39. Xiong, T.Y., and Yuen, M.C., "Evaporation of a liquid droplet on a hot plate", Int. J. Heat Mass Transfer. Vol.34, No.7, pp.1881-1894, 1991.

40. Makino, A., and Law, C.K., "On the controlling parameter in the gasification behaviour of multicomponent droplets", Combust Flame Vol.73, pp.331-336, 1988.

41. Rangel, R.H., and Sirignano, W.A., "Combustion of parallel fuel droplet streams", Combust Flame Vol.81, pp.325-340, 1990.

42. Megahed, M.M., Saeed, M.N., Sorour, M.M., and Madi, M.B., "Unsteady vaporization of stationary dodecane and alcohol droplets suspended in a hot non-reactive environment", Int. J. Heat Mass Transfer. Vol.32, No.7, pp.1299-1308, 1989.

43. Tadrist, L., Shehu Diso, I., Santini, R., and Pantaloni, J., "Vaporization of a liquid by direct contact in another immiscible liquid; Part I: vaporization of a single droplet; Part II: vaporization of rising multidroplets", Int. J. Heat Mass Transfer. Vol.30, No.9, pp.1773-1785, 1987.

44. Chen, Steven J., and Tong, Albert Y., "Application of elliptic grid generation technique to the solution of hydrodynamics and heat transfer of droplet arrays at intermediate Reynolds numbers", Int. J. Heat Mass Transfer. Vol.31, No.5, pp.1063-1072, 1988.

FUEL DROPLETS AND SPRAY VAPORIZATION THEORY

45. Sirignano, W.A., "Fuel Droplet Vaporization and Spray Combustion Theory", PROGRESS IN ENERGY AND COMBUSTION SCIENCE, vol 9, pp 291-322, 1983.

46. Tsue, M., et al., "Numerical analysis of fuel vapour concentration fields in a spark ignition engine", SAE Paper 912347, 1991.

47. Abramzon, B., and Sirignano, W.A., "Droplet vaporization model for spray combustion calculations" Intl Jnl Heat Mass Transfer, v 32, n 9, Sept 1989, pp 1605-1608.

48. Mawid, M., and Aggarwal, S.K., "Analysis of dropwise ignition for dilute multicomponent sprays", Combust Flame Vol.81, pp.59-72, 1990.

SPRAY VAPORIZATION

49. Aggarwal, S.K, Tong, A.Y., and Sirignano, W.A., "A comparison of vaporization models in spray calculations", AIAA J. Vol.22, No.10, pp.1448-1457, 1984.

50. Bracco, F.V., "Modeling of Engine Sprays", SAE Paper 850394, 1985.

51. Lin, T.H., Law, C.K. and Chun, S.H., "Theory of laminar flame propagation in off-stoichiometric dilute sprays", Intl Jnl Heat Mass Transfer, v 31, n 5, May 1988, pp 1023-1034.

52. Continillo, G., and Sirignano, W.A., "Counterflow spray combustion modeling", Combust Flame Vol.81, pp.325-340, 1990.

53. Aggarwal, Suresh K., "Modeling of a dilute vaporizing multicomponent fuel spray", Int. J. Heat Mass Transfer. Vol.30, No.9, pp.1949-1961, 1987.

54. Rangel, R.H., and Sirignano, W.A., "An evaluation of the point-source approximation in spray calculations", Numer. Heat Transfer, Vol.16, pp.37-57, 1989.

EXPERIMENTAL ANALYSES AND FLOW PROCESS STUDIES

55. Wells, M.R., and Melton, L.A., "Temperature measurements of falling droplets", ASME Transactions Vol.112, pp.1008-1013, Nov. 1990.

56. Ekchian, A., and Hoult, D.P., "Flow Visualization Study of the Intake Process of an Internal Combustion Engine", SAE Paper 790095, 1979.

57. Ghodbane, M., and Holman, J.P., "Experimental study of spray cooling with Freon-113", Int. J. Heat Mass Transfer. Vol.34, No.4&5, pp.1163-1174, 1990.

58. Lo, R.S. and Lalas, D.P., "Parametric study of fuel-droplet flow in an idealized automotive system", SAE Paper 770645, 1977.

59. Ingebo, R.D., "Vaporization Rates and Drag Coefficients for Iso-octane Sprays in Turbulent Air Streams", National Advisory Committee for Aeronautics, 1954, TN3265.

DROPLET SIZE STUDIES

60. Coy, E.B., and Santavicca, D.A., "Simultaneous droplet velocity and size measurements in fuel sprays", SAE Paper 912399, 1991.

61. Mao, C-P., Oechsle, V., and Chigier, N., "Drop size distribution and air velocity measurements in air assist swirl atomizer sprays", ASME Transactions Vol.109, pp.64-69, March 1987.

62. Kadota T., et al., "Fuel droplet size measurements in the combustion chamber of a motored SI engine via laser Mie scattering", SAE Paper 900477, 1990.

63. Gelman, M.E., "A photographic investigation into fuel droplet formation in an automotive carburettor", Undergraduate thesis, Mechanical Engineering Department, University of Cape Town, 1992.

64. Rizkalla, A., and Lefebvre, A.H., "The influence of air and liquid properties on airblast atomization", Journal of Fluids Engineering, 1975, Vol 97, 316-320.

65. Lefebvre, A.H., "Atomization and combustion of alternative fuels", The South African Mechanical Engineer, 1988, Vol 38, 131-137.

66. Bhatia, J.C., and Durst, F., "Description of sprays using joint hyperbolic distribution in particle size and velocity", Combust Flame Vol.81, pp.203-218, 1990.

67. Richards, G., Sojka, P.E., and Lefebvre, A.H., "Drop-size studies in a radially-uniform fuel spray", SAE Paper 852083, 1985.

68. Kashiwaya, M., Kosuge, T., Nakagawa, K., and Okamoto, Y., "The effect of atomization of fuel injectors on engine performance", SAE Paper 900261, 1990.

OCTANE NUMBER AND COMPRESSION RATIO

69. Overington, M.T., and Thring, R.H., "Gasoline engine combustion - compression ratio and knock", Int Symp Knocking of Combustion Engines, Wolfsburg, West Germany, Nov 1981.

70. Douaud, A., "Modeling the knocking phenomenon in engines", Int Symp Knocking of Combustion Engines, Wolfsburg, West Germany, Nov 1981.

71. van Gulick, H., "Refineries and engines as a single technical system", Imeche 1975, The Journal of Automotive Engineering, 11-16.

72. Eatwell, H.J., and Withers, J.G., "The significance of Octane Numbers in relation to road performance", Proc. Instn Mech. Engrs, Paper presented 22nd February 1952.

OCTANE NUMBER AND SPARK ADVANCE

73. Williams, C.G., "Fuel anti-knock requirements of automobile engines", Proc. Instn Mech. Engrs, 1948-49, Part III, 111-127.

74. Caris, D.F., Mitchell, B.J., McDuffie, A.D., and Wyczalec, F.A., "Mechanical Octanes for higher efficiency", Trans SAE, Vol 64, 1956.

75. Leng, I.J., "Petrol engined cars: influence of spark timing on Octane requirement and vehicle performance", Energy Research Institute Report 97, Jan 1986.

OCTANE NUMBER MEASUREMENTS WITH VARIOUS FUEL TYPES

76. 1988 ANNUAL BOOK OF ASTM STANDARDS, Section 5, Volume 05.04, "Test methods for rating motor, diesel and aviation fuels", American Society for Testing and Materials, 1988.

77. Rifkin, E.B., and Walcutt, C., "A basis for understanding antiknock action", Trans SAE, Vol 65, 1957.

78. Nicholls, R.J., "Investigation of the Octane rating and autoignition temperature of methanol-gasoline blends", SAE Paper 800258, 1980.

BIBLIOGRAPHY

79. Botha, J., "A comparative study for 97 octane fuel and a 12% methanol blend to establish the effect of bends in an intake manifold on evaporative cooling", Undergraduate thesis, Mechanical Engineering Department, University of Cape Town, 1991.

80. Raznjevic, K., HANDBOOK OF THERMODYNAMIC TABLES, Washington, Hemisphere, 1976.

81. Heywood, J.B., INTERNAL COMBUSTION ENGINE FUNDAMENTALS, McGraw-Hill, 1988.

82. Taylor, C.F., THE INTERNAL COMBUSTION ENGINE IN THEORY AND PRACTICE, MIT Press, 3rd printing, 1979.

83. Fischer, C.H., CARBURETION AND CARBURETTORS, Chapman and Hill Ltd., London, 1939.

84. Judge, A.W., CARBURETTORS AND FUEL SYSTEMS, Chapman and Hill Ltd., London, 1943.

85. Goodger, E.M., PETROLEUM AND PERFORMANCE IN INTERNAL COMBUSTION ENGINES, Butterworth Scientific Publishers, London, 1953.

86. Bleimschein, G.E., "The octane requirements of spark ignition engines", M.Sc. Thesis Dissertation, University of Cape Town, April 1991.

87. Rose, J.W., and Cooper, J.R., TECHNICAL DATA ON FUEL, Seventh Ed., Scottish Academic Press, Edinburgh, 1977.

88. Holman, J.P., HEAT TRANSFER, McGraw-Hill, 1989.

89. Reid, R.C., Prausnitz, J.M., and Poling, B.E., THE PROPERTIES OF GASES AND LIQUIDS, McGraw-Hill, Fourth Ed., 1986.

90. British Standard 1042, MEASUREMENT OF FLUID FLOW IN CLOSED CONDUITS, Part 1, "Pressure differential devices", Sections 1.1-4, British Standards Institution, 1981.

91. Massey, B.S., MECHANICS OF FLUIDS, London, Van Nostrand, 1968.

92. Shapiro, A.H., THE DYNAMICS AND THERMODYNAMICS OF COMPRESSIBLE FLUID FLOW, New York, N.Y.: The Ronald Press, 1953.

93. Douglas, J.F., Gasiorek, J.M., and Swaffield, J.A., FLUID MECHANICS-2nd ed., Longman Scientific & Technical, 1986.

Text and Figures produced on Word Perfect 5.1, Harvard Graphics 2.3 (with Draw Partner) and Quattro Pro3, by D P Moran.

APPENDIX A. DERIVATION OF MODEL EQUATIONS

NOTATION

A_c	Cross-sectional area
A_s	Surface area
C_D	Drag coefficient
c	Specific heat capacity
D	Diffusion coefficient
d	Diameter
f	Friction factor
H	Manifold wall heat flux
h	Specific enthalpy
h_{fg}	Latent heat of vaporization
k	Thermal conductivity
M	Mass flow-rate
m	Number of components in the liquid fuel
MW	Molecular weight
n	Number of droplets passing any section per second
Pr	Prandtl number $\{= c_g\mu_g/k_g\}$
P	Pressure
PV	Effective vapour pressure of a component in a mixture
Q	Droplet flux
R	Specific gas constant
Re_d	Droplet Reynolds number $\{= \rho_g(V_g-V_d)d_d/\mu_g\}$
Re_M	Duct Reynolds number $\{= \rho_g V_g d_M/\mu_g\}$
r_h	Hydraulic radius
Sc	Schmidt number $\{= \mu_g/(\rho_g D)\}$
t	Temperature
t^*	Absolute temperature
V	Velocity
x	Distance measured in the direction of flow (x = 0 at the fuel inlet)
α	Heat-transfer coefficient
β	Mass-transfer coefficient
μ	Absolute viscosity
ρ	Density

Subscripts

a	Of air
aw	Adiabatic surface condition
D	By deposition
d	Of droplet
E	By entrainment
e	By evaporation
f	Of film
g	Of gas
i	Of i-th component

L	Of liquid
M	Of manifold
m	Of mixture
S	Saturated vapour
T	Total
t	At temperature t
v	Of vapour

EQUATIONS

Conservation of energy applied to the gas stream (air and fuel vapour):

$$[M_a c_a + \sum_{i=1}^{m} M_{v,i} c_{v,i}] \frac{dt_a}{dx} = \frac{\alpha_d n \pi d_d^2}{V_d}(t_d - t_{aw,d})$$

$$+ \pi d_M \alpha_f (t_f - t_{aw,f}) - \sum_{i=1}^{m} c_{v,i} [\frac{dM_{de,i}}{dx}(t_d - t_a)$$

$$+ \frac{dM_{fe,i}}{dx}(t_f - t_a)] + \frac{1}{2} \sum_{i=1}^{m} [\frac{dM_{de,i}}{dx}(V_a^2 - V_d^2)$$

$$+ \frac{dM_{fe,i}}{dx} V_a^2] - V_a \frac{dV_a}{dx}[M_a + \sum_{i=1}^{m} M_{v,i}]$$

$$- V_d \frac{dV_d}{dx} \sum_{i=1}^{m} M_{d,i}$$

where the **heat transfer coefficients** are

$$\alpha_d = \frac{k_a}{d_d}(2 + 0.6 Re_d^{0.5} Pr_a^{0.33})$$

$$\alpha_f = \frac{k_a}{d_M} \times 0.023 Re_M^{0.8} Pr_a^{0.4}$$

Conservation of energy applied to the liquid wall film:

$$[\sum_{i=1}^{m} M_{f,i}c_{L,i}]\frac{dt_f}{dx} = \pi d_M[H - \alpha_f(t_f - t_{aw,f})$$

$$+ (t_d - t_f)\times\sum_{i=1}^{m}(Q_D c_L)] + \sum_{i=1}^{m} h_{fg,i}\frac{dM_{fe,i}}{dx}$$

where

$$Q_D = \frac{Nmk_c}{AV_d}$$

and

$$\frac{k_c}{V_g} = Function(f,Sc)$$

the correlations of which can be found in Friedlander and Johnstone (17).

Conservation of energy applied to the liquid fuel droplets:

$$[\sum_{i=1}^{m} M_{d,i}c_{L,i}]\frac{dt_d}{dx} = -\frac{\alpha_d \pi n d_d^2}{V_d}(t_d - t_{aw,d})$$

$$+ \sum_{i=1}^{m} h_{fg,i}\frac{dM_{de,i}}{dx} + Q_E \pi d_M c_L(t_f - t_{aw,d})$$

Conservation of mass applied to the gas stream (air and fuel vapour):

$$A_c V_a \rho_a + \sum_{i=1}^{m} A_c V_g \rho_{v,i} = M_a + \sum_{i=1}^{m} M_{v,i}$$

from which, if Va = Vg

$$\frac{1}{V_g}\frac{dV_g}{dx} + \frac{1}{A_c}\frac{dA_c}{dx} + \frac{\frac{d\rho_a}{dx} + \sum_{i=1}^{m}\frac{d\rho_{v,i}}{dx}}{\rho_a + \sum_{i=1}^{m}\rho_{v,i}} = \frac{\sum_{i=1}^{m}\frac{dM_{v,i}}{dx}}{A_c V_g[\rho_a + \sum_{i=1}^{m}\rho_{v,i}]}$$

Conservation of mass applied to the liquid fuel droplets:

$$\frac{d(d_d)}{dx} = \frac{2}{\pi d_d^2 \rho_L n} \times \sum_{i=1}^{m}\frac{dM_{de,i}}{dx}$$

Conservation of momentum applied to the liquid fuel droplets: Equating the rate of change of momentum to the drag force on the droplets gives

$$\frac{dV_d}{dx} = \frac{2}{n\pi d_d^2 \rho_L} \times \sum_{i=1}^{m}\frac{dM_{de,i}}{dx}$$

where, from Ingebo (59)

$$C_D = 27Re_d^{-0.84}$$

Conservation of momentum applied to the system:

$$A_c\frac{dP_T}{dx} - \pi r_H f \rho_m V_a^2 + [M_a + \sum_{i=1}^{m}\rho_{v,i}]\frac{dV_g}{dx}$$

$$+ (V_g - V_d)\sum_{i=1}^{m}\frac{dM_{de,i}}{dx} - \frac{dV_d}{dx}\times\sum_{i=1}^{m}M_{d,i}$$

$$- V_g\times\sum_{i=1}^{m}\frac{dM_{fe,i}}{dx} + Q_D\pi d_M V_d - Q_E\pi d_M V_d = 0$$

where from the laws of partial pressures

$$\frac{dP_T}{dx} = \frac{dP_a}{dx} + \sum_{i=1}^{m} \frac{dP_{v,i}}{dx}$$

and from the gas laws

$$\frac{1}{P_a}\frac{dP_a}{dx} - \frac{1}{\rho_a}\frac{d\rho_a}{dx} - \frac{1}{t_a^*}\frac{dt_a^*}{dx} = 0$$

also from the gas laws

$$\frac{dP_{v,i}}{dx} = \frac{R_{v,i}}{M_a R_a} \times \frac{\left[\frac{dM_{de,i}}{dx} + \frac{dM_{fe,i}}{dx}\right]\left[P_T - \sum_{i=1}^{m} P_{v,i}\right]^2}{\left[P_t + P_{v,i} - \sum_{i=1}^{m} P_{v,i}\right]}$$

where mass transfer equations yield

$$\frac{dM_{de,i}}{dx} = \frac{n\pi d_d^2}{V_d}\beta_{d,i}(PV_{Std,i} - P_{v,i})$$

$$\frac{dM_{fe,i}}{dx} = \pi d_M \beta_{f,i}(PV_{Stf,i} - P_{v,i})$$

with **mass transfer coefficients**

$$\beta_{d,i} = \frac{D_i}{d_d R_{v,i} t_L}(2 + 0.6Re_d^{0.5} Sc_i^{0.33})$$

$$\beta_{f,i} = \frac{D_i}{d_M R_{v,i} t_L} 0.023 Re_M^{0.8} Sc_i^{0.4}$$

Vapour pressure:

In a multicomponent liquid, the saturation vapour pressure of each component is affected by the presence of the other components in proportion to its mole concentration.

$$Mole\ concentration = \frac{\frac{MW_{L,i}}{MW_i}}{\sum_{i=1}^{m} \frac{MW_{L,i}}{MW_i}}$$

thus

$$PV_{St,i} = P_{St,i} \frac{\frac{MW_{L,i}}{MW_i}}{\sum_{i=1}^{m} \frac{MW_{L,i}}{MW_i}}$$

APPENDIX B. PROGRAM DOCUMENTATION

The mathematical model involves differential equations which can be solved only numerically, by methods such as a Runge-Kutta technique. The model inherently requires enormous amounts of computation to be performed, and this necessitated the use of a computer program. It was decided to write the program using the 'Borland C' environment, since this package offers advanced features such as 'object orientated programming' while being supported on the available range of personal computers.

The program comprises approximately 6000 lines of 'object orientated' '**C++**' code, and hence it would be impractical to include a listing in this document. The purpose of Appendix B, therefore is simply to outline the rudiments of the program. The main workings of the program are depicted in the flow-chart below.

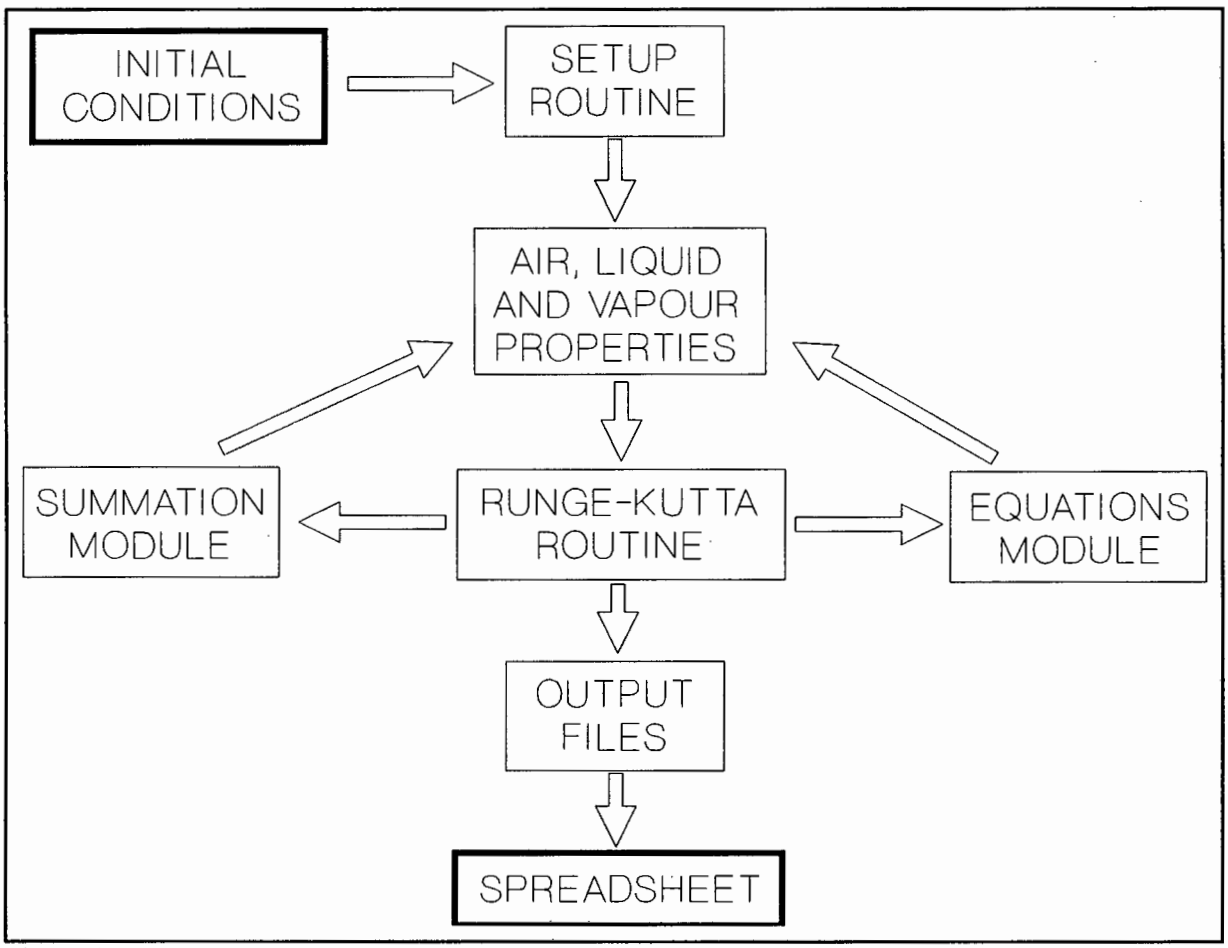

Figure 1 - Flow-chart of the computer program. (Bold boxes depict the user domain)

The program is not user-friendly, insofar as all run-to-run setup changes must be performed from within the program body itself. The program output consists of data files, which are of a suitable format to be imported to a spreadsheet package, where the data may be analyzed and graphics produced using the functions offered by the spreadsheet environment.

The complete program is a synthesis of modules, each of which performs a specific function, whilst simultaneously being dependent on the other modules. The functions performed by some of the modules are discussed briefly here.

Thermal properties

Each component of the fuel is completely described by cubic equations of relevant properties.

Fuel project initializer module

All initial conditions such as the names of the output files are specified here, together with initial temperatures, velocities, fuel composition, droplet sizes etc. These parameters are then passed to the 'setup' module.

Setup module

The data structures required for the program are generated here, and are initialized with the relevant values. Control is then passed to the Runge-Kutta control module which instigates the numerical solving technique for the set of conditions selected by the initializer module.

Runge-Kutta control module

This module contains the primary routines which perform the numerical solving on the set of differential equations discussed in Appendix A. The module calls up many external routines which determine the net effect of the interaction of the various fluid properties.

Fuel equations module

The main system differential equations (see Appendix A) are housed here. These include heat and mass transfer coefficients and various dimensionless groups, as well as the manifold geometry considerations.

Summation module

Some quantities are used frequently by the various equations which involve summing the contributions of the various chemicals (for example total evaporative cooling enthalpy is the sum of the cooling for each substance), and these are defined in this module.

Fuel properties module

The nett effect of having a multi-component mixture on certain values (such as fuel viscosity, vapour pressures, evaporation rates etc.) are calculated in this module in order that the lumped values can be used in the main equations. Each property has to be recalculated as surrounding conditions (such as temperature) are altered by the functioning and nature of the Runge-Kutta procedure.

'Gasoline' constituents

The constituents of the 'gasoline' approximation in the model are listed below, with their mass proportions:

Toluene = 20.63%, m_Xylene = 28.04%, Heptane = 7.652%, Hexane = 13.18%, Pentane = 16.41%, Propane = 0.092%, Isopentane = 14.03%.

The model is capable, in theory, of modelling as many components as required (provided their properties are defined). Other chemicals that were completely described in the model included Methanol, Octane, Ethanol, Heptene, Hexene, and Pentene. These were useful for certain analyses that were undertaken in this investigation.

Default 'run' setup

The standard initial conditions assumed for most of the analyses presented in the main body of this document were:

Initial droplet size = 50 μm,
Proportion of fuel initially in droplet phase = 60%,
Initial droplet velocity = 5 m/s.

APPENDICES

Bigger droplets to wall

Due to the geometry of the injector nozzle setup, the bigger droplets were the most likely to join the wall film initially. The smaller droplets, due to their lower inertia, will be most readily carried off by the air-stream, and thus the mean droplet size in the 'manifold' will be somewhat smaller than the average size produced by the nozzles (60-70μm see Appendix D). The mean droplet size in the manifold was thus assumed to be approximately 50μm. The bigger droplets are shot onto the wall very soon after leaving the nozzle, and in order to simplify the model, this liquid body is assumed to be part of the wall film from the start. This simplification is not expected to cause significant inaccuracies, because the bigger droplets are more thermally inert than the smaller droplets.

Film shape approximator

One of the most interesting facets of the model which was dictated by empirical observations concerns the shape of the wall film. At first (when the computer program was being written) it was assumed that the film was evenly distributed around the manifold, as in the Boam and Finlay model[10]. After the experimental effort was completed, and the model predictions were compared with the empirical data, it was found that the film reheat rate, as predicted by the model, was too great. The model predictions were correct close to the nozzles ($x <= 0.3$m) but overshot the experimental temperatures by up to 15°C at 1m down the 'manifold'. Several factors were investigated to explain this behaviour, but all were capable of only shifting the film temperature curve vertically, without moderating the slope of the curve.

It had been observed in the experimental rig that the film was indeed evenly distributed around the manifold up to 0.2m down the 'manifold'. Beyond this distance, however, the film congregated exclusively at the bottom of the pipe (succumbing to gravity), and a fuel rivulet resulted. At higher speeds, the evenly distributed film existed up to 0.4m (approximately), before giving way to the rivulet shape.

This rivulet had a very much lower surface area as compared with the evenly distributed film. It was then realized that the initial assumption of an evenly-distributed film (which had been long-forgotten) was responsible for this over-heating.

The film-shape used for all the results presented this document was defined as follows:

1. Evenly-distributed film from x=0 to x=0.2m.
2. A ramp function from even distribution (surface occupied = pipe perimeter) at 0.2m to 0.4m, where the film is assumed to have a surface width of approximately 1cm.
3. For x>=0.4m the surface maintains a width of 1cm.

These assumptions resulted in dramatically improved film temperature predictions by the model, but it remains a crude approximation (for example the shape was observed to be radically changed at different speeds), and it is anticipated that a more detailed description of the film-shape will result in even better model performance.

Cone shape

Provision was made for the droplets to spread out from the point of inlet in the shape of a cone (as in Figure 1). It was found, however, that this did not influence the downstream (x>0.1m) temperatures significantly, and hence this setup was not used for the main simulations, and uniform initial distributions were assumed throughout.

Example of the main data structures

The main data structures are outlined briefly here because they illuminate how the program works. These are contained in the universal header file below.

```
class cubic {  // Values of temperature dependent properties
private:
   double a0,a1,a2,a3;
   int positive_only;  // if quantity is necessarily positive (eg. vapour pressure)
public:
   cubic( double a, double b, double c, double d, int postv ) {
        a0=a; a1=b; a2=c; a3=d; positive_only=postv;
   }
   double eval_at( double xK) {      // Kelvin temperature parsed in
        double xC=xK-273;            // Cubic equations based on Celsius temperatures
        double fit=a0 +a1*xC +a2*xC*xC +a3*xC*xC*xC;
        if(positive_only&&(fit<0)) fit=0;
        return fit;  // cubic fit
   }
};
```

```
class quality { // General properties
private:
   double current;  // current value at x
   double next;     // next value at x+h worked out by Runge-Rutta routine
   int positive_only;
public:
   quality( double c, double n, int postve ) {
        positive_only=postve;
        if( postve && (c<0) ) c=0;
        if( postve && (n<0) ) n=0;
        current=c; next=n;
        }
   void swap();
   double set_next( double nx);
   double val() { return current; }
};

inline void quality::swap()  {
   current=next;
};

inline double quality::set_next( double nx)  {
   if(positive_only&&(nx<0)) nx=0;
   next=nx;
   return nx;
};

class air_or_vapour {  // Properties common to gaseous components
public:
  quality *dens;       //density
  quality *mass;       // mass flow-rate
  quality *press;      // vapour pressures contribution
  double R;            // gas const
  cubic *mew;          // absolute viscosity
  cubic *Cp;           // specific *heat
  cubic *k;            // thermal conductivity

// Setup command
  air_or_vapour( quality *d, quality *m, quality *p, double rr,
                 cubic *mw, cubic *c, cubic *kk )
  {  dens=d; mass=m; press=p;
     R=rr;
     mew=mw; Cp=c; k=kk;
  }

};
```

```
class air_and_fuel_vapour {  // full descriptor of the gas body
public:
  quality *temp;       // Gas temperature
  quality *vel;        // Gas velocity
  quality *Ptotal;     // Total pressure
  air_or_vapour *air;          // air qualities
  air_or_vapour *vap[12];   // individual vapour component qualities

// Setup command
  air_and_fuel_vapour( quality *t, quality *vl, quality *pt,
                       air_or_vapour *a, air_or_vapour *v[12] )
  {   temp=t; vel=vl; Ptotal=pt; air=a;
     vap[0]=v[0]; vap[1]=v[1]; vap[2]=v[2]; vap[3]=v[3]; vap[4]=v[4]; vap[5]=v[5];
     vap[6]=v[6]; vap[7]=v[7]; vap[8]=v[8]; vap[9]=v[9]; vap[10]=v[10]; vap[11]=v[11];
  }
};

class fuel_droplets {  // General descriptor of the fuel droplet stream
public:
  quality *temp;       // temperature
  quality *vel;        // velocity
  quality *diam;       // mean droplet diameter
  quality *n;          // number of droplets passing any section per second
  quality *mass[12];  // mass of each individual component

// Setup command
  fuel_droplets( quality *t, quality *v, quality *d, quality *nn, quality *m[12] )
  {   temp=t; vel=v; diam=d; n=nn;
        mass[0]=m[0]; mass[1]=m[1]; mass[2]=m[2]; mass[3]=m[3]; mass[4]=m[4];
        mass[5]=m[5]; mass[6]=m[6]; mass[7]=m[7]; mass[8]=m[8]; mass[9]=m[9];
        mass[10]=m[10]; mass[11]=m[11];
  }
};

class liquid_fuel_film { // General descriptor of wall film
public:
  quality *temp;       // temperature
  quality *vel;        // velocity
  quality *mass[12];  // mass of each individual component

// Setup command
  liquid_fuel_film( quality *t, quality *v, quality *m[12] )
  {   temp=t; vel=v;
        mass[0]=m[0]; mass[1]=m[1]; mass[2]=m[2]; mass[3]=m[3]; mass[4]=m[4];
        mass[5]=m[5]; mass[6]=m[6]; mass[7]=m[7]; mass[8]=m[8]; mass[9]=m[9];
        mass[10]=m[10]; mass[11]=m[11];
  }
};
```

```
class fuel_properties {
public:
  double mol_mass;
  double diff_coeff;  // diffusion coefficient m^2/s (for Methanol = 0.159E-4)
  cubic *density;
  cubic *cl;          // Liquid specific heat
  cubic *h_fg;        // Heat of vaporization
  cubic *Vp_cub;      // Vapour pressure
        // Methanol = { 0.010647 +0.000288125 -9.048975E-06 +4.69762E-07 };

// Setup routine
  fuel_properties( double mm, double dc, cubic *d, cubic *c, cubic *h, cubic *vp )
  {   mol_mass=mm; diff_coeff=dc;
      density=d; cl=c; h_fg=h; Vp_cub=vp;
  }
};
```

APPENDIX C. EXPERIMENTAL PROCEDURES AND RESULTS

The procedures employed when using the rig are described, and certain limitations are outlined. A summary of the experimentation is presented, and tables are included showing a history of the results.

DESCRIPTION OF EXPERIMENTAL PROCEDURES, AND DISCUSSION OF TECHNIQUES

A specific 'run' consisted of data collection for specific air and fuel inlet temperatures, over a range of air speeds, starting with low air flow-rates, and building up to the system's capacity (limited by both the air and the fuel supplies). The composition (proportion methanol content in the gasoline base) of the fuel was chosen, and the rig was run for several minutes to flush the system, to ensure the integrity of the new blend.

The air mass flow-rate was very easy to control, and therefore was repeatable from day to day. Hence this was the datum for which the fuel flow-rate was set, for purposes of comparison. The fuel flow-rate was more difficult to set at a target value, and the flow at a particular 'throttle' setting varied from day-to-day, and with each different fuel mix. Thus it was necessary to measure the flow-rate for each setting, and this was done volumetrically. The desired flow-rate (to provide a stoichiometric mixture, for example) was usually sufficiently accurate on the third iteration (typically). Once the desired flow-rate had been attained, the fuel supply was very reliable in maintaining that flow-rate with a precision to within $\pm 2\%$. This procedure was employed for each new fuel and air flow-rate.

The temperature of the air being delivered by the fan was subject to the flow-rate (as well as being dependent on the ambient conditions), and hence the air heater had to be adjusted to correct for these changes. The minimum air temperature produced by the fan was 40°C, and this corresponded to minimum offered by the rig (no cooling method was implemented). The heater was designed to deliver 2.2 kW, which facilitated heating of the maximum air flow-rates to 80°C (and initial air temperatures of up to 150°C were tested for low flow-rates).

At each new setting, a waiting period was necessary to ensure that equilibrium conditions had been established before the relevant temperature data were gathered. The analogue output of the data-logger was monitored until it was clear that final temperatures were prevalent. Data samples were then gathered, comprising two instantaneous readouts, and, in addition, an analogue history of not fewer than 30 samples (read at a rate of one every five seconds) of each temperature measuring station. These 30 sample points formed the window for the 'mean and range' format of data presentation necessary for the statistical analysis of variance (described in Appendix E).

SUMMARY OF AND COMMENTS ON EXPERIMENTATION

Justification for the use of fuel injector nozzles for most experimentation

Many experiments were performed using a 'carburettor'-type hypodermic needle fuel-jet, both in this study, and in a subsidiary project[79]. The data gathered using this type of setup proved useful in confirming trends, but the interpretation of these data was confounded by the lack of definition surrounding the droplet sizes and their distribution. In order to clarify the behaviour of the droplets, an in-depth investigation was launched (as mentioned in section 3.3, which is more fully described in Appendix D). The behaviour of droplets produced by fuel injector nozzles (Bosch K-Jetronic type) was readily described, but the droplets emanating from the 'carburettors' (needles as well as real carburettors) proved more elusive to classify accurately, and a special investigation[63] was initiated to encompass this aspect of inlet systems. The results of the special investigation[63] were to have been available at the conclusion of this project, and hence it was decided to perform most of the bulk of the experimentation using injector nozzles. These were configured as they were in the droplet size investigation.

General overview of the experimentation

The table below provides a summary of the experimentation that was performed using fuel injector nozzles. For this experimentation only one AV probe (gas temperature probe, AV being an acronym for 'air and vapour') was used, since it was considered likely to corrupt downstream readings, due to its intrusive nature. Therefore, data readings downstream of the AV probe were not expected to be accurate (especially in the case of the droplet

temperatures). For 'runs' with no AV probe in use, the droplet and film temperatures have been shown to be insignificantly affected by the inclusion of other droplet or film thermocouple wires upstream. Hence, for these 'runs' (after Aug/04) the full array of temperature readings are considered to be accurate.

Date '92	Fuel type	No.s	Comments
Jul/06	100G	50-67	AV probe at 0.2m [1]
Jul/06A	100G	70-92	AV probe at 1.0m [5]
Jul/08	100G	100-121	AV probe at 0.6m [3]
Jul/08A	10M90G	130-155	AV probe at 0.6m [3]
Jul/09	100G	170-189	AV probe at 0.1m [0]
Jul/10	10M90G	200-216	AV probe at 0.1m [0]
Jul/10A	10M90G	220-235	AV probe at 1.0m [5]
Jul/27	100G	300-307	AV probe at 1.0m [5]
Jul/28	10M90G	320-336	AV probe at 1.0m [5]
Aug/04	100G	499-519	$A_i \approx 60°C$; $F_i \approx 30°C$ (no AV probe)
Aug/05	100G	529-540	$A_i \approx 80°C$; $F_i \approx 30°C$ (no AV probe)
Aug/06	100G	549-559	$A_i \approx 60°C$; $F_i \approx 20°C$ (no AV probe)
Aug/07	10M90G	599-611	$A_i \approx 60°C$; $F_i \approx 20°C$ (no AV probe)
Aug/10	10M90G	699-714	$A_i \approx 80°C$; $F_i \approx 20°C$ (no AV probe)
Aug/12	20M80G	750-760	$A_i \approx 60°C$; $F_i \approx 15°C$ (no AV probe)
Aug/13	20M80G	799-807	$A_i \approx 60°C$; $F_i \approx 25°C$ (no AV probe)
Aug/24	100G	1000-1020	$A_i \approx 50°C$; $F_i \approx 20°C$ (no AV probe)
Aug/25	10M90G	1040-1050	$A_i \approx 50°C$; $F_i \approx 20°C$ (no AV probe)
Aug/26	20M80G	1070-1093	$A_i \approx 50°C$; $F_i \approx 20°C$ (no AV probe)
Aug/27	20M80G	1100-1121	$A_i \approx 80°C$; $F_i \approx 20°C$ (no AV probe)
Aug/28	20M80G	1130-1147	$A_i \approx 70°C$; $F_i \approx 20°C$ (no AV probe)
Sep/01	20M80G	1160-1175	$A_i \approx 80°C$; $F_i \approx 20°C$ (no AV probe)
Sep/03	100G	1200-1210	$A_i \approx 60°C$; $F_i \approx 25°C$; AV probe 0.2m
Sep/04	100G	1230-1238	$A_i \approx 80°C$; $F_i \approx 20°C$; AV probe 0.2m
Sep/04A	10M90G	1250-1260	$A_i \approx 60°C$; $F_i \approx 25°C$; AV probe 0.2m

In the above table, A_i and F_i stand for the supply temperatures of the air and fuel respectively. The numbers in square brackets correspond to standard measuring positions in the test-section, and these are explained further below.

Explanation of the tabulated data
The tabulated experimental data is presented in the remainder of this Appendix, the key to the interpretation of which is set out below.

Run No
Every data set has been distinctly numbered, and this is listed at the top of each column. These data sets are thus grouped in columns.

Row key
A key to the rows is provided in the tables. This key features acronyms, the meanings of which are spelt out below.

T.op
Thermocouple temperature measurement of the air just before the air flow orifice plate. This temperature is used in the spreadsheet in the calculation of the air flow-rate.

D
Thermocouple droplet temperature measurements.

AV
Thermocouple gas temperature measurements using the specially developed probe (see section 3.1).

F
Thermocouple film temperature measurements.

Ai
Initial air temperature (measured with a thermocouple in the air-stream positioned immediately upstream of the fuel inlet point).

Fi
Initial fuel temperature (measured with a thermocouple positioned immediately before upstream of one of the four fuel injector nozzles).

[-1], [0], [1], [2], [3], [4], [5]
Shorthand for the standard positions of the temperature measurement probes. These positions correspond to distances downstream of the fuel inlet point of 0.03m, 0.1m, 0.2m, 0.4m, 0.6m, 0.8m and 1.0m respectively.

Composites
The pseudonym F3, for example, would therefore correspond to the film temperature thermocouple placed at position [3] (0.6m downstream).

VS
This corresponds to the fan's throttle position. The scale is printed on the fan, but is an arbitrary, non-linear scale where VS=19 corresponds to a fully closed throttle, with VS≈4 for wide-open throttle.

Airflow
This is the mass flow-rate of the supply air, calculated from the orifice plate reading.

Velocity
The air velocity (upstream of the fuel inlet) is calculated from the air mass flow-rate, together with the initial air temperature (Ai) and pipe pressure (mentioned below).

F.req
The required fuel flow-rate (to ensure a stoichiometric fuel/air mixture. This is calculated from the air mass flow-rate assuming a 1/14.7 fuel/air mass ratio to be stoichiometric for all blends (100G, 10M90G and 20M80G).

SS
This corresponds to an arbitrary, but approximately linear scale by which the fuel flow-rate may be coarsely set. SS=0 corresponds to zero fuel flow, with SS≈13 offering the maximum fuel flow-rate of about 7 g/s.

F.actual
The actual fuel flow-rate, measured by timing the consumption of a fixed volume (150 ml) of fuel.

Equiv ratio
The equivalence ratio of actual fuel/air mass flow ratio divided by the assumed stoichiometric ratio of 1/14.7 (fuel/air ratio by mass).

(1, 2), (3, 4), (5, 6), (7, 8)
Head readings (in millimetres of water) for four U-tubes. ('2'-'1') + ('3'-'4') yields the head loss over the orifice plate, ('5'-'6') + ('7'-'8') gives the pressure head upstream of the orifice plate.

Pipe press A and B
The pressure of the supply air, measured immediately upstream of the fuel inlet point. 'A' and 'B' are the two sides of U-tube (in millimetres of water).

Tot int
The total internal pressure (air supply) which is the difference in head between 'B' and 'A' (in millimetres of water).

Density
The density of the supply air ($kg.m^{-3}$) calculated from the total internal pressure (above) and the measured air temperature.

Sample column of one such spreadsheets
(*) = Thermocouple measurement (in °C)
(**) = U-tube reading (in millimetres of water)

E10: +D10+1 (Run number)

E11: 28.5 (*)
E12: 26.7 (*)
E13: 9.2 (*)
E14: 10.6 (*)
E15: 14.2 (*)
E16: 15.7 (*)
E17: 63.1 (*)
E18: 18.1 (*)
E19: 23.3 (*)
E20: 27.9 (*)
E21: 27 (*)
E22: 28.7 (*)
E23: 18.5 ('VS' read off the fan scale)

E24: (Air mass flow-rate calculated for the orifice plate)
0.0006*@SQRT(10000*(E31-E32+E33-E34)/1000*((101325+10000*(E35-E36+E37-E38)/1000)/(287*(273+E11))))

E25: +E24/(E43*@PI/4*0.034^2) (Air velocity)

E26: +E24*357142.857143 (Fuel mass flow-rate required for stoichiometric mix)

E27: 1.75 ('SS' fuel supply indicator)
E28: 3868 (Volumetrically measured 'actual fuel flow-rate')

E29: +E28/E26 (Equivalence ratio)

E31: 394 (**) \ First U-tube \
E32: 547 (**) / \ => Orifice plate head
E33: 583 (**) \ Second U-tube /
E34: 403 (**) / /
E35: 490 (**) \ Third U-tube \
E36: 512 (**) / \ => Air density before orifice plate
E37: 510 (**) \ Fourth U-tube /
E38: 513 (**) / /
E40: 500 (**) \ U-tube for internal pressure after the fan
E41: 503 (**) /

E42: +E41-E40

E43: (101325+9.81*E42)/(287*(E17+273)) (Density of supply air)

Run #	--->	50	51	52	53	54	55	56
Station	Dist							
T.op		37.6	38.4	37.1	36.8	37.3	37.8	36
D	0.17	19.1	17.9	25.1	25.4	21.1	21.9	25.2
AV	0.2	23.3	21	28.5	28.7	22.2	23.2	26.6
Ai	0	46.1	46.1	54.2	54.3	51.9	51.9	55.6
Fi	0	27.9	31.3	33.4	33.8	29	29.1	29.8
F-1	0.03	3.1	5.5	7.1	7.8	7.7	8.6	12.1
F0	0.1	5.6	7.1	8.3	8.6	8.3	8.9	13.3
F1	0.2	8.1	8.7	9.5	9.4	8.9	9.2	14.5
F2	0.4	8.1	8.3	11.6	12	9.3	9.7	16.5
F3	0.6	9.1	9	12.7	12.8	9.3	9.7	17.2
F4	0.8	8.2	7.9	12.6	12.8	7.1	7.6	16.9
F5	1	9.9	9.2	14.2	14.5	8.3	8.8	18.2
VS		18.5	18.5	18	18	18	18	17
Airflow (kg/s)		0.011	0.011	0.018	0.018	0.018	0.018	0.029
Velocity (m/s)		11.17	11.15	18.39	18.4	18.25	18.24	29.75
F.req (ml/hr)		4009	4003	6452	6455	6450	6445	10469
SS		1.2	1.3	1.3	1.3	2.1	1.9	1.9
F.actual		3639	4457	4457	4457	7763	7007	7007
Equiv ratio		0.908	1.113	0.691	0.69	1.204	1.087	0.669
1		411	411	427	427	427	427	464
2		532	532	517	517	517	517	478
3		568	568	575	575	575	575	596
4		418	418	410	410	410	410	389
5		636	636	636	636	636	636	641
6		368	368	367	367	367	367	362
7		690	690	690	690	690	690	895
8		334	334	334	334	334	334	338
Pipe press A		500	500	486	486	486	486	450
B		504	504	517	517	517	517	554
Tot int (mm)		4	4	31	31	31	31	104
Density (kg/m^3)			1.107	1.082	1.082	1.09	1.09	1.085

57	58	59	60	61	62	63	64	65
36	36	34.8	34.8	32.9	33.3	33.6	33.7	33.9
21.3	21.3	20.7	20.5	17.6	17.7	17.5	17.8	17.9
19.05	20.1	20.1	19.4	18.8	17.7	16.8	16	15.6
52.4	52.1	51.2	50.8	51.8	50.6	49.9	48.4	48
25.5	25.4	25.4	25.3	23.5	23.3	22.9	22.3	22.3
12.5	13.7	20.6	19.1	4.3	2.9	4	10.2	11.8
12	12.7	22	20.9	10.8	10.2	10.6	15.3	16.3
11.5	11.7	23.4	22.7	17.3	17.5	17.2	20.4	20.8
12.4	12.2	26.7	26.2	18.9	18.8	18.4	24.2	24.4
12.1	11.8	23.4	23.4	18.2	17.9	17.6	21.7	21.8
9.8	9.5	21.3	21.3	16.3	15.7	15	19.2	19.1
11.1	10.9	21.8	21.7	17.3	16.5	15.9	19.3	19.2
17	17	15	15	15	15	15	13	13
0.029	0.029	0.043	0.043	0.043	0.043	0.043	0.049	0.049
29.76	29.73	42.32	43.31	42.97	43.87	43.75	49.36	49.28
10469	10469	15314	15314	15529	15519	15511	17581	17576
3	3	3	3	4.4	4.4	4.4	4.4	4.4
11187	11187	11187	11187	15271	15271	15271	15271	15271
1.069	1.069	0.731	0.731	0.983	0.984	0.985	0.869	0.869
464	464	530	530	534	534	534	574	574
478	478	408	408	408	408	408	369	369
596	596	642	642	644	644	644	665	665
389	389	345	345	342	342	342	320	320
641	641	647	647	644	644	644	647	647
362	362	357	357	360	360	360	356	356
895	895	685	685	690	690	690	687	687
338	338	340	340	334	334	334	337	337
		373		372				
		630		633				
0	0	257	0	261	0	0	0	0
1.085	1.086	1.116	1.09	1.114	1.091	1.093	1.098	1.1

66	67		70	71	72	73	74	75
35	35.2		38.1	39.1	39.5	38	37.7	37.6
16.7	16.5		24	24	23.9	30.2	30.9	27.1
13	12.7		24	24	24	30.9	31.4	26.9
46.1	45.5		46.5	46.2	46.1	55.1	55.1	54.2
20.1	19.7		31.3	32.3	33.3	35.1	35.5	33.8
18.6	19		5.8	5.5	5.8	5.8	6.5	7.9
20.3	20.5		7.6	7.5	7.6	9	9.7	9
22	22		9.4	9.5	9.4	12.2	12.9	10.1
23.7	23.5		9.2	9.2	9.2	15.4	16.3	11.4
19.5	19.3		10.4	10.2	10.2	16.8	17.7	12.2
15	14.9		9.2	9.1	9.1	18.3	19	11.5
15.2	15		11.8	11.5	11.4	18.9	20.1	13.4
13	13		18.5	18.5	18.5	18	18	18
0.049	0.049		0.011	0.011	0.011	0.018	0.018	0.018
48.9	48.8		11.12	11.09	11.08	18.65	18.66	18.61
17544	17539		4005	3998	3996	6525	6529	6530
5.5	5.5		1.2	1.2	1.2	1.2	1.2	1.8
17521	17521		3616	3616	3616	3616	3616	6200
0.999	0.999		0.903	0.904	0.905	0.554	0.554	0.95
574	574		420	420	420	433	433	433
369	369		524	524	524	510	510	510
665	665		560	560	560	570	570	570
320	320		427	427	427	416	416	416
647	647		643	643	643	642	642	642
356	356		362	362	362	363	363	363
687	687		682	682	682	681	681	681
337	337		342	342	342	343	343	343
			450	450	450	487	487	487
			500	500	500	518	518	518
0	0		50	50	50	31	31	31
1.106	1.108		1.11	1.111	1.112	1.079	1.079	1.082

76	77	78	79	80	81	82	83	84
37.7	37.9	36	35.5	35.8	36.2	34.8	34.6	35.1
26.3	26.3	30.9	30.8	25.8	25.8	27.6	27.4	25.5
25.7	25.5	31.5	31.3	25	24.5	27	26.7	23.4
53.3	53.3	55.9	54.9	52.7	52.1	51.6	51.1	49.2
31.9	31.7	32.1	31.7	27.7	26.4	26.3	26.1	23.4
8.1	8.3	20	20	12.8	12.6	17.2	17.9	9.8
8.9	9	17.7	17.7	12.4	12.3	20.1	20.4	14.8
9.7	9.7	15.4	15.4	12	12	23	22.9	19.8
10.6	10.8	17.9	17.6	12.8	12.7	23.2	22.9	19.1
11.3	11.3	19.3	19	13.1	12.8	22.7	22.3	17.3
10.1	10.2	19.8	19.5	11.7	10.9	21.6	21.3	14.8
11.7	11.6	20.9	20.6	13	12.2	22	21.7	15.9
18	18	17	17	17	17	15	15	15
0.018	0.018	0.029	0.029	0.029	0.029	0.043	0.043	0.043
18.55	18.55	29.42	29.36	29.15	29.07	42.8	42.75	42.46
6529	6527	10341	10349	10344	10338	15477	15482	15470
1.9	1.9	1.9	1.9	3	3	3	3	4.4
6505	6505	6505	6505	10825	10825	10825	10825	14921
0.996	0.997	0.629	0.629	1.046	1.047	0.699	0.699	0.965
433	433	467	467	467	467	540	540	540
510	510	476	476	476	476	403	403	403
570	570	593	593	593	593	638	638	638
416	416	392	392	392	392	347	347	347
642	642	643	643	643	643	648	648	648
363	363	362	362	362	362	357	357	357
681	681	683	683	683	683	684	684	684
343	343	340	340	340	340	340	340	340
487	487	453	453	453	453	371	371	371
518	518	554	554	554	554	633	633	633
31	31	101	101	101	101	262	262	262
1.085	1.085	1.084	1.087	1.095	1.097	1.115	1.117	1.124

85	86	87	88	89	90	91	92
35.3	35.4	35.5	35.8	35.8	36	35.8	35.2
25.2	25.2	25.1	25.1	25.1	25.4	24.4	24.4
22.7	22.6	22.5	22.4	22.4	22.6	23.2	24.2
48.4	48.2	47.7	47.2	46.9	46.6	50.9	52.4
22.4	22.2	21.8	21.8	21.7	21.8	24	24.6
9.7	11.6	19	17.6	20.6	22.9	20.5	21.8
14.1	15.2	21.1	20.6	22.8	24	22.1	
18.5	18.8	23.2	23.6	25	25.1	23.7	23.2
17.7	18.2	25	24.7	25.4	25.9	24.4	24.4
16.3	16.4	22	21.9	21.7	21.3	20.6	21.4
13.7	13.8	19.3	19	18.7	18.2	18.7	20.8
14.6	14.8	19.3	19.2	19	18.9	19.3	20.3
15	15	13	13	13	13	13	13
0.043	0.043	0.049	0.049	0.049	0.049	0.049	0.049
42.34	42.31	47.37	47.27	47.23	47.17	47.82	48.09
15465	15462	17480	17471	17471	17466	17471	17488
4.4	4.4	4.4	4.4	4.4	4.4	5.5	5.5
14921	14921	14921	14921	14921	14921	17250	17250
0.965	0.965	0.854	0.854	0.854	0.854	0.987	0.986
540	540	577	577	577	577	577	577
403	403	365	365	365	365	365	365
638	638	660	660	660	660	660	660
347	347	325	325	325	325	325	325
648	648	651	651	651	651	651	651
357	357	353	353	353	353	353	353
684	684	682	682	682	682	682	682
340	340	342	342	342	342	342	342
371	371	329	329	329	329	329	329
633	633	677	677	677	677	677	677
262	262	348	348	348	348	348	348
1.126	1.127	1.138	1.14	1.141	1.142	1.127	1.122

Run No.	---->	100	101	102	103	104	105	106
Station	Dist					Ambient 20.2°C		
T.op		36.5	37.3	37.6	37.7	36.1	35.9	35.8
D	0.57	41.5	18.5	19.5	19.8	27.1	37.5	23.5
AV	0.6	41.6	19.5	20.4	20.8	29.1	29.9	25
Ai	0	46.3	46.4	46.5	46.5	55.7	55.7	54.8
Fi	0	17	28.4	30.9	31.9	33.4	33.9	31.9
F0	0.1	35.2	6.1	6.5	6.6	9	9.1	8.1
F1	0.2	31.3	8.1	8.2	8.4	10.8	11	9
F2	0.4	33.7	7.8	8.5	8.7	13.7	14.1	10.5
F3	0.6	29.8	9.9	10.4	10.6	15.1	15.4	11.5
F4	0.8	32	9.6	9.3	9.4	16.8	17	11.9
F5	1	29.7	11.1	11.2	11.2	18.1	18.4	13.1
VS		18.5	18.5	18.5	18.5	18	18	18
Airflow (kg/s)		0.011	0.011	0.011	0.011	0.018	0.018	0.018
Velocity (m/s)		11.2	11.19	11.19	11.18	18.63	18.63	18.58
F.req (ml/hr)		4017	4012	4010	4009	6506	6508	6509
SS		off	1.3	1.3	1.3	1.3	1.3	1.875
F.actual		0	4016	4016	4016	4016	4016	6758
Equiv ratio		0	1.001	1.002	1.002	0.617	0.617	1.038
1		398	398	398	398	415	415	415
2		544	544	544	544	528	528	528
3		580	580	580	580	587	587	587
4		405	405	405	405	398	398	398
5		621	621	621	621	622	622	622
6		380	380	380	380	380	380	380
7		706	706	706	706	704	704	704
8		316	316	316	316	320	320	320
Pipe press A		500	500	500	500	487	487	487
B		504	504	504	504	517	517	517
Tot int (mm)		4	4	4	4	30	30	30

107	108	109	110	111	112	113	114	115
			Ambient 18.3°C					
35.8	34	33.8	33.6	33.7	32.2	32.1	32.1	32.8
23.5	27.7	27.3	23.6	23.5	25.4	24.9	22.2	22
24.9	30.3	30.1	25.3	25.2	28	27.3	23.8	23.3
54.9	57.5	57	56.1	55.9	55.6	54.7	53.8	53.5
31.7	30.9	31.1	28.7	28.5	27.9	27.6	25.4	24.2
8.2	16.6	16.8	11.1	11.4	20.9	19.8	15.9	15.8
9	16.4	16.5	12.2	12.3	23.7	23.2	19.5	18.8
10.4	18	18.2	13.3	13.4	25.6	25	19.9	19.2
11.5	19.8	19.8	14.2	14.4	25	24.6	19.4	18.6
11.9	22	21.9	15.2	15.1	27.4	26.7	21.5	20.4
13.1	22.7	22.6	16.4	16.1	27	26.5	21.1	19.6
18	17	17	17	17	15	15	15	15
0.018	0.029	0.029	0.029	0.029	0.044	0.044	0.044	0.044
18.59	30	29.96	29.89	29.87	43.7	43.59	43.47	43.38
6509	10486	10489	10493	10491	15600	15603	15603	15585
1.875	1.875	1.875	2.9	2.9	2.9	2.9	4.4	4.8
6758	6758	6758	10997	10997	10997	10997	14921	15590
1.038	0.644	0.644	1.048	1.048	0.705	0.705	0.956	1
415	451	451	451	451	527	527	527	527
528	492	492	492	492	417	417	417	417
587	611	611	611	611	659	659	659	659
398	374	374	374	374	327	327	327	327
622	626	626	626	626	360	360	360	360
380	377	377	377	377	373	373	373	373
704	703	703	703	703	704	704	704	704
320	320	320	320	320	320	320	320	320
487	454	454	454	454	375	375	375	375
517	549	549	549	549	629	629	629	629
30	95	95	95	95	254	254	254	254

116	117	118	119	120	121		130	131
	Amb 19.5°C				Ambient 20.3°C			
33	32.7	32.8	33.2	33.1	33.2		38.4	38.4
22.3	22.3	22.3	21.4	21.6	21.5		18.7	17.9
23.6	24.2	24	22.3	22.8	22.9		20.2	19.4
53.5	53.2	53	52.7	52.9	53		46.1	46.9
24.2	24	24	23.3	23.6	23.7		32.9	33.5
16.3	20	19.8	16.5	16.6	17.2		5.2	5.2
19.3	22.4	22.4	20.4	20.6	20.8		6.5	5.9
19.5	25.2	25	21.5	21.7	22		6	6
18.9	23.4	23.3	19.7	20.2	20.7		7.9	8.2
20.7	24.9	24.7	21.3	21.7	22		6.7	7.6
19.8	23.8	23.8	20	20.6	20.5		9.2	9.5
15	13	13	13	13	13		18.5	18.5
0.044	0.05	0.05	0.05	0.05	0.05		0.011	0.011
43.37	49.34	49.3	49.22	49.26	49.27		10.76	11.18
15580	17884	17881	17869	17872	17869		3863	4003
4.8	4.8	4.8	5.9	5.9	5.9		1.3	1.3
15590	15590	15590	18018	17810	17810		3795	3795
1.001	0.872	0.872	1.008	0.997	0.997		0.982	0.948
527	568	568	568	568	568		404	405
417	373	373	373	373	373		539	538
659	678	678	678	678	678		574	575
327	306	306	306	306	306		412	413
360	637	637	637	637	637		625	625
373	366	366	366	366	366		378	378
704	699	699	699	699	699		700	700
320	325	325	325	325	325		323	323
375	333	333	333	333	333		500	500
629	672	672	672	672	672		504	504
254	339	339	339	339	339		4	4

132	133	134	135	136	137	138	139	140
				Ambient 18.5°C				
38.5	37.3	36.7	36.5	36.5	36.3	36.5	34.6	34.4
17.9	24.8	26.1	26.3	19.4	18.8	18.7	23.2	24
19.5	28.2	29.6	29.4	21.7	21	21.1	26.3	27.5
47.3	55.5	55.7	55.4	55	54.9	54.9	57.6	56.9
33.7	34.1	34.2	34	30.9	30.5	30.4	30.5	30.6
5.3	4.1	3.6	3.6	2.9	2.9	2.7	8.4	8.7
6.1	6.2	5.8	5.8	4.4	4.5	4.6	9.4	10.2
5.7	7.8	7.4	7.3	4.7	4.8	4.9	10.9	11.5
8.1	9.9	9.4	9.6	6	6.1	6.2	12.7	13.4
7.1	11.5	10.6	10.8	5.8	5.9	6.1	14	14.5
9.6	12.5	13.1	13.4	9	8.8	8.8	15.7	16.2
18.5	18	18	18	18	18	18	17	17
0.011	0.018	0.018	0.018	0.018	0.018	0.018	0.03	0.03
11.19	18.57	18.6	18.59	18.57	18.57	18.56	31.06	31
4003	6492	6498	6500	6500	6503	6500	10842	10846
1.3	1.3	1.3	1.3	2.3	2.3	2.3	2.3	2.3
3795	3795	3795	3795	6562	6562	6562	6562	6562
0.948	0.585	0.584	0.584	1.009	1.009	1.009	0.605	0.605
405	419	419	419	419	419	419	450	450
538	525	525	525	525	525	525	493	493
575	584	584	584	584	584	584	628	628
413	402	402	402	402	402	402	375	375
625	625	625	625	625	625	625	629	629
378	378	378	378	378	378	378	375	375
700	700	700	700	700	700	700	700	700
323	324	324	324	324	324	324	324	324
500	486	486	486	486	486	486	460	460
504	518	518	518	518	518	518	545	545
4	32	32	32	32	32	32	85	85

141	142	143	144	145	146	147	148	149
			Ambient 19.1°C					
34.2	34.3	32.9	32.5	32.7	32.8	32.6	32.6	32.9
17.9	18.1	20.1	20.3	15.5	15.8	17.2	17	15.9
20	20.2	23.6	23.7	17.5	17.5	18.8	18.6	16.5
55.9	55.9	55.9	55.3	54	53.8	53.3	53.1	52.8
26.7	26.6	26.7	26.7	23.8	23.4	22.9	22.9	21.8
4.4	4.5	11.2	11.3	6.5	6.5	10.6	11.2	6.7
6.5	6.7	16.5	17.3	11.5	11.5	13.8	14	11.8
7.8	7.9	19.8	20.7	11.9	11.8	16.1	16.3	12.5
9.1	9.2	20.1	20.5	11.5	11.2	14.1	14.5	11.5
9.4	9.5	22.5	23	13.4	13.2	17.3	17.5	13.1
10.6	10.7	22.3	22.8	13.7	13.4	17.7	17.8	13.1
17	17	15	15	15	15	13	13	13
0.029	0.029	0.044	0.044	0.044	0.044	0.05	0.05	0.05
29.48	29.48	44.01	43.96	43.77	43.73	49.4	49.37	49.3
10347	10345	15691	15702	15697	15694	17901	17901	17893
5	5	5	5	9.5	9.5	9.5	9.5	12.7
10330	10330	10330	10330	15638	15638	15638	15638	18096
0.998	0.999	0.658	0.658	0.996	0.996	0.874	0.874	1.011
450	450	528	528	528	528	570	570	570
487	487	413	413	413	413	372	372	372
607	607	654	654	654	654	678	678	678
379	379	332	332	332	332	308	308	308
629	629	633	633	633	633	636	636	636
375	375	370	370	370	370	367	367	367
700	700	700	700	700	700	700	700	700
324	324	323	323	323	323	325	325	325
460	460	375	375	375	375	333	333	333
545	545	627	627	627	627	672	672	672
85	85	252	252	252	252	339	339	339

150	151	152	155		170	171	172	173
			Petrol in again (155)					
33.1	33.2	33.4	33.5		38.2	38.5	38.5	37.1
16.1	16.2	16.3	22.6		13	12.3	12.6	16.5
16.9	16.9	17.3	23.8		17.1	16.3	16.3	25
52.8	52.8	52.9	52.8		46	46.3	46.7	55.8
21.5	21.4	21.6	22		33.3	33.3	33.1	33
6.9	7.4	8.5	17.9		6.3	6.9	6.7	8.2
12	12.2	12.5	20		8	8.3	8.5	9.8
12.9	13.1	13.5	22.5		8.3	8	8	12.3
11.7	11.9	11.9	20.2		9.9	9.3	9.1	13.4
13.5	13.8	14	23.2		9.9	8.6	8.7	14.3
13.2	13.5	13.8	22		10.1	8.8	9	15
13	13	13	13		18.5	18.5	18.5	18
0.05	0.05	0.05	0.05		0.011	0.011	0.011	0.018
49.29	49.28	49.28	49.26		11.16	11.16	11.18	18.72
17887	17884	17878	17875		4005	4003	4003	6537
12.7	12.7	12.7	12.7		1.1	1.25	1.25	1.25
18096	18096	18096	16000		3314	4234	4234	4234
1.012	1.012	1.012	0.895		0.827	1.058	1.058	0.648
570	570	570	570		401	401	401	419
372	372	372	372		542	542	542	524
678	678	678	678		578	578	578	584
308	308	308	308		408	408	408	402
636	636	636	636		620	620	620	623
367	367	367	367		382	382	382	378
700	700	700	700		705	705	705	702
325	325	325	325		317	317	317	322
333	333	333	333		500	500	500	487
672	672	672	672		504	504	504	516
339	339	339	339		4	4	4	29

174	175	176	177	178	179	180	181	182
			Ambient 18.3°C					
36.8	36.7	36.7	34.8	34.5	34.5	34.8	34.8	33
16.7	14.3	14.3	14.9	14.8	11.5	11.7	11.7	13.4
25.1	19.4	19.3	19.9	20.1	16	16.9	17.3	17.1
55.9	55.7	55.7	58.4	58	56.5	56.5	56.5	55.1
32.9	31.4	31.2	31.1	31	28.2	28.1	28.1	27.9
8.4	7.6	7.5	15.9	15.9	11.4	11.7	11.7	22.9
10	8.3	8.1	14.1	14.3	12.9	13.5	13.7	25.8
12.5	9.5	9.4	17.7	17.9	14.6	15.2	15.3	30.6
13.6	10.6	10.6	19.1	19.2	15.4	15.8	16	30
14.6	10.8	10.6	20.6	20.5	16	16.2	16.3	30.4
15.4	11.4	11.1	21.5	21.5	16.3	16.6	16.5	29.4
18	18	18	17	17	17	17	17	15
0.018	0.018	0.018	0.029	0.029	0.029	0.029	0.029	0.044
18.74	18.73	18.73	30.04	30.02	29.88	29.87	29.87	44.14
6541	6542	6542	10472	10477	10477	10472	10472	15778
1.25	1.9	1.9	1.9	1.9	3.5	3.5	3.5	3.5
4234	6606	6606	6606	6606	10277	10277	10277	10277
0.647	1.01	1.01	0.631	0.631	0.981	0.981	0.981	0.651
419	419	419	455	455	455	455	455	532
524	524	524	488	488	488	488	488	410
584	584	584	607	607	607	607	607	653
402	402	402	378	378	378	378	378	333
623	623	623	627	627	627	627	627	633
378	378	378	375	375	375	375	375	370
702	702	702	702	702	702	702	702	700
322	322	322	323	323	323	323	323	324
487	487	487	454	454	454	454	454	375
516	516	516	548	548	548	548	548	627
29	29	29	94	94	94	94	94	252

183	184	185	186	187	188	189
32.9	33.5	33.7	33.4	33.4	33.8	33.9
13.4	10.5	10.4	12.2	12.3	13.1	12.9
17	13.8	13.7	12.9	13.1	13.5	13.3
54.8	54.1	54.2	54	53.8	53.6	53.8
27.8	24.3	24.2	24.3	24.4	23.8	23.7
23	15.6	15.2	23.1	23.5	22.7	23
26.1	18.8	19.1	22.6	22.9	22	22.3
30.7	23.9	24	27.6	28	27.4	27.7
29.9	23.4	23.4	27.1	27.2	26.7	26.8
30.4	22.7	22.8	27.1	27.4	26.9	26.8
29.5	20.4	20.6	25.9	26.3	24.4	24.4
15	15	15	13	13	13	13
0.044	0.044	0.044	0.05	0.05	0.05	0.05
44.11	43.97	43.97	49.34	49.31	49.25	49.27
15780	15765	15760	17832	17832	17820	17817
3.5	7.4	7.4	7.4	7.4	12.8	12.8
10277	15638	15638	15638	15638	16493	16493
0.651	0.992	0.992	0.877	0.877	0.926	0.926
532	532	532	573	573	573	573
410	410	410	368	368	368	368
653	653	653	673	673	673	673
333	333	333	313	313	313	313
633	633	633	640	640	640	640
370	370	370	363	363	363	363
700	700	700	696	696	696	696
324	324	324	328	328	328	328
375	375	375	334	334	334	334
627	627	627	668	668	668	668
252	252	252	334	334	334	334

		200	201	202	203	204	205	206
Station	Dist (m)	Petrol	Ambient 18°C					
T.op	-------	38.8	38.8	39	37.5	37.8	37.1	36.9
D	0.57	14.1	6.2	5.8	8.3	8.5	6.4	6.4
AV	0.6	17.9	11.1	10.4	16.7	16.5	12	12.9
Ai	0	48	48.3	48.4	56.5	56.4	56.1	56
Fi	0	27.4	32.7	32.1	31.9	31.8	30.7	30.3
F0	0.1	5.6	2.7	2.9	2.3	2.4	1.7	1.7
F1	0.2	7.6	1.8	1.5	3.2	3.7	1.9	1.7
F2	0.4	9.6	4.8	5.2	6.5	6.7	4	4
F3	0.6	10.8	6.1	6.7	9	9.2	5.8	5.8
F4	0.8	11.1	5.7	5.4	9.2	9.4	5	5.1
F5	1	13.2	8.6	7.6	11.5	12.1	8.3	7.9
VS		18.5	18.5	18.5	18	18	18	18
Airflow (kg/s)		0.011	0.012	0.012	0.018	0.018	0.018	0.018
Velocity (m/s)		11.4	11.6	11.6	18.87	18.85	18.86	18.86
F.req (ml/hr)		4069	4136	4135	6575	6572	6579	6581
SS		1.1	1.4	1.4	1.4	1.4	2.35	2.35
F.actual		≈ 3500	4173	4173	4173	4173	6897	6897
Equiv ratio		0	1.009	1.009	0.635	0.635	1.048	1.048
1		407	410	410	423	423	423	423
2		536	534	534	520	520	520	520
3		572	570	570	580	580	580	580
4		413	415	415	405	405	405	405
5		624	626	626	627	627	627	627
6		378	376	376	375	375	375	375
7		700	698	698	697	697	697	697
8		323	325	325	325	325	325	325
Pipe press A		498	499	499	485	485	485	485
B		503	504	504	517	517	517	517
Tot int (mm)		5	5	5	32	32	32	32

207	208	209	210	211	212	213	214	215
35.3	34.8	34.9	35	33.4	33.4	33.4	33.1	33.1
6	5.8	3.8	3.9	4.9	4.6	5	5.8	5.9
11.1	11	7	7.2	6.7	6.9	6.6	5.8	5.2
59	58.4	57.3	57.3	56.5	55.9	55.5	54.7	54.3
29.6	29.6	27.4	27.1	25	24.5	24.2	22.8	22.4
5.8	5.6	2.6	3	3.5	2.3	2.5	4.2	3.8
6.4	6.1	3.8	4	4.5	4.4	4	5.8	5.4
10.5	10.5	7	7.1	16.6	16.7	16.6	17.9	18.2
12.7	12.9	8.5	8.7	16.4	16.3	16.3	18.9	18.9
13.9	14	8.5	8.7	15	15	14.9	18.8	19
15.3	15.7	10.1	10.2	14.1	13.9	13.8	17.2	17.5
17	17	17	17	15	15	15	12	12
0.029	0.029	0.029	0.029	0.043	0.043	0.043	0.051	0.051
29.99	29.96	29.85	29.85	43.58	43.5	43.44	50.11	51.81
10437	10445	10443	10442	15518	15518	15518	18122	18122
2.35	2.35	3.7	3.7	5.9	5.9	5.9	8	8
6897	6897	11117	11117	15849	15849	15849	18569	18569
0.661	0.66	1.065	1.065	1.021	1.021	1.021	1.025	1.025
459	459	459	459	530	530	530	580	580
483	483	483	483	411	411	411	362	362
603	603	603	603	647	647	647	675	675
384	384	384	384	338	338	338	310	310
630	630	630	630	636	636	636	640	640
372	372	372	372	366	366	366	362	362
698	698	698	698	697	697	697	695	695
325	325	325	325	325	325	325	328	328
453	453	453	453	372	372	372	320	
550	550	550	550	630	630	630	683	
97	97	97	97	258	258	258	363	0

216		220	221	222	223	224	225	226
33.2		38.6	38.7	38	37.7	37.4	37.2	37
5.9		15	15	21.8	23.7	24.1	19.5	19.1
5.3		15	14.7	24.4	26.1	26.3	21	20.8
54.1		47	47.3	55.1	56.4	56.5	56.3	56.1
22.2		31.4	31.4	31.7	31.9	32	30.9	30.1
3.8		2.4	2.5	0.8	1	1.2	0.9	0.6
5.4		3.8	3.8	0.9	1.2	1.3	0.1	-0.2
18.2		2.8	2.5	3.5	4.3	4.7	2.2	1.9
19		6.1	6	6.3	7.5	7.9	4.4	4
19		4.6	4.3	7.2	8.5	9	4	3.8
17.5		6.4	6.1	8.9	10.6	11.2	6.7	6.1
12		18.5	18.5	18	18	18	18	18
0.051		0.011	0.011	0.018	0.018	0.018	0.018	0.018
51.77		11.37	11.38	18.45	18.54	18.55	18.55	18.54
18119		4070	4070	6442	6445	6448	6450	6452
8		1.39	1.39	1.39	1.39	1.39	2.3	2.3
18569		4272	4272	4272	4272	4272	6796	6796
1.025		1.05	1.05	0.663	0.663	0.663	1.054	1.053
580		408	408	423	423	423	423	423
362		535	535	520	520	520	520	520
675		571	571	579	579	579	579	579
310		414	414	407	407	407	407	407
640		626	626	626	626	626	626	626
362		376	376	376	376	376	376	376
695		698	698	698	698	698	698	698
328		325	325	325	325	325	325	325
		498	498	498	498	498	498	498
		503	503	503	503	503	503	503
0		5	5	5	5	5	5	5

227	228	229	230	231	232	233	234	235
							Ambient	20.3°C
35	34.8	33.3	33.4	33.4	32.9	32.8	33.1	33.2
18.7	18.3	15.7	15.9	16	13.6	13.8	14	14.2
20.7	20.4	16.7	17.1	17.3	14	14.5	14.7	14.9
58.4	57.8	55.8	55.3	55.2	53.7	53.6	53.6	53.6
28.2	27.2	23.6	23.2	23.2	21.5	21.1	21.4	21.5
4.7	5.6	8.7	4.8	5.4	5	5.3	5.2	5.6
2.9	2.7	10.3	11.9	12.1	10.3	10.6	10.1	10.6
3.6	3.6	7.2	9.6	9.8	10.3	10.8	11.1	11.5
6.6	6.6	10.4	11.9	12	11.5	12.1	12.5	12.7
7.3	7.5	11.9	13.2	13.4	12.1	12.7	12.7	13.1
9	9	12	13.1	13.3	11.6	12.1	12.2	12.5
17	17	15	15	15	12	12	12	12
0.029	0.029	0.043	0.043	0.043	0.051	0.051	0.051	0.051
29.71	29.67	43.2	43.13	43.12	50.51	50.5	50.47	50.47
10361	10364	15427	15425	15425	18140	18143	18134	18131
3.55	3.55	6	6	6	12	12	12.7	12.7
10291	10291	15327	15327	15327	19101	19101	17916	17916
0.993	0.993	0.993	0.994	0.994	1.053	1.053	0.988	0.988
458	458	531	531	531	577	577	577	577
485	485	411	411	411	364	364	364	364
603	603	650	650	650	679	679	679	679
384	384	335	335	335	308	308	308	308
629	629	634	634	634	635	635	635	635
373	373	669	669	669	367	367	367	367
699	699	700	700	700	697	697	697	697
324	324	323	323	323	325	325	325	325
453	453	369	369	369	372	372	372	372
550	550	634	634	634	630	630	630	630
97	97	265	265	265	258	258	258	258

300	301	302	303	304	305	306	307	
Ambient 17.3°C						Ambient 18.7°C		
28.4	28.3	29.6	29.8	29.8	30.1	29	29.1	
24.2	24.1	24.7	25	24.2		24	24	
24.8	25	26.6	26.7	26.7	26.5	25.8	26.2	
60.4	60.8	59.8	59.8	60.1	59.8	60.1	60.1	
28.7	29	29.8	29.7	29.7	29.6	30.7	30.6	
11.3	11.3	9.9	9.9	11.6	11.9	14.4	15	
11.7	11.6	10.4	10.3	11.2	11.3	14.4	15.2	
10.3	10.6	7.9	7.9	9	9	13.5	14.1	
11.9	12.2	9.4	9.4	10.8	10.9	15.8	16.3	
12.7	12.9	10.2	10.3	12	12	17.7	18.2	
14.3	14.1	11.6	11.5	13.2	13.2	18.8	18.6	
18.5	18.5	18.2	18.2	17	17	15	15	
0.011	0.011	0.021	0.021	0.03	0.03	0.045	0.045	
11.29	11.31	21.31	21.3	31.19	31.15	45.49	45.48	
3878	3879	7353	7350	10804	10799	15919	15917	
1.8	1.8	3	3	4	4	5.8	5.8	
3834	3834	7471	7471	10946	10946	15512	15512	
0.989	0.988	1.016	1.016	1.013	1.014	0.974	0.975	
397	397	421	421	457	457	534	534	
544	544	521	521	484	484	407	407	
580	580	593	593	615	615	665	665	
405	405	393	393	370	370	320	320	
492	492	594	594	497	497	497	497	
510	510	508	508	504	504	504	504	
514	514	515	515	515	515	516	516	
510	510	508	508	507	507	507	507	
500	500	485	485	460	460	407	407	
503	503	516	516	540	540	595	595	
3	3	31	31	80	80	188	188	

320	321	322	323	324	325	326	327	328
Ambient 17.3°C							Ambient	19.2°C
28.5	28.5	28.5	28.5	29.8	29.6	29.8	29.9	30.1
22.2	22	20.8	20.9	20.7	20.9	46.1	51.8	23.2
23.1	22.8	21.9	22.3	22	22	52	56.6	23.6
61.1	61.2	60.9	60.9	60.2	60.3	118.5	121.8	60.1
34.8	35	35.9	35.9	36.5	36.2	35.9	35.7	35.7
8.5	8.4	8.7	8.8	6.7	6.4	10.7	12.4	7.3
8.5	8.7	9	9.3	7.6	7.2	12.2	14.1	8.2
6.4	6.7	6.1	6.3	3.8	3.8	12.4	13.8	4
7.8	8.1	8.8	9	6	5.8	15.6	17.4	6
8.7	8.8	8.4	8.4	6.2	5.9	18.6	20.9	6.1
10.5	10.8	10.8	10.6	7.2	7.1	19.1	22.4	7.9
18.5	18.5	18.5	18.5	17.8	17.8	17.8	17.8	17.8
0.011	0.011	0.011	0.011	0.019	0.019	0.019	0.019	0.019
11.13	11.13	11.12	11.12	19.95	19.96	23.44	23.63	19.93
3814	3814	3814	3814	6873	6875	6873	6872	6869
1.75	1.75	1.75	1.75	2.7	2.7	2.7	2.7	2.7
3761	3761	3761	3761	7361	7361	7361	7361	7361
0.986	0.986	0.986	0.986	1.071	1.071	1.071	1.071	1.072
402	402	402	402	421	421	421	421	421
540	540	540	540	521	521	521	521	521
575	575	575	575	586	586	586	586	586
410	410	410	410	398	398	398	398	398
504	504	504	504	506	506	506	506	506
498	498	498	498	495	495	495	495	495
518	518	518	518	519	519	519	519	519
505	505	505	505	504	504	504	504	504
500	500	500	500	487	487	487	487	487
503	503	503	503	515	515	515	515	515
3	3	3	3	28	28	28	28	28

329	330	331	332	333	334	335	336
						Ambient 21.6°C	
30.1	30.3	30.4	31.1	31.1	31.7	32.1	32.5
22.7	21.3	21.6	17.8	17.7	17.2	17.4	26.1
23.3	22.4	22.7	17.4	17.4	16.7	17	26.5
59.5	60.5	60.5	59.8	59.9	60.1	60.4	81.6
35.3	34.7	34.2	33.6	33.2	32.9	32.6	32.4
6.9	6.6	6.6	8.4	8.4	8.8	8.9	10.4
7.7	7.1	7.3	12.3	11.9	13.8	13.6	16.7
3.8	4.4	4.5	6.9	6.7	10.2	10.2	17.7
5.8	6.5	6.7	7.1	6.9	7.9	7.9	13.5
6.1	7.3	7.3	7.3	7	7.8	7.6	14.5
7.6	8.2	8.3	7.7	7.1	7.8	7.6	14.2
17.8	17	17	15	15	12	12	12
0.019	0.029	0.029	0.044	0.044	0.053	0.053	0.053
19.9	29.7	29.69	45.01	45.03	53.29	53.3	56.66
6869	10264	10262	15762	15762	18781	18769	18757
2.7	4	4	6	6	7.5	7.5	7.5
7361	10114	10114	15711	15711	19217	19217	16993
1.072	0.985	0.986	0.997	0.997	1.023	1.024	0.906
421	458	458	540	540	605	605	605
521	484	484	400	400	335	335	335
586	604	604	654	654	686	686	686
398	382	382	331	331	300	300	300
506	518	518	523	523	538	538	538
495	484	484	480	480	464	464	464
519	523	523	524	524	529	529	529
504	500	500	500	500	495	495	495
487	465	465	408	408	370	370	370
515	536	536	594	594	633	633	633
28	71	71	186	186	263	263	263

Station	Dist (m)	499	500	501	502	503	504	505
T.op	-------	27.7	28.5	28.7	30.1	30.3	30.8	31.2
Fi	0	25.2	26.7	26.6	27.9	28.1	28.7	29.2
F0	0.1	49.2	9.2	9.6	7.1	7.1	8.1	8.1
F1	0.2	45.3	10.6	10.4	8.4	8.3	7.6	7.6
F3	0.6	42.6	14.2	13.5	12.6	12.3	11.9	11.9
F5	1	40.9	15.7	15.2	13.8	13.7	14.7	14.8
Tai	0	61.7	63.1	62.9	62.4	62.4	61.1	61.1
D-1	0.03	61.3	18.1	18.1	20	23.4	13.1	12.9
D0	0.1	62.9	23.3	22	22.9	23	15.1	14.9
D1	0.2	61.1	27.9	27.2	29	29	22.9	23.2
D3	0.6	57.8	27	27.2	28.4	28.7	26.5	26.6
D5	1	55.2	28.7	28.2	29.2	29.2	27.7	27.7
VS		18.5	18.5	18.5	17.8	17.8	17	17
Airflow (kg/s)		0.011	0.011	0.011	0.02	0.02	0.029	0.029
Velocity (m/s)		11.14	11.17	11.16	20.38	20.37	29.95	29.93
F.req (ml/hr)		3811	3806	3804	6973	6970	10334	10327
SS		0	1.75	1.75	2.85	2.85	4.05	4.05
F.actual		0	3868	3868	7167	7167	10686	10686
Equiv ratio		0	1.016	1.017	1.028	1.028	1.034	1.035
1		394	394	394	416	416	451	451
2		547	547	547	525	525	490	490
3		583	583	583	592	592	612	612
4		403	403	403	392	392	373	373
5		490	490	490	495	495	502	502
6		512	512	512	506	506	500	500
7		510	510	510	512	512	514	514
8		513	513	513	512	512	510	510
Pipe press A		500	500	500	488	488	465	465
B		503	503	503	514	514	537	537
Tot int (mm)		3	3	3	26	26	72	72
Density (kg/m^3)		1.055	1.051	1.051	1.055	1.055	1.064	1.064

506	507	508	509	510	511	512	513	514
31.3	31.3	31.6	32.8	33.2	33.8	33.9	34.5	35.2
29.5	29.5	29.8	30.5	30.6	30.9	30.9	31.3	31.9
17.9	18.4	8.3	10.8	10.8	11	10.6	16.3	16.5
17.3	17.5	8.1	10.8	10.6	11.9	11.7	16.8	15.8
23.5	24.4	13	14.6	14.6	17.3	17.6	24.6	24.4
29	29.8	15.5	17.6	17.5	21.1	21.5	30.9	31.6
99.7	100.6	61	60.3	60.5	60.6	60.6	79.1	80.1
26.3	26.6	13.8	15.3	14.1	15.9	18	23.4	24.4
29.2	29.4	16.1	12.1	12.2	10.7	11	17.1	18.5
41.3	41.9	23.7	17.5	17.7	14.9	15.4	23.6	24
46.7	47.6	27.3	23.6	24	22.3	22.4	31.6	31.9
48.3	48.8	28.5	25.1	25.4	24.3	24.7	34.7	35.3
17	17	17	15	15	12	12	12	12
0.029	0.029	0.029	0.044	0.044	0.052	0.052	0.052	0.052
33.38	33.46	29.9	44.71	44.71	52.63	52.62	55.48	55.58
10325	10325	10320	15641	15631	18540	18536	18518	18497
4.05	4.05	4.05	5.95	5.95	7.5	7.5	7.5	7.5
10686	10686	10686	16235	16235	18776	18776	18776	18776
1.035	1.035	1.035	1.038	1.039	1.013	1.013	1.014	1.015
451	451	451	538	538	600	600	600	600
490	490	490	403	403	340	340	340	340
612	612	612	654	654	685	685	685	685
373	373	373	330	330	300	300	300	300
502	502	502	520	520	532	532	532	532
500	500	500	481	481	470	470	470	470
514	514	514	520	520	524	524	524	524
510	510	510	504	504	500	500	500	500
465	465	465	406	406	364	364	364	364
537	537	537	597	597	638	638	638	638
72	72	72	191	191	274	274	274	274
0.954	0.952	1.064	1.079	1.078	1.086	1.086	1.029	1.026

515	516	517	518	519		529	530	531
36.5	36.5	36.4	35	34.4		28.2	28.8	29
35.2	36.5	38.2	38	38.2		25.9	27.2	27.7
11.1	11.1	11	54	54.7		58.6	11.7	11.9
7.8	8.1	8.3	49.2	51.4		52.6	13.6	13.5
15.2	15.8	15.8	45	48.8		48.6	19.4	18.6
21.3	22.1	21.8	49.5	51		46.7	22.7	21.3
61.2	60.9	60.9	60.3	59.6		80.9	82.1	82.9
26.2	13.9	14.2	59.2	58.8		79.3	28	28.8
13.5	14	14.2	58.6	58.3		82.2	37.1	36.3
17.5	17.6	17.6	56.6	56.9		79.3	42.3	42.4
23.1	23.8	23.7	55.9	56.4		74	38.9	37.7
26.1	26.5	26.5	55.7	56.1		69.8	40.9	39.7
12	12	12	12	12		18.5	18.5	18.5
0.052	0.052	0.052	0.052	0.052		0.011	0.011	0.011
52.49	52.45	52.45	52.48	52.42		11.8	11.83	11.85
18458	18458	18461	18503	18521		3819	3815	3814
7.5	7.5	7.5	0	0		0	1.75	1.75
18776	18776	18776	0	0		0	3868	3868
1.017	1.017	1.017	0	0		0	1.014	1.014
600	600	600	600	600		405	405	405
340	340	340	340	340		536	536	536
685	685	685	685	685		572	572	572
300	300	300	300	300		414	414	414
532	532	532	532	532		512	512	512
470	470	470	470	470		488	488	488
524	524	524	524	524		518	518	518
500	500	500	500	500		507	507	507
364	364	364	364	364		500	500	500
638	638	638	638	638		503	503	503
274	274	274	274	274		3	3	3
1.084	1.085	1.085	1.087	1.09		0.998	0.995	0.992

532	533	534	535	536	537	538	539	540
31.1	31.1	31.6	32.5	32.7	34.8	35	36.3	36.7
28.5	29	29.3	30.6	30.5	32	32.2	33	33.3
9.9	11	11.3	14	14	12.5	12.5	15.1	15.4
10.6	11.5	11.8	11.9	12.1	11.2	11.1	12.7	12.9
15.6	16.8	17.3	18.1	18.2	20	19.8	21.6	22.1
18.3	19.8	20.3	22.8	22.9	25.4	25.3	28.2	29
74.4	81.1	81.8	80.9	81	80.5	80.6	81.4	81.6
30.2	35.3	36.2	21.9	22	31.9	40.1	35.5	41.6
28.9	32.3	33	25.1	25.2	19.8	20.2	20	20.6
35.8	39.2	39.8	34	33.7	25.4	26.2	24	24.7
34.8	38.1	38.8	37.8	38	32.9	33	31.2	31.9
36	39.1	39.8	39.2	39.3	36.3	36.5	35.3	36
17.8	17.8	17.8	17	17	15	15	12	12
0.02	0.02	0.02	0.029	0.029	0.043	0.043	0.051	0.051
21.13	21.54	21.56	31.82	31.82	47.06	47.06	55.36	55.35
6982	6982	6976	10365	10362	15528	15523	18358	18346
2.85	2.85	2.85	3.95	3.95	9	9	12.7	12.7
7212	7212	7212	10634	10634	15697	15697	18776	18776
1.033	1.033	1.034	1.026	1.026	1.011	1.011	1.023	1.023
427	427	427	464	464	546	546	606	606
515	515	515	477	477	395	395	333	333
582	582	582	599	599	644	644	673	673
403	403	403	385	385	342	342	312	312
518	518	518	528	528	540	540	553	553
483	483	483	474	474	462	462	448	448
520	520	520	523	523	527	527	532	532
505	505	505	503	503	497	497	493	493
487	487	487	465	465	404	404	364	364
516	516	516	537	537	599	599	639	639
29	29	29	72	72	195	195	275	275
1.019	1	0.998	1.005	1.004	1.018	1.017	1.023	1.022

	549	550	551	552	553	554	555	556
	27.3	29.9	30	32.1	32.1	32.5	32.4	34.9
	20.2	22.8	22.5	22.9	22.9	22.8	22.9	23.7
	47.2	10.5	10.3	6.4	6.5	7.7	7.7	7
	44.4	10.5	10.2	6.9	6.9	6.1	6	5.3
	41.7	13.9	13.6	11.4	11.4	9.8	9.6	11.3
	39.8	15.6	15.2	13.4	13.4	13.1	12.9	15
	60.4	62.6	59.9	60.7	60.5	59.7	59.5	60.5
	60.1	9	8.8	8.5	8.6	29.1	29.5	14.2
	61.7	17	16.3	20.4	20.2	15	15.1	11.9
	59.9	23	21.5	25.5	25.2	22.3	22.2	16.1
	56.9	23.7	22.6	27.1	27.1	25.1	24.7	21.8
	54.3	26.1	24.9	27.7	27.4	26.9	26.6	24.4
	18.5	18.5	18.5	17.8	17.8	17	17	15
	0.011	0.01	0.01	0.019	0.019	0.029	0.029	0.043
	10.93	10.95	10.86	20.16	20.14	29.38	29.37	44.33
	3754	3738	3737	6933	6933	10181	10183	15488
	0	1.7	1.7	2.8	2.8	3.9	3.9	9
	0	3722	3722	7171	7171	10158	10158	15600
	0	0.996	0.996	1.034	1.034	0.998	0.998	1.007
	406	406	406	428	428	462	462	541
	535	535	535	513	513	480	480	398
	570	570	570	580	580	598	598	647
	415	415	415	405	405	386	386	338
	515	515	515	520	520	526.5	526.5	531
	487	487	487	481	481	475	475	471
	518	518	518	519	519	521	521	523
	506	506	506	505	505	502	502	502
	500	500	500	487	487	465	465	409
	503	503	503	515	515	537	537	593
	3	3	3	28	28	72	72	184
	1.059	1.052	1.061	1.061	1.061	1.069	1.069	1.077

557	558	559		599	600	601	602	603
35.2	33.6	34.3		27.2	28.5	29	30.1	30
23.8	19.8	20.2		18	18	18	18.3	18.2
7	5.8	6.7		47.2	2.2	2.6	-1.4	-1.4
5.4	6.1	6.7		44.4	2.3	2.1	-1.3	-1.3
11.5	12	13.6		11.1	5.2	4.9	2.7	2.7
15.2	15.2	16.9		13.1	7.3	6.2	3.6	3.6
60.8	57.5	60.6		60.8	61	59.8	59.6	59.6
16.3	12.2	13.9		21.7	7.9	4.8	2.2	2.4
12.2	11.1	12.5		25.8	17	12.7	12.4	12.9
16.5	15.4	17.3		29.2	21.1	17.7	18.7	19.8
22.2	20.6	22.4		27.7	21.5	19	20.6	21.1
24.7	23.4	25.5		29	24.1	23	22	22
15	12	12		18.5	18.5	18.5	18	18
0.043	0.052	0.052		0.011	0.011	0.011	0.019	0.019
44.35	52.2	52.63		11.12	11.1	11.05	19.41	19.41
15481	18553	18532		3815	3806	3803	6698	6699
9	12.7	12.7		1.7	1.86	1.86	3.4	3.4
15600	15652	15652		3722	3900	3900	6757	6757
1.008	0.844	0.845		0.976	1.025	1.025	1.009	1.009
541	605	605		396	397	397	415	415
398	335	335		544	544	544	527	527
647	679	679		580	580	580	591	591
338	305	305		405	406	406	395	395
531	542	542		494	494	494	495	495
471	460	460		508	508	508	505	505
523	526	526		509	509	509	509	509
502	498	498		515	515	515	514	514
409	367	367		500	500	500	488	488
593	636	636		503	503	503	515	515
184	269	269		3	3	3	27	27
1.077	1.096	1.086		1.058	1.057	1.061	1.064	1.064

604	605	606	607	608	609	610	611
30.7	30.7	34	35	36	36.1	36.5	36.5
18.3	18.5	20.5	21.1	21.7	21.7	22	22
-1.6	-1.4	0	0.2	0.4	0.5	0.6	0.6
-2.5	-2.5	-3.4	-3.8	-3.8	-3.8	-3.2	-3.3
1.7	1.8	1.7	1.3	1.5	1.3	2.5	2.8
4.1	4.1	4.2	3.8	4.7	4.6	6.4	7
60.3	60.3	60.2	60.7	61	61.2	61.5	61.5
3.5	3.5	6.2	6.9	5.1	5.6	7.4	8.2
4	4.3	1.6	2.1	2.3	2.3	2.7	2.8
14.2	15.4	0.8	1.2	0.6	0.6	1.6	1.7
18.5	18.6	7.2	7.2	6.7	6.9	8.3	8.5
20.5	20.5	10.8	10.9	10.6	10.6	12.2	12.5
17	17	11.8	11.8	8	8	8	8
0.029	0.029	0.052	0.052	0.054	0.053	0.053	0.053
30.44	30.44	52.83	52.82	54.18	54.2	54.22	54.22
10533	10533	18645	18615	19109	19106	19093	19093
6	6	10	10	10	10	9	9
10444	10444	20995	21234	20761	20761	19169	19169
0.992	0.992	1.126	1.141	1.086	1.087	1.004	1.004
452	452	595	595	612	612	612	612
489	489	345	345	328	328	328	328
615	615	695	695	696	696	696	696
370	370	290	290	290	290	290	290
498	498	519	519	533	533	533	533
503	503	483	483	468	468	468	468
510	510	520	520	523	523	523	523
513	513	504	504	500	500	500	500
462	462	360	360	352	352	352	352
540	540	642	642	652	652	652	652
78	78	282	282	300	300	300	300
1.067	1.067	1.088	1.087	1.088	1.087	1.086	1.086

699	700	701	702	703	704	705	706	707
27.7	28.2	28.4	30	30.1	30.9	31.1	29.4	30.5
17.5	18.3	18.8	19.9	20.4	21.5	21.7	22.5	23.3
3.9	4.5	4.7	2.2	2.3	3.4	3.4	3.5	4.3
5	5	5	2.1	2.2	2.2	2.2	5.6	5.8
8.1	7.2	7.2	7.5	7.6	7.1	7.2	9	8.8
9.8	9	9	10	10.1	11.7	11.7	13.6	13.9
80.6	80.5	80.3	80.3	80.3	80.3	80.1	80.1	80.8
10.8	12.3	12.9	4.4	4.6	7.6	7.7	5.8	5.8
17.3	16.7	16.3	14.2	14.3	9.5	9.7	9.9	8.8
25.2	24.2	24.4	24.6	24.6	19	19.5	18.1	15.7
26.8	25.4	25.1	29.1	29.1	26.5	26.7	27.4	25.4
30.2	30.3	29.6	30.8	30.5	29	29.4	30.1	28.8
18.5	18.5	18.5	17.8	17.8	17	17	15.8	15.8
0.01	0.011	0.011	0.02	0.02	0.029	0.029	0.04	0.04
11.51	11.72	11.71	21.52	21.52	32.11	32.22	43.86	43.87
3729	3798	3796	6994	6993	10482	10526	14426	14400
1.86	1.86	1.82	2.8	2.8	6	6	5	5
3987	4031	3943	7110	7110	10724	10444	14240	14100
1.069	1.061	1.039	1.017	1.017	1.023	0.992	0.987	0.979
384	383	383	405	405	441	452	498	498
558	558	558	536	536	500	489	443	443
593	593	593	604	604	625	615	660	660
393	391	391	381	381	359	370	325	325
470	468	468	476	476	481	498	483	483
530	533	533	524	524	519	503	518	518
501	501	501	504	504	505	510	506	506
522	513	513	520	520	518	513	518	518
500	500	500	486	486	462	462	426	426
503	503	503	515	515	540	540	576	576
3	3	3	29	29	78	78	150	150
0.999	0.999	1	1.002	1.002	1.007	1.007	1.014	1.012

708	709	710	711	712	713	714		750
31.6	31.9	33.6	33.4	33.7	34	34.2		28.7
23.6	23.8	24.5	24.5	23.8	23.9	23.8		13.5
3	3.1	7.3	7.2	5.3	5.1	3.5		1.1
3.9	3.3	9.7	9.9	7.8	7.3	5.6		1.8
8.1	7.8	12.9	13.7	12.7	12.8	8.1		4.7
13.2	12.2	16.5	17.1	15.9	16.5	10		6.6
80.3	81.1	80.1	80.1	80.9	80.7	81		60.1
8	6.4	7	10.7	5.8	14.3	5.9		2.2
8.3	8.6	6.1	6.3	5.2	5.7	5.1		5.6
16.2	17.4	9.1	9.5	8.9	9.1	8.4		11.6
25.7	26.1	20.2	20.5	19	19.4	16.8		11.6
29	29	23	23.4	21.6	22.1	19.3		16.1
15.8	15.8	12	12	12	12	12		18.5
0.04	0.04	0.052	0.052	0.052	0.052	0.052		0.011
43.72	43.8	55.34	55.36	55.46	55.4	55.43		11.32
14374	14367	18464	18470	18461	18452	18446		3891
5	5	6.8	6.8	7.5	7.5	7.5		1.8
14100	13828	18531	18531	18800	18531	21531		3929
0.981	0.963	1.004	1.003	1.018	1.004	1.167		1.01
498	498	581	581	581	581	581		408
443	443	359	359	359	359	359		533
660	660	704	704	704	704	704		569
325	325	281	281	281	281	281		416
483	483	499	499	499	499	499		523
518	518	503	503	503	503	503		477
506	506	513	513	513	513	513		520
518	518	513	513	513	513	513		504
426	426	352	352	352	352	352		500
576	576	652	652	652	652	652		503
150	150	300	300	300	300	300		3
1.014	1.012	1.029	1.029	1.027	1.027	1.026		1.06

751	752	753	754	755	756	757	758	759
29	29.2	31.3	31.1	32	32.1	32.9	33.2	34.6
13.3	13.6	14	14.2	14.8	15	15.6	15.6	16.6
1.4	1.6	-1.9	-1.9	-1.7	-1.6	-0.8	-0.6	-0.3
1.7	1.9	-1.1	-1.1	-1.8	-1.9	0	0	0.2
3.9	3.6	1.6	1.6	0.8	0.6	0.7	0.8	1.5
5.8	5.2	1.5	1.5	0.8	0.6	0.9	0.8	1.1
59.6	59.4	61	61	59.6	59.2	59.1	60.1	59.7
1.7	1.7	3.5	2.8	0.2	0.8	0.8	0.3	1.4
5.4	4.6	4.9	4.6	1.3	1.5	0.3	0.6	-0.3
10.1	9.4	10.9	10.8	5.2	5.2	2.2	2.4	0.8
10.2	9.2	12.9	13	9.4	9.4	6.3	6.6	3.6
14.5	13.1	15.4	14.7	11.5	11.5	7.6	8	4.8
18.5	18.5	17.8	17.8	17	17	15.8	15.8	15.8
0.011	0.011	0.019	0.019	0.029	0.029	0.04	0.04	0.052
11.29	11.28	19.9	19.9	29.63	29.59	40.45	40.55	52.15
3889	3887	6837	6839	10272	10270	14151	14144	18418
1.8	1.8	2.8	2.8	3.85	3.85	5.1	5.1	6.75
3929	3929	6871	6871	10291	10291	14236	14236	18894
1.01	1.011	1.005	1.005	1.002	1.002	1.006	1.007	1.026
408	408	430	430	463	463	520	520	605
533	533	512	512	478	478	420	420	335
569	569	577	577	599	599	629	629	675
416	416	407	407	387	387	355	355	310
523	523	428	428	530	530	540	540	553
477	477	473	473	470	470	460	460	448
520	520	519	519	520	520	524	524	529
504	504	505	505	503	503	500	500	496
500	500	488	488	464	464	425	425	365
503	503	514	514	538	538	578	578	637
3	3	26	26	74	74	153	153	272
1.062	1.062	1.06	1.06	1.069	1.07	1.079	1.076	1.089

760		799	800	801	802	803	804	805
35.1		29.5	29.1	29.2	31	30.9	31.7	31.6
16.9		22.9	23.7	23.8	24	24	24.2	24.2
-0.2		46.7	3.8	3.8	1.3	1.4	1.5	1.5
0.1		42.8	4.2	4.3	2	2	1.8	1.7
1.5		39.7	6.5	6.3	5	4.9	4.9	4.8
1.1		38.1	8.3	8.2	5.3	5	5.6	5.5
59.8		60.9	58.4	58.8	61.1	61	60.5	60.1
1.8		60.5	5.6	5.6	7.6	8	3.3	3.3
-0.2		62.2	8.6	8.3	8.5	7.4	5.5	5.5
1		60	12.5	13.1	13.1	12.7	9.6	9.2
3.5		56.8	13.4	13.6	14.5	14	13.6	13.5
4.8		53.9	26.4	26.2	23.5	20.8	23.2	21.5
15.8		18.5	18.5	18.5	17.8	17.8	17	17
0.052		0.011	0.011	0.011	0.02	0.02	0.028	0.028
52.13		11.31	11.24	11.25	20.3	20.3	29.17	29.14
18403		3880	3883	3882	6974	6975	10082	10083
6.75		0	1.8	1.8	2.85	2.85	3.85	3.85
18894		0	3857	3857	6870	6870	9964	9964
1.027		0	0.993	0.994	0.985	0.985	0.988	0.988
605		404	404	404	423	423	455	455
335		537	537	537	518	518	486	486
675		573	573	573	585	585	604	604
310		412	412	412	400	400	381	381
553		514	514	514	515	515	419	419
448		487	487	487	486	486	481	481
529		514	514	514	515	515	517	517
496		508	508	508	408	408	506	506
365		500	500	500	488	488	465	465
637		503	503	503	515	515	537	537
272		3	3	3	27	27	72	72
1.089		1.058	1.066	1.064	1.059	1.06	1.066	1.067

806	807		1000	1001	1002	1003	1004	1005
32.5	32.5		27.2	27.4	27.8	29	28.9	28.9
24.2	24.3		18.6	18.7	18.9	19.5	19.5	19.8
2	2		6.3	7.4	7.3	3.4	3.2	2.4
3.3	3.3		9	9	8.5	5.9	5.7	4.1
4.7	4.4		11.9	11.6	11.8	12.7	11.9	7.8
5.6	4.9		13.6	13.8	13.6	15	14.5	8.2
58.8	58.4		64.8	65.2	65	48.6	48.6	48.5
4	3.5		30.8	33.2	35.3	22.9	17	6.9
3.7	3.8		41.9	40.9	34.3	21.3	20.5	15
6.9	6.3		34.2	34.8	29.5	24.2	23.8	18.7
10.4	10.2		28.2	28	27.7	23.3	23.2	17.8
18.9	17.7		35.5	35.3	33	31.5	31.4	23.8
15.8	15.8		18.5	18.5	18.5	17.8	17.8	17.8
0.04	0.04		0.011	0.011	0.011	0.017	0.017	0.017
40.43	40.38		11.08	11.08	11.07	17.47	17.47	17.46
14159	14159		3754	3753	3751	6234	6235	6235
5.1	5.1		1.7	1.7	1.7	1.7	1.7	2.8
14165	14073		3829	3829	3829	3829	3829	6986
1	0.994		1.02	1.02	1.021	0.614	0.614	1.12
515	515		406	406	406	420	420	420
425	425		535	535	535	519	519	519
635	635		570	570	570	578	578	578
350	350		415	415	415	407	407	407
530	530		515	515	515	522	522	522
472	472		487	487	487	480	480	480
521	521		518	518	518	519	519	519
503	503		506	506	506	505	505	505
423	423		500	500	500	487	487	487
579	579		503	503	503	515	515	515
156	156		3	3	3	28	28	28
1.08	1.081		1.045	1.044	1.045	1.101	1.101	1.101

1006	1007	1008	1009	1010	1011	1012	1013	1014
29.3	30.2	29.4	29.8	29.8	29.6	29.7	29.8	29.8
20	20.2	20	20.2	20.5	20.6	20.7	21.1	20.8
2.5	6.1	6.4	4.2	4.3	7.9	7.6	5.8	5.3
4	6.6	7.1	3.5	3.6	8.9	9.1	6.2	6
7.2	12.1	12.8	7	6.8	11.4	11.5	9.6	9.3
8	16.4	17.2	9.2	9.2	14.9	14.8	11.9	11.5
48.6	53	52.5	51.9	51.9	52.6	52.3	51.4	51.1
7.3	10.7	10.5	18.9	20	24.6	24.2	6.8	6.7
15.3	16	14.9	10.8	11.2	10	10	7.4	7.1
19	23.8	21.5	18.6	19.2	18.1	18	12.5	12
17.8	26.7	25.8	20.7	20.7	22.8	22.7	19.3	18.8
23.9	34.2	33.8	27.5	27.7	28.2	28	23.2	22.6
17.8	17	17	17	17	15	15	15	15
0.017	0.028	0.028	0.028	0.028	0.04	0.04	0.04	0.04
17.46	28.61	28.61	28.53	28.53	40.07	40.03	39.91	39.87
6231	10110	10124	10117	10117	14294	14291	14289	14289
2.8	2.7	2.7	3.9	3.9	3.9	3.9	5.5	5.5
6986	6640	6640	10372	10372	10372	10372	15258	15258
1.121	0.657	0.656	1.025	1.025	0.726	0.726	1.068	1.068
420	458	458	458	458	514	514	514	514
519	483	483	483	483	425	425	425	425
578	600	600	600	600	637	637	637	637
407	385	385	385	385	347	347	347	347
522	525	525	525	525	525	525	525	525
480	475	475	475	475	475	475	475	475
519	518	518	518	518	518	518	518	518
505	505	505	505	505	505	505	505	505
487	468	468	468	468	426	426	426	426
515	533	533	533	533	576	576	576	576
28	65	65	65	65	150	150	150	150
1.101	1.09	1.091	1.093	1.093	1.1	1.101	1.104	1.105

1015	1016	1017	1018	1019	1020		1040	1041
30.1	30.2	31.5	32.1	33.3	33.6		27.6	28.2
21.2	21.2	21.5	21.7	22	22.1		19.3	19.8
9.4	8.9	5.2	5.3	5.6	5.8		0	0.8
10.9	9.7	7.3	7.3	6.9	6.7		1.3	1.2
15.1	14.7	11.5	11.3	9.9	9.9		5.9	3.8
18.4	17.9	13.4	13.5	11.4	11.5		7	5.2
51.4	50.7	50.9	51.4	52.4	52.6		38.8	39.1
6.8	6.4	6.4	6.6	7.3	7.9		0.1	1.5
6.9	6.5	5.6	5.9	6.3	6.6		5.8	5.2
11.7	11.4	8.8	9.1	8.9	9.4		9.8	9.5
20	19.4	15.9	16.1	15.2	15.5		10.4	9.6
22	21.9	16.4	16.6	14.2	14.5		13.8	13.4
12	12	12	12	12	12		18.5	18.5
0.052	0.052	0.052	0.052	0.052	0.052		0.011	0.011
51.71	51.59	51.51	51.54	51.6	51.6		10.38	10.38
18714	18711	18671	18652	18616	18607		3812	3808
5.5	5.5	8	8	11	11		1.7	1.7
15258	15258	19850	19850	22222	22222		3550	3550
0.815	0.815	1.063	1.064	1.194	1.194		0.931	0.932
601	601	601	601	601	601		394	394
338	338	338	338	338	338		547	547
686	686	686	686	686	686		582	582
300	300	300	300	300	300		402	402
535	535	535	535	535	535		493	493
466	466	466	466	466	466		507	507
522	522	522	522	522	522		507	507
501	501	501	501	501	501		516	516
369	369	369	369	369	369		500	500
633	633	633	633	633	633		503	503
264	264	264	264	264	264		3	3
1.116	1.119	1.118	1.116	1.113	1.112		1.133	1.132

1042	1043	1044	1045	1046	1047	1048	1049	1050
28	29	29.1	29.2	29.3	30.1	29.8	29.4	29.6
19.8	20.1	20.2	20.5	20.9	20.9	20.9	21.1	21.1
0.8	-1.4	-1.3	-2.1	-2.1	0.2	0.2	-1.7	-1.8
1.1	0.7	0.8	-1.2	-1.2	0.3	0.4	-1.4	-1.5
3.4	6.8	6.9	2.3	1.7	5	5.2	2.3	2.3
4.8	9.6	9.8	2.3	1.9	9.2	9.4	4.4	4.3
38.8	48.5	48.6	48.4	48.6	53.1	52.6	51.9	51.8
0.5	3.9	4	2	4.6	19.1	18.2	0.7	0.6
4.8	10.6	10.4	5.9	6.8	6.4	6.4	3.3	3.2
9.2	16.9	16.8	11	11.3	15.1	14.8	9.4	9.2
8.9	19.5	19.8	12.3	11.7	20.5	20.3	15.4	15.4
13.4	27.4	27.7	19.8	20	26.9	26.6	19.8	19.8
18.5	17.8	17.8	17.8	17.8	17	17	17	17
0.011	0.017	0.017	0.017	0.017	0.028	0.028	0.028	0.028
10.37	17.37	17.38	17.36	17.37	28.77	28.74	28.69	28.68
3809	6197	6196	6195	6194	10166	10171	10178	10175
1.7	1.7	1.7	2.7	2.7	2.7	2.7	3.8	3.8
3550	3550	3550	6813	6813	6813	6813	10273	10273
0.932	0.573	0.573	1.1	1.1	0.67	0.67	1.009	1.01
394	407	407	407	407	440	440	440	440
547	533	533	533	533	500	500	500	500
582	591	591	591	591	618	618	618	618
402	394	394	394	394	366	366	366	366
493	593	593	593	593	488	488	488	488
507	507	507	507	507	412	412	412	412
507	507	507	507	507	506	506	506	506
516	516	516	516	516	517	517	517	517
500	492	492	492	492	466	466	466	466
503	510	510	510	510	535	535	535	535
3	18	18	18	18	69	69	69	69
1.133	1.1	1.1	1.1	1.1	1.09	1.092	1.094	1.094

Station	Dist (m)	1070	1071	1072	1073	1074	1075	1076
T.op		27.2	27.8	28.2	28.7	28.5	28.8	30.1
Fi	0	18.6	18.6	18.8	19.2	19.2	19.6	20
F0	0.1	-2	-1.8	-1.2	-1.6	-1.9	-1.5	-2.1
F1	0.2	-0.9	-1.1	-0.7	-0.1	0.5	1.1	-0.3
F3	0.6	1.1	1.1	1.1	4.4	5	6.4	4.5
F5	1	1.7	1.4	1.3	5.1	5.8	6.6	5.3
Tai	0	39.6	39.6	40.1	40.9	40.7	41.1	51.1
D-1	0.03	0.8	1.3	1.9	0.3	-0.9	1.4	0.3
D0	0.1	-0.9	4.9	-0.8	19.8	11.8	13.1	8.4
D1	0.2	6.3	6.1	9.3	19.2	16.3	16.1	13.4
D3	0.6	7.6	8.1	7	18.9	19.5	19	19.5
D5	1	16.5	15.6	16.1	28.7	28.1	27.7	30.3
VS		18.5	18.5	18.5	18.5	18.5	18.5	17.8
Airflow (kg/s)		0.011	0.011	0.011	0.011	0.011	0.011	0.019
Velocity (m/s)		10.8	10.79	10.8	10.82	10.82	10.82	19.15
F.req (ml/hr)		3957	3953	3950	3947	3948	3946	6780
SS		1.7	1.7	1.7	1	1	1	1.8
F.actual		4000	4000	4000	1512	1512	1512	3960
Equiv ratio		1.011	1.012	1.013	0.383	0.383	0.383	0.584
1		397	397	397	397	397	397	414
2		543	543	543	543	543	543	525
3		580	580	580	580	580	580	590
4		405	405	405	405	405	405	393
5		500	500	500	500	500	500	500
6		500	500	500	500	500	500	502
7		510	510	510	510	510	510	509
8		513	513	513	513	513	513	514
Pipe press A		500	500	500	500	500	500	490
B		503	503	503	503	503	503	513
Tot int (mm)		3	3	3	3	3	3	23
Density (kg/m^3)		1.13	1.13	1.128	1.125	1.126	1.124	1.092

1076	1077	1078	1079	1080	1081	1082	1083	1084	1085
30.1	30.1	29.9	30.1	30.9	30.9	31.1	31.4	31.2	31
20	20.1	20.2	20.4	20.6	20.8	20.9	21.2	21.3	21.3
-2.1	-1.9	-2.3	-2.1	-1.5	-1.3	-2.1	-1.4	0.2	0.2
-0.3	-0.2	-1.3	-1.3	-0.7	-0.6	-1.6	-1.3	1.2	1.1
4.5	4.8	1.1	1.1	3.8	3.9	1.5	1.5	3.9	3.9
5.3	5.6	0.9	1.1	5.6	5.6	1.9	2.2	5.7	5.7
51.1	51.1	50.5	50.6	53.5	53.2	52.9	53	53.5	53.2
0.3	0.6	1.9	2.3	1.1	1.1	1.1	1.3	1.1	1.1
8.4	8.9	3.5	4	2.8	2.5	1.8	1.9	1.6	1.5
13.4	15.6	8.3	8.5	7.9	8.1	5.6	5.2	4.6	4.6
19.5	20.2	9.7	9.6	15.5	15.2	10.4	10.1	11.6	11.4
30.3	30.8	21.9	21.9	23.2	22	16.2	14.2	16.5	17.3
17.8	17.8	17.8	17.8	17	17	17	17	15	15
0.019	0.019	0.019	0.019	0.029	0.029	0.029	0.029	0.04	0.04
19.15	19.15	19.12	19.12	29.41	29.39	29.35	29.34	39.92	39.89
6780	6780	6782	6780	10385	10385	10381	10376	14205	14210
1.8	1.8	2.7	2.7	2.7	2.7	3.8	3.8	3.8	3.8
3960	3960	6770	6770	6770	6770	10336	10336	10336	10336
0.584	0.584	0.998	0.999	0.652	0.652	0.996	0.996	0.728	0.727
414	414	414	414	450	450	450	450	510	510
525	525	525	525	489	489	489	489	429	429
590	590	590	590	613	613	613	613	640	640
393	393	393	393	372	372	372	372	344	344
500	500	500	500	504	504	504	504	519	519
502	502	502	502	496	496	496	496	482	482
509	509	509	509	511	511	511	511	515	515
514	514	514	514	511	511	511	511	508	508
490	490	490	490	465	465	465	465	424	424
513	513	513	513	537	537	537	537	578	578
23	23	23	23	72	72	72	72	154	154
1.092	1.092	1.094	1.093	1.089	1.09	1.091	1.091	1.097	1.098

1086	1087	1088	1089	1090	1091	1092	1093
31.1	31.3	31.4	31.4	31.9	32.2	32.9	33.2
21.5	21.7	22	22.2	22.4	22.5	22.5	22.6
-0.6	-0.7	1.4	1.5	0	-0.1	-1.2	-1.2
0.2	0.2	3.1	2.9	0.8	0.7	-0.4	-0.4
1.7	1.6	4.8	4.9	2.9	2.8	1.8	1.8
2.3	2.3	7.5	6.9	3.2	3.1	1.8	2.1
52.7	52.8	52.4	52.1	52.1	52.2	52.6	52.8
0.7	1.7	1.9	1.2	2.3	2.2	2.1	2.3
1.1	1	0.9	1.1	0.3	0.2	0.4	0.6
2.9	2.7	2.6	2.9	1.3	1.3	1.2	1.5
8.1	8	8.3	8.5	5.5	5.6	4.8	5.5
10.2	10.5	14.5	14.8	7.6	6.9	4.4	6.7
15	15	12	12	12	12	12	12
0.04	0.04	0.052	0.052	0.052	0.052	0.052	0.052
39.83	39.83	51.38	51.34	51.3	51.29	51.29	51.3
14207	14203	18559	18559	18544	18535	18513	18504
5.1	5.1	5.1	5.1	6.7	6.7	8	8
14248	14248	14248	14248	18096	18096	21176	21176
1.003	1.003	0.768	0.768	0.976	0.976	1.144	1.144
510	510	592	592	592	592	592	592
429	429	347	347	347	347	347	347
640	640	691	691	691	691	691	691
344	344	293	293	293	293	293	293
519	519	523	523	523	523	523	523
482	482	477	477	477	477	477	477
515	515	518	518	518	518	518	518
508	508	505	505	505	505	505	505
424	424	364	364	364	364	364	364
578	578	639	639	639	639	639	639
154	154	275	275	275	275	275	275
1.1	1.1	1.114	1.115	1.115	1.115	1.113	1.112

1100	1101	1102	1103	1104	1105	1106	1107	1108
29	29.4	29.5	29.4	29.5	29.6	30.9	30.8	30.7
20.5	20.6	20.7	21.7	21.7	21.9	22.2	22.3	22.5
4.9	6	6.1	11	11.1	11.4	4.6	4.4	3.6
7.1	7.4	7.5	15	14.9	15.2	6.6	6.4	4.8
10.2	10.2	10.2	23.8	24	24	12.9	12.6	9.2
10.7	10.5	10.4	18.9	19.1	19	14.6	14.4	9.6
90	90.7	90.9	91.3	91.5	91.6	80.1	79.7	80.6
6.4	6.5	6.5	9.5	9.2	9.5	5.8	5.7	6.3
17.5	17.2	16.5	28.9	28.2	27.9	14	13.4	11.8
26.1	25	24.4	43	45.8	42.1	23.2	23.1	20.2
22.9	22.9	21.8	49.5	49.2	47.5	31.7	31.4	25.5
38.1	36.4	35.2	59.8	59.5	59.7	43.1	42.6	37.2
18.5	18.5	18.5	18.5	18.5	18.5	17.8	17.8	17.8
0.011	0.011	0.011	0.011	0.011	0.011	0.019	0.019	0.019
12.1	12.11	12.12	12.13	12.14	12.14	20.76	20.74	20.79
3816	3814	3813	3814	3813	3813	6748	6749	6751
1.7	1.7	1.7	1	1	1	2.1	2.1	2.7
3901	3901	3901	1505	1505	1505	4878	4878	6977
1.022	1.023	1.023	0.395	0.395	0.395	0.723	0.723	1.034
406	406	406	406	406	406	422	422	422
533	533	533	533	533	533	517	517	517
569	569	569	569	569	569	583	583	583
415	415	415	415	415	415	403	403	403
520	520	520	520	520	520	517	517	517
480	480	480	480	480	480	482	482	482
516	516	516	516	516	516	516	516	516
506	506	506	506	506	506	507	507	507
500	500	500	500	500	500	486	486	486
503	503	503	503	503	503	515	515	515
3	3	3	3	3	3	29	29	29
0.973	0.971	0.97	0.969	0.969	0.969	1.003	1.004	1.001

1109	1110	1111	1112	1113	1114	1115	1116	1117
30.7	31.6	31.2	31.2	31.4	31.6	31.5	32.3	32.5
22.5	22.8	22.8	22.9	23.1	23.1	23.3	23.4	23.4
3.6	4.9	4.8	4.7	4.8	6.9	6.9	5.1	5
4.8	6	5.8	4.9	5	8.9	8.9	6.3	6.1
8.8	11.7	11.5	9	9.1	13.4	13.6	8.2	8.1
9.6	16.5	15.9	11.1	11.3	18.2	18.2	9.4	9.3
80.5	73.6	72.8	81.5	81.9	79.5	79.4	78.1	78.3
6.3	4.9	4.8	7.1	7.4	6.4	6.4	8.8	8.9
12.1	8.5	8.5	9.2	9.4	8.7	8.8	6.4	6.4
20.4	16.1	15.5	15.5	15.7	14.5	14.6	9.2	9.2
25.5	27.1	26.9	24.7	25.2	25.2	24.9	17.3	17.3
36.5	34	33.6	31.7	32.3	29.6	30.9	19.3	19.3
17.8	17	17	17	17	15	15	15	15
0.019	0.028	0.028	0.028	0.028	0.039	0.039	0.039	0.039
20.79	30.23	30.18	30.94	30.96	42.7	42.7	42.49	42.5
6751	10056	10063	10063	10059	14082	14084	14066	14061
2.7	2.7	2.7	3.7	3.7	3.7	3.7	5.5	5.5
6977	6977	6977	10118	10118	10118	10118	14742	14742
1.034	0.694	0.693	1.005	1.006	0.719	0.718	1.048	1.048
422	455	455	455	455	512	512	512	512
517	485	485	485	485	427	427	427	427
583	602	602	602	602	635	635	635	635
403	383	383	383	383	350	350	350	350
517	522	522	522	522	528	528	528	528
482	479	479	479	479	473	473	473	473
516	517	517	517	517	519	519	519	519
507	506	506	506	506	503	503	503	503
486	463	463	463	463	421	421	421	421
515	538	538	538	538	580	580	580	580
29	75	75	75	75	159	159	159	159
1.002	1.026	1.028	1.003	1.002	1.017	1.017	1.021	1.02

1118	1119	1120	1121		1130	1131	1132	1133
32.6	32.5	33.5	33.7		29.3	30.1	30.3	31.5
23.6	23.6	23.6	23.6		18.4	19.2	19.3	19.8
9.1	9.3	4.8	4.9		0	3.8	3.8	0.9
10.8	10.8	6.1	6.1		0.4	5.2	5	2.3
14.7	14.8	9.5	9.5		2.5	7.9	7.8	6
23.2	23.5	12.3	12.7		2.7	8.1	8	6.3
79.6	79.7	79.8	80.3		41.1	76.9	77.3	69.7
10.4	10.1	9.1	9.2		-1	6.4	6.3	7.3
7.2	6.9	6	6.1		1.8	11.3	11.3	7.4
10.2	10.2	8.1	8		4	16.9	16.6	15
19.3	19.5	14.2	14.3		4	15.9	15.3	19.4
25.9	26.4				8.7	24.9	24.2	30.7
12	12	12	12		18.5	18.5	18.5	17.8
0.051	0.051	0.052	0.052		0.011	0.011	0.011	0.019
54.88	54.91	55.52	55.58		10.64	11.84	11.85	20.5
18309	18312	18495	18489		3881	3875	3874	6866
5.5	5.5	8.5	8.5		1.7	1.7	1.7	2.5
14742	14742	19700	19700		3323	3323	3323	5932
0.805	0.805	1.065	1.065		0.856	0.857	0.858	0.864
597	597	592	592		402	402	402	426
341	341	347	347		537	537	537	514
677	677	691	691		573	573	573	580
308	308	293	293		410	410	410	404
543	543	523	523		512	512	512	524
457	457	477	477		488	488	488	475
525	525	518	518		514	514	514	518
499	499	505	505		509	509	509	505
359	359	364	364		500	500	500	488
643	643	639	639		503	503	503	514
284	284	275	275		3	3	3	26
1.029	1.029	1.027	1.026		1.124	1.009	1.008	1.033

1134	1135	1136	1137	1138	1139	1140	1141	1142
31.6	31.6	31.8	32.6	32.4	32.6	32.7	33.1	33
20	20.4	20.5	20.9	21.1	21.4	21.5	21.7	21.8
1	1	0.9	1.9	1.9	1.2	1.1	1.7	1.5
2.3	1.9	1.7	2.5	2.5	1.3	1.4	3.1	2.8
6	4.4	4.3	6.3	6.4	4.5	4.4	6	5.7
6.6	4.9	4.8	9	9.3	5.5	5.6	7.9	7.3
69.5	70.1	70.7	68.9	68.6	70.7	70.9	68.4	67.7
7	4.1	4.1	5.6	6.1	4.7	5.8	12.9	12.9
7.9	6.4	6.5	5.8	6	4.8	5	4.2	3.5
15.8	12.9	12.9	11.9	11.9	9.4	9.6	7.2	6.8
19.9	17	17.2	21.4	22	16.9	17.4	14.3	14.5
30.7	25.2	25.2	28.6	28.5	21.9	21.5	17.9	16.7
17.8	17.8	17.8	17	17	17	17	15	15
0.019	0.019	0.019	0.028	0.028	0.028	0.028	0.04	0.04
20.49	20.52	20.55	29.82	29.81	29.98	29.99	41.53	41.45
6865	6865	6862	10054	10057	10054	10052	14144	14146
2.5	2.9	2.9	2.9	2.9	4.3	4.3	5.5	5.5
5932	6951	6951	6951	6951	9902	9902	12408	12408
0.864	1.013	1.013	0.691	0.691	0.985	0.985	0.877	0.877
426	426	426	459	459	459	459	519	519
514	514	514	480	480	480	480	420	420
580	580	580	597	597	597	597	630	630
404	404	404	387	387	387	387	355	355
524	524	524	533	533	533	533	539	539
475	475	475	468	468	468	468	461	461
518	518	518	521	521	521	521	523	523
505	505	505	503	503	503	503	500	500
488	488	488	466	466	466	466	420	420
514	514	514	536	536	536	536	582	582
26	26	26	70	70	70	70	162	162
1.033	1.032	1.03	1.04	1.041	1.034	1.034	1.05	1.052

1143	1144	1145	1146	1147		1160	1161	1162
33.4	33.7	33.8	33.6	34		29.3	29.9	30.1
22.1	22.4	22.6	22.6	22.8		16.9	17.3	17.4
1.3	1.2	2.4	2.3	1.7		4.9	5.6	5.4
1.9	1.9	3.8	3.8	3		6.4	6.9	6.8
4.4	4.3	8.3	8.3	6.9		9	9.6	9.4
5.1	5.1	15	15.2	11.4		9.2	9.8	9.9
70.8	70.4	68.1	67.6	71.5		81.8	81.6	81.8
18.2	19.9	18.1	16.8	18.4		8.8	8.9	9
3.5	3.5	3.2	3.1	3.7		14	13.1	12.9
6	6.1	5.4	5.3	5.6		19.2	18	16.9
12.6	12.4	12.3	12.5	11.8		18.7	17.8	16.9
13.8	13.7	15.6	15.9	15		27.3	24.8	23.8
15	15	12	12	12		18.5	18.5	18.5
0.04	0.04	0.051	0.051	0.051		0.01	0.01	0.01
41.8	41.73	53.14	53.08	53.66		11.61	11.59	11.59
14137	14130	18323	18329	18317		3746	3743	3741
7	7	7	7	12.5		1.7	1.7	1.7
13982	13982	13982	13982	16765		3890	3890	3890
0.989	0.99	0.763	0.763	0.915		1.038	1.039	1.04
519	519	601	601	601		410	410	410
420	420	337	337	337		530	530	530
630	630	674	674	674		565	565	565
355	355	311	311	311		419	419	419
539	539	552	552	552		527	527	527
461	461	449	449	449		473	473	473
523	523	528	528	528		518	518	518
500	500	496	496	496		505	505	505
420	420	360	360	360		500	500	500
582	582	642	642	642		503	503	503
162	162	282	282	282		3	3	3
1.043	1.044	1.063	1.065	1.053		0.995	0.996	0.995

1163	1164	1165	1166	1167	1168	1169	1170	1171
31.7	31.8	32.1	31.9	32.1	32	30.9	31.6	32.3
17.8	18	18.4	18.6	19	19.1	20.1	20.4	20.9
2.9	2.9	3.7	3.8	5.1	5.2	4	4.1	5.2
3.7	3.8	3.8	3.9	6.7	6.6	5.8	5.9	6.9
7.1	7.3	7.6	7.6	9.6	9.6	7.7	7.8	9.3
7.9	7.9	9.4	9.4	11.8	11.7	8.9	8.9	10.3
76.1	75.9	79.8	79.1	80.1	79.4	79.4	80.5	79.5
7.6	7.5	10.1	10.9	26.6	27.6	8.7	12.1	17.9
10.2	10.2	8.5	8.5	7.2	7.6	6.1	6.4	7
16.5	16.4	13.8	14.2	10.9	11.2	8.9	9.4	9.1
20.4	20.6	20.5	20.8	17.3	17.5	14	14.7	13.8
29.4	29.8	26.9	27.6	24.8	23.4	19.2	19.2	20.2
17.8	17.8	17	17	15	15	15	15	12
0.019	0.019	0.028	0.028	0.043	0.043	0.044	0.044	0.051
20.41	20.39	30.78	30.72	47	46.91	47.27	47.36	55.03
6710	6709	10058	10061	15532	15534	15646	15628	18365
2.8	2.8	4.3	4.3	7	7	8	8	12.7
7000	7000	10142	10142	14244	14244	16172	16172	18411
1.043	1.043	1.008	1.008	0.917	0.917	1.034	1.035	1.002
429	429	461	461	542	542	539	539	601
510	510	477	477	396	396	399	399	337
575	575	595	595	644	644	650	650	674
410	410	390	390	340	340	334	334	310
530	530	531	531	536	536	526	526	545
469	469	469	469	463	463	474	474	455
519	519	517	517	520	520	517	517	524
504	504	505	505	503	503	505	505	498
487	487	464	464	401	401	403	403	358
515	515	538	538	600	600	598	598	643
28	28	74	74	199	199	195	195	285
1.014	1.015	1.008	1.01	1.019	1.021	1.021	1.018	1.029

1172	1173	1174	1175		Station	Dist (m)	1200	1201
32.4	32.6	33	33		T.op		28.6	28.6
20.9	21.1	21.3	21.5		Fi	0	21.1	21.1
5.6	5.4	5.6	5.6		F0	0.1	6.7	6.7
6.8	6.7	6.9	6.9		F1	0.2	7.6	7.6
9.1	9.2	9.6	9.7		F3	0.6	11	11.1
9.9	10.2	10.6	11		F5	1	12.5	12.9
79.7	80	80.3	80.1		Tai	0	59.2	59
16.5	17.7	17.7	17.8		D-1	0.03	20.9	22.7
6.5	6.9	7	7.2		D0	0.1	18.7	18.5
9	9.1	9.1	9.3		D1	0.2	26	26.6
13.6	13.8	13.8	13.9		D3	0.6	24	23.5
19.2	18.6	20	20.2		AV	0.2	34.5	33.7
12	12	12	12		VS		18.5	18.5
0.051	0.051	0.051	0.051		Airflow (kg/s)		0.01	0.01
55.05	55.08	55.09	55.06		Velocity (m/s)		10.86	10.86
18362	18356	18344	18344		F.req (ml/hr)		3744	3744
12.7	12.7	12.7	12.7		SS		1.7	1.7
18411	18411	18411	18411		F.actual		3840	3840
1.003	1.003	1.004	1.004		Equiv ratio		1.026	1.026
601	601	601	601		1		403	403
337	337	337	337		2		535	535
674	674	674	674		3		571	571
310	310	310	310		4		413	413
545	545	545	545		5		514	514
455	455	455	455		6		485	485
524	524	524	524		7		513	513
498	498	498	498		8		510	510
358	358	358	358		Pipe press A		500	500
643	643	643	643		B		503	503
285	285	285	285		Tot int (mm)		3	3
1.029	1.028	1.027	1.027		Density (kg/m^3)		1.063	1.064

1202	1203	1204	1205	1206	1207	1208	1209	1210
28.7	30.7	30.9	31.9	31.4	32.3	32.3	32.1	32.5
21.5	21.8	22	22.5	22.5	22.7	22.9	23.1	23.2
7.1	5.4	5.6	6.5	6.3	6.7	6.9	5.2	5.4
7.9	6.3	6.4	6.9	6.6	8.5	9	5.2	5.4
11	9.6	9.7	10.6	10.4	14.8	15.6	8.4	8.6
12.7	12.4	12.4	14	14	17.7	18.4	11.1	11.3
59.5	61.3	61.3	60	59.5	60.1	60.1	61.5	62.1
16.1	23.3	22.6	17.5	16.7	22.5	22	22.6	23.4
17.9	21.5	22.5	14.9	14.5	12.9	12.8	14.5	15
26.1	30.4	31.2	24.8	23.8	20.9	20.4	26.1	26.8
23.6	26.9	27.4	26.3	26.1	25.3	25.8	25.8	26.2
31.9	40.6	40.8	35	34.7	32.9	32.7	34	34.4
18.5	17.8	17.8	17	17	15	15	17	17
0.01	0.019	0.019	0.028	0.028	0.044	0.044	0.028	0.028
10.87	19.99	19.99	29.35	29.33	44.6	44.6	29.47	29.51
3744	6865	6863	10161	10170	15626	15626	10158	10151
1.7	3.2	3.2	5	5	12.7	12.7	9	9
3840	7014	7014	10159	10159	13626	13626	11349	11349
1.026	1.022	1.022	1	0.999	0.872	0.872	1.117	1.118
403	422	422	458	458	545	545	458	458
535	517	517	480	480	394	394	480	480
571	584	584	600	600	644	644	600	600
413	401	401	385	385	340	340	385	385
514	515	515	525	525	542	542	525	525
485	485	485	474	474	458	458	474	474
513	514	514	517	517	523	523	517	517
510	510	510	505	505	500	500	505	505
500	487	487	464	464	400	400	464	464
503	515	515	537	537	601	601	537	537
3	28	28	73	73	201	201	73	73
1.062	1.059	1.059	1.068	1.069	1.081	1.081	1.063	1.061

1230	1231	1232	1233	1234	1235	1236	1237	1238
28	28.1	28.3	30.3	30.2	31.1	31.1	31.3	31.2
20.5	20.6	20.7	21.3	21.7	22.3	22.4	22.9	22.9
10.9	11.3	11.8	10.2	9.8	8.1	10.4	24.8	24
13	13.1	13.4	11.8	11.8	10.8	11.4	23	21.4
17.6	17.5	17.7	17	17	16.2	16.7	26.9	26.6
19.9	19.5	19.8	21.3	21.6	20.7	21.1	31.7	31.4
81.5	81.6	81.7	80.5	80.1	78.6	78.6	80.3	79.9
32.9	33.8	32.7	39.9	43.6	27.3	27.9	24.4	25.5
39.1	38.3	37	35.9	38.3	28.7	29.8	25.4	24.7
28.7	29.5	32.3	41	41.9	32.7	33.1	32.1	33.7
34.6	35.5	33.4	39.2	40.9	37.4	37.8	41.8	42.5
39.8	38.6	38.3	50.7	51.9	46.4	43.5	46.3	46.8
18.5	18.5	18.5	17.8	17.8	17	17	15.8	15.8
0.01	0.01	0.01	0.019	0.019	0.029	0.029	0.039	0.039
11.39	11.4	11.39	20.82	20.8	31.13	31.13	42.52	42.48
3680	3680	3679	6762	6763	10215	10215	14008	14011
1.7	1.7	1.7	3.1	3.1	6.1	6.1	12.7	12.7
3722	3722	3722	6767	6767	10080	10080	10133	10133
1.011	1.011	1.012	1.001	1.001	0.987	0.987	0.723	0.723
409	409	409	427	427	464	464	520	520
530	530	530	512	512	475	475	419	419
565	565	565	577	577	595	595	624	624
419	419	419	407	407	390	390	361	361
525	525	525	527	527	535	535	547	547
475	475	475	473	473	465	465	453	453
516	516	516	517	517	521	521	525	525
505	505	505	505	505	501	501	498	498
500	500	500	486	486	460	460	415	415
503	503	503	515	515	542	542	587	587
3	3	3	29	29	82	82	172	172
0.996	0.996	0.996	1.002	1.003	1.012	1.012	1.016	1.017

1250	1251	1252	1253	1254	1255	1256	1257	1258
29.2	29.2	29.4	30.8	30.7	31.1	31.1	32.3	32.1
23.7	24	24.4	24.9	24.9	25	25.1	25.3	25.2
3.6	4	4.4	1.9	2	1.5	1.6	2.9	2.9
4.6	5.1	5.6	3.1	3.1	2.2	2.2	4.6	4.4
7.1	6.8	7.9	6.8	6.9	6.7	6.7	7.3	7.2
9	8.8	8.5	8.3	8.2	8.8	9	9.2	9
60.5	60.9	60.9	60.1	59.9	59.1	59	59.7	59.5
17.5	11.5	14.8	8.3	6.7	3.4	3.5	7.5	5
17.5	14.6	13.6	10.3	10.6	6.6	6.7	5.2	5.2
24.2	21.1	20.7	20.4	20.1	13.8	13.7	10.4	10.4
22.5	20.5	20	22	22.5	19	18.8	16.1	16.2
31.7	31	29.4	29.8	29.8	23.9	23.6	16.8	17
18.5	18.5	18.5	17.8	17.8	17	17	15.8	15.8
0.011	0.011	0.01	0.018	0.018	0.029	0.029	0.039	0.039
10.92	10.93	10.93	18.69	18.68	29.4	29.39	39.7	39.69
3750	3750	3749	6440	6441	10215	10215	13890	13895
1.85	1.85	1.85	2.62	2.62	4	4	5.4	5.4
3862	3862	3862	6404	6404	10436	10436	13906	13906
1.03	1.03	1.03	0.994	0.994	1.022	1.022	1.001	1.001
413	413	413	429	429	464	464	519	519
527	527	527	510	510	475	475	420	420
562	562	562	571	571	595	595	622	622
422	422	422	413	413	390	390	362	362
534	534	534	537	537	535	535	548	548
466	466	466	463	463	465	465	452	452
520	520	520	521	521	521	521	525	525
503	503	503	501	501	501	501	498	498
499	499	499	486	486	460	460	414	414
503	503	503	515	515	542	542	588	588
4	4	4	29	29	82	82	174	174
1.059	1.058	1.058	1.063	1.064	1.072	1.072	1.079	1.08

1259	1260
33.3	33.7
25.2	25.2
2.5	2.5
3.8	3.6
7.6	7.6
8.4	8.3
60.1	60.3
8.1	6.5
4.1	4.5
8.1	8.9
13	13.3
14.5	14
12	12
0.05	0.05
50.86	50.86
17996	17984
8	8
18188	18188
1.011	1.011
596	596
341	341
666	666
318	318
557	557
442	442
528	528
494	494
348	348
653	653
305	305
1.091	1.091

APPENDIX D :- DROPLET SIZES AND FUEL DISTRIBUTION

Droplet sizes produced by a fuel injector nozzle

A Malvern 2200D laser particle sizer was used to perform the required droplet size measurements. The particle sizer, which is based on diffraction techniques, was capable of gauging the number of particles in particular size ranges as a proportion of the total measured range. From this information, the mean droplet size (SMD - Sauter Mean Diameter, which is a mathematical lumping of the size distribution into a single 'representative' droplet size) could be calculated. The laser beam was very directional, however, and any set of measurements corresponded only to the slender column of droplets illuminated by the laser. This meant that in order to characterize a wide spray (such as that produced by the nozzles), several readings have to be made through different locations in the spray. Due to time constraints using the hired equipment, it was decided for this study to sample at a few specific sites, as shown in Figure D1.

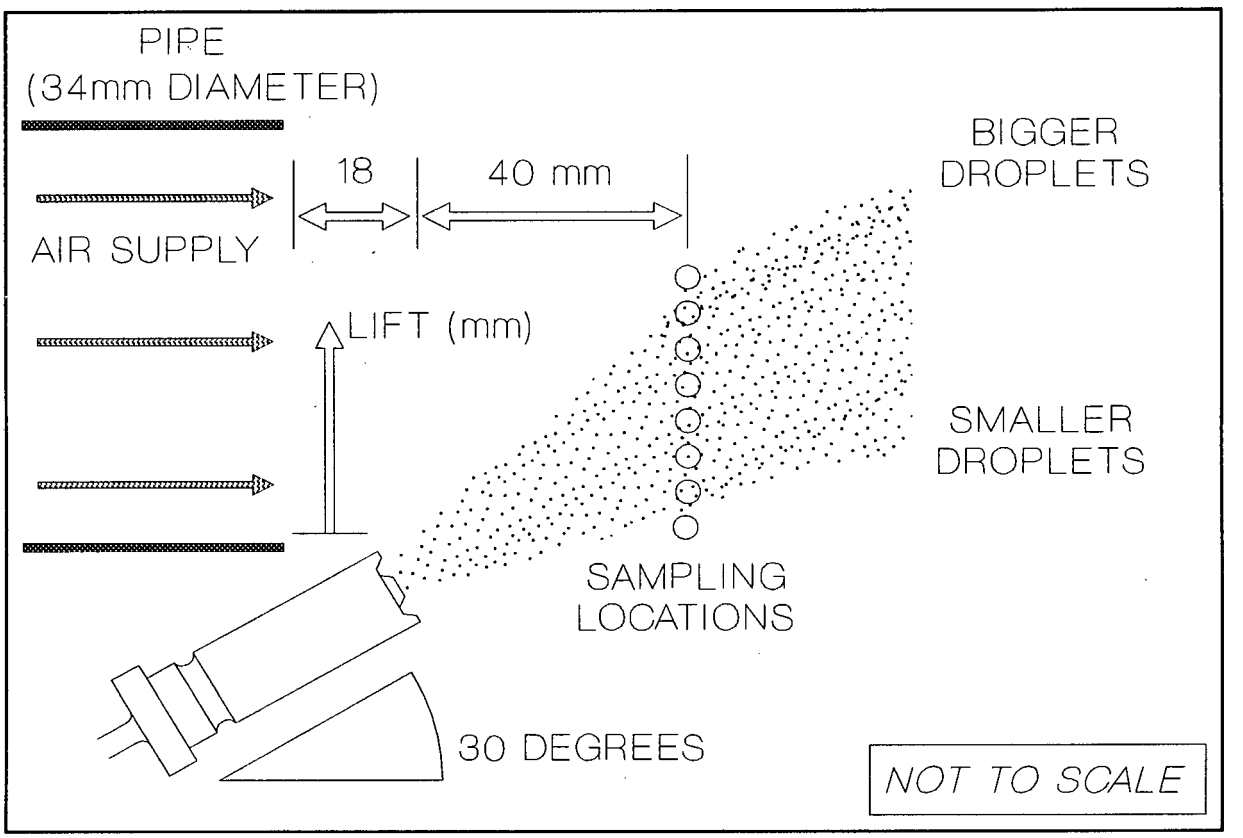

Figure D1 - *The location of sampling points during fuel injector spray particle sizing*

To facilitate the measurements, the air-supply pipe ended immediately before the single nozzle, allowing the laser to pass directly through the spray.

Results

Figures D2 and D3 are graphical representations of the results. 'Lift' corresponds to certain positions in the spray (see Figure D1). 'Concentration' is an indication of the suitability of the sample (0 to 0.05 = too low; 0.05 to 0.1 = low; 0.1 to 0.3 = ideal; 0.3 to 0.5 = high; 0.5 to 1 = too high).

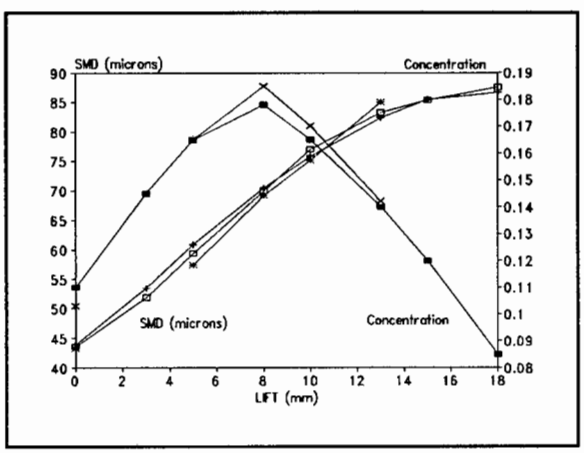

Figure D2

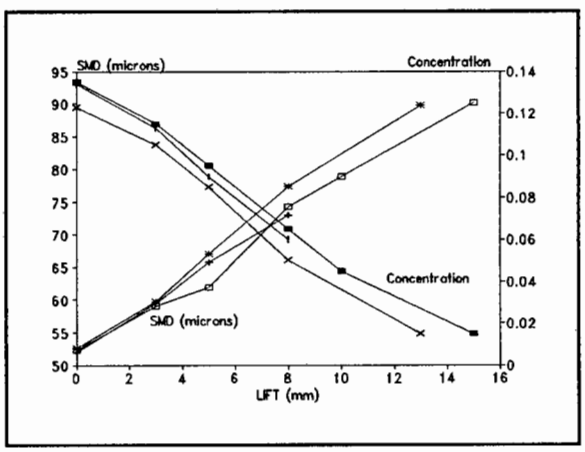

Figure D3

Figures D2 and D3 - *Graphs of fuel injector droplet size (SMD) and spray 'concentration' versus 'lift' for various fuel types at low speeds (left - 20 g/s air mass flow-rate) and high speeds (right - 50 g/s air mass flow-rate). Key: Drop sizes of 100G, 10M90G and 'unleaded' are represented by hollow squares, plus signs and asterisks respectively. 'Concentrations' for 100G, 10M90G and 'unleaded' correspond with solid squares, vertical lines and crosses respectively.*

Lumped spray SMD

The droplet size study was initiated to discover what size droplets the fuel injectors produce, and whether these sizes are significantly affected by changes in air speed and fuel composition. The study was important insofar as if the droplet sizes changed significantly in concert with changes in velocity and fuel composition, the nett effect may be overpowering enough so as to negate any conclusions drawn if these effects were ignored. For purposes of this comparison, it was instructive to lump the data spread over the spray to gain an indication of the 'overall mean droplet size'. This was done by weighting the

SMD readings by their 'concentrations', and it was hoped that this would yield a representative mean droplet size for the whole spray. The results of this spray droplet size calculation is shown in Table D1, with the original data shown later in this Appendix.

AIR SPEED (Mass flow-rate)	Fuel type	Weighted SMD (μm)
Slow (20 g/s)	100G	69.11
Slow (20 g/s)	100G ('unleaded')	67.39
Fast (50 g/s)	100G	60.16
Fast (50 g/s)	100G ('unleaded')	62.67
Fast (50 g/s)	10M90G	62.08

Table D1 - *Lumped SMD data for the whole spray*

These data (Table D1) serve to show that, for the purposes of this study, droplet sizes do not change significantly with fuel composition. Although the physical setup used here differs from that used for the temperature measurements insofar as the latter comprised a closed tube, the apparent trend was that the bigger droplets were more likely to join the wall film (for the present study) due to their trajectories. The fact that smaller droplets are found at a lower 'lift' can be attributed to their lower inertia, allowing them to be carried more readily by the air-stream.

The change in mean droplet size associated with higher air-speeds is therefore a trade-off between influences acting to decrease the mean size (better droplet shattering at the nozzle, as well as greater shattering and shearing by a faster-moving, more turbulent air-stream), and other influences tending to introduce the opposite trend (for example, bigger droplets are more readily carried off in suspension by higher air-speeds). The major factor giving rise to different droplet sizes at different speeds for the fuel injector setup used for the main experimentation in this study would seem to be geometric distribution and trajectories of the droplets, rather than any significant changes in the initial droplet sizes at the different speeds. The results of this investigation into the size and distribution of droplets provided valuable insights into and guidelines for the conditions assumed for the computer model.

Droplet sizes produced by automotive carburettors

Although the emphasis for the test-rig experimentation was placed almost exclusively on fuel injector nozzles, the behaviour of carburettors was considered important for follow-up studies (as well as for CFR engine studies). A photographic investigation into the droplets produced by typical gasoline engines was initiated (as a subsidiary to the high-speed knock investigation)[63], which dealt specifically with wide open throttle conditions. For safety, water was the only fluid tested (and little loss of generality was assumed), and the findings of the study were then compared with formulations described in the literature based on physical properties. The experimental data were found to compare well with the expected performance, and that the formulae could therefore be applied to other fluids. Figure D4 shows the experimentally based droplet size versus air velocity, and fuels such as gasoline are anticipated to behave similarly (within 5%).

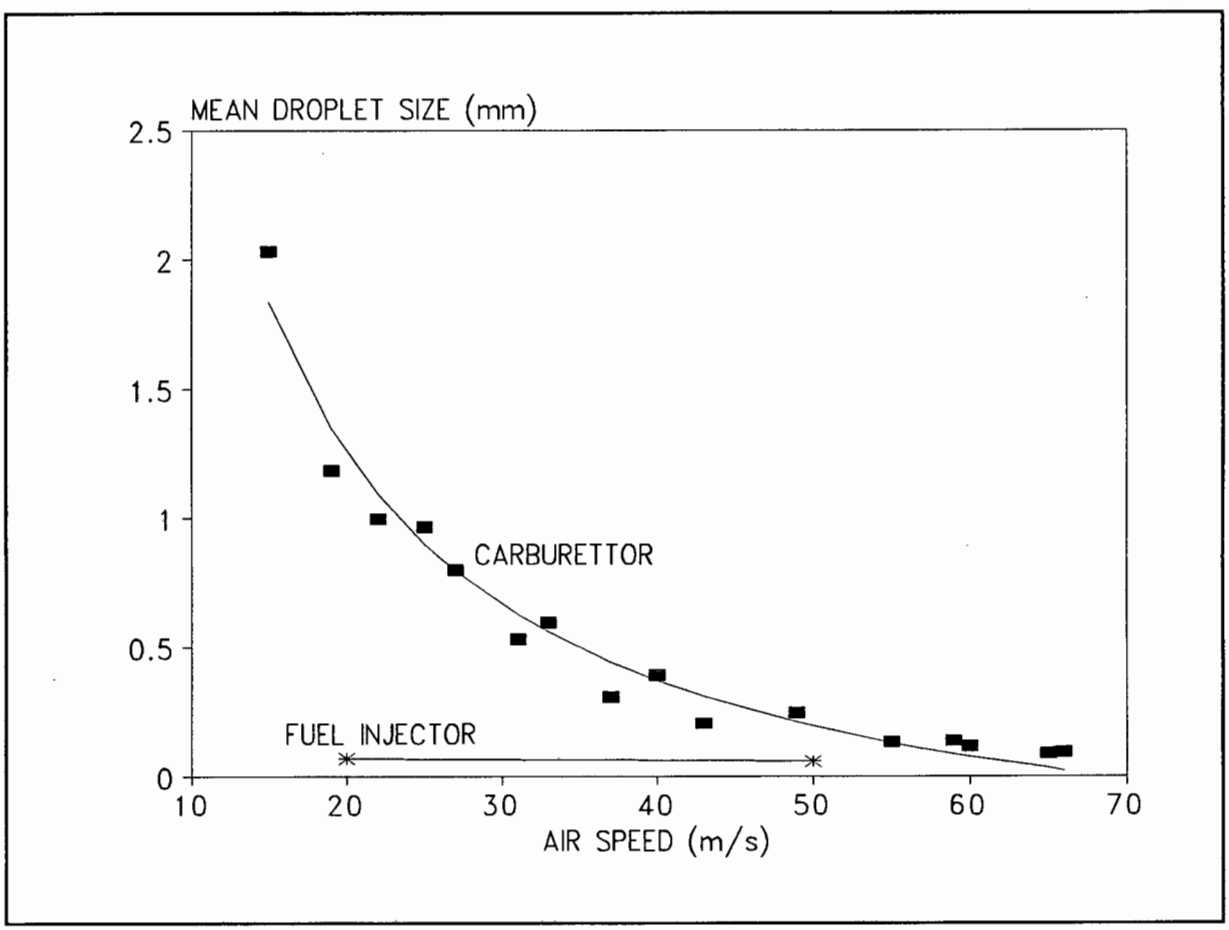

Figure D4 - *Droplet sizes versus air-speed measured using a simulated carburettor*

RAW DATA - MALVERN

Key to the tables

The Malvern particle sizer incorporated a computer that calculated relevant data on-line. These data, which are explained below, are tabulated and included in this Appendix.

Run no. - The samples are numbered, but these numbers have nothing to do with corresponding numbers in Appendix D. The fuels tested are 10M90G (Runs 301 to 315), 100G (316 to 334), and 'unleaded' 100G (400 to 410).

% < (x) - The cumulative percentage mass of the total droplets measured, which is contained in droplets below a certain size (x micron).

D50% - 50% of the fuel mass is contained in droplets smaller than this size (and 50% in bigger droplets).

VMD - Volume Mean Diameter (more specifically defined as D_{43}).

SMD - Sauter Mean Diameter (D_{32}).

$$D_{43} = \frac{\sum_{i=1}^{m} N(x_i)x_i^4}{\sum_{i=1}^{m} N(x_i)x_i^3} \qquad D_{32} = \frac{\sum_{i=1}^{m} N(x_i)x_i^3}{\sum_{i=1}^{m} N(x_i)x_i^2}$$

where N( ) is the number frequency and x is the particle diameter

Log fit - 'Log difference' which is a measure of the 'goodness' of fit. The reading should be discarded for ld > 6.0. (lc( ) is the calculated light coefficient, lm( ) is the measured light coefficient)

$$ld = \log_{10}[\sum_{i=1}^{15} (lc(i)-lm(i))^2]$$

Ma - The mass flow-rate of air in g/s.

Lift - The vertical position of the laser (see Figure D1).

'Conc' - The concentration of the sample (as explained before).

'Conc' OK? - The interpretation of the concentration reading.

Run no	301	302	303	304	305	306	307	308
% < 188	100	100	100	100	100	100	100	100
% < 87.2	73.7	66.3	61.3	55.7	56.6	53	47.3	45.3
% < 53.5	49.7	37.6	29.7	20.5	21.1	16.9	11.8	8.9
% < 37.6	28.4	19.4	15.1	8.8	9.1	6	3.9	3.1
% < 28.1	15.4	10	5.7	1.8	2	0.9	0.3	0.4
% < 21.5	9.3	4.9	2.5	0.6	0.6	0.3	0.1	0.1
% < 16.7	4.3	1.7	0.9	0.2	0.2	0.1	0	0
% < 13.0	1.5	0.4	0.2	0	0	0	0	0
% < 10.1	0.7	0.2	0	0	0	0	0	0
% < 7.9	0.2	0.1	0	0	0	0	0	0
% < 6.2	0.1	0	0	0	0	0	0	0
% < 4.8	0	0	0	0	0	0	0	0
% < 3.8	0	0	0	0	0	0	0	0
% < 3.0	0	0	0	0	0	0	0	0
% < 2.4	0	0	0	0	0	0	0	0
% < 1.9	0	0	0	0	0	0	0	0
D50%	53.9	68.1	75.1	81.7	81	84.4	92.3	95.9
VMD	70.1	80.1	86.4	93.7	93	96.9	102	105
SMD	44	53.5	60.9	71.2	70.5	75.8	82.4	85.4
Log fit	5.01	4.89	4.78	4.66	4.55	4.59	4.55	4.54
Ma*100	1.99	1.94	1.95	2.02	1.96	2.02	1.99	2.01
Lift (mm)	0	3	5	8	8	10	13	15
'Conc'*1000								
'Conc' OK ?		Ideal	Ideal	Ideal	Ideal	Ideal	Ideal	

309	310	311	312	313	314	315	316	317
100	100	100	100	100	100	100	100	100
44.6	51.4	57.7	64	64.9	65.3	68.2	67	63.8
8.2	11.2	16.9	23.5	30.5	29.7	36.6	37.6	36.5
2.3	3.2	6.3	11.2	14.4	15.4	20.3	21.8	21.1
0.3	0.3	1.4	2.6	5.3	6.5	10.1	11.3	11.6
0.1	0.1	0.5	0.9	2.5	2.7	5.4	6.6	6.2
0	0	0.3	0.4	1.3	1.2	2.7	3.3	3.6
0	0	0.2	0	0.3	0.4	1.1	1.4	1.7
0	0	0.1	0	0	0.1	0.4	0.6	0.3
0	0	0	0	0	0	0.1	0.2	0.1
0	0	0	0	0	0	0	0	0
0	0	0	0	0	0	0	0	0
0	0	0	0	0	0	0	0	0
0	0	0	0	0	0	0	0	0
0	0	0	0	0	0	0	0	0
0	0	0	0	0	0	0	0	0
97	86.1	80.8	75.5	72.6	72.7	67.8	67.7	70.1
105	99.8	93.6	87	86.9	83.7	78.8	78.9	81.5
86.7	81.2	73	65.8	59.7	59.1	52	50.4	50.9
4.53	4.48	4.54	4.8	4.86	4.84	4.98	4.8	4.97
1.98	5.08	4.92	5.09	5.06	5.01	4.98	4.97	4.98
18	15	8	5	3	3	0	0	0
50	50	60	90	117	109	134	135	130
Low	Low	Ideal	Ideal	Ideal	Ideal	Ideal	Ideal	Ideal

319	320	321	322	323	324	325	326	327
100	100	100	100	100	100	100	100	100
71.3	68.4	66.6	67.2	63.3	57.6	51.2	40.7	43.1
36.2	36.2	33.5	30.9	25.1	15.7	11.9	2.8	8.9
19.7	20.1	19.6	14.6	13	6.1	4.6	2.5	2.2
8.7	10.3	10.8	6	4.2	1.4	0.5	0.5	0.3
4.1	4.9	7.3	2.4	2.5	0.2	0.4	0.3	0.1
1.8	2.5	4.7	1	1.8	0.1	0.3	0.3	0
0.7	1	2.4	0.3	0.5	0	0.2	0.3	0
0.4	0.4	1.4	0.1	0.2	0	0.1	0.2	0
0.2	0.1	0.6	0	0.1	0	0.1	0.1	0
0.1	0	0.1	0	0	0	0	0	0
0.1	0	0	0	0	0	0	0	0
0.1	0	0	0	0	0	0	0	0
0	0	0	0	0	0	0	0	0
0	0	0	0	0	0	0	0	0
0	0	0	0	0	0	0	0	0
66.7	67.9	70.3	71.2	75.45	81.1	86.1	103	99.4
77.1	78.8	80.4	82.2	86.6	94.1	99.5	109	106
52.4	52.3	49.7	59.1	62	74.3	78.9	90.1	87.5
4.5	4.67	5.11	4.78	4.84	4.26	4.56	4.66	4.28
5.01	4.93	4.99	5.02	4.99	5	5.01	5.01	2.05
0	0	3	3	5	8	10	15	18
135	135	115	115	95	65	45	15	85
Ideal	Ideal	Ideal	Ideal	Low	Low	Too low	Too low	Low

328	329	330	331	332	333	334	400	401
100	100	100	100	100	100	100	100	100
44.6	44.6	51.2	56.4	62.6	66.3	71.8	71.6	70.9
10.4	10.7	16	21.7	31.7	38.2	48.3	47	47.3
2.7	3.8	5.9	9.4	15.9	22.7	28.5	30.2	31.2
0.3	0.5	1.1	2.4	6.4	11.2	17.3	16.7	17.2
0.1	0.1	0.3	0.7	2.7	5.1	10.1	9.2	9.8
0	0	0.1	0.2	0.9	2.2	4.4	5	5.1
0	0	0	0.1	0.2	0.6	1.9	2	2.2
0	0	0	0	0	0.2	0.9	0.8	0.8
0	0	0	0	0	0.1	0.3	0.3	0.2
0	0	0	0	0	0	0.1	0.1	0.1
0	0	0	0	0	0	0	0	0
0	0	0	0	0	0	0	0	0
0	0	0	0	0	0	0	0	0
0	0	0	0	0	0	0	0	0
0	0	0	0	0	0	0	0	0
97.1	93.2	83	81	73.4	67.6	56	57.5	57.3
105	103	98.3	92.9	84.8	79.4	71.5		72
85.3	83.2	76.9	69.9	59.4	51.9	43.6		43.2
4.24	4.35	4.3	4.59	0	0	5.15		5.09
2.02	1.96	2.08	2.03	1.98	1.95	2	1.96	1.96
15	13	10	8	5	3	0	0	0
120	140	165	178	165	145	110	103	103
Ideal	Ideal	Ideal	Ideal	Ideal	Ideal	Ideal	Ideal	Ideal

402	403	404	405	406	407	408	409	410
100	100	100	100	100	100	100	100	100
65.4	57.7	53.3	43.6	43.7	53.8	60.1	65.9	66.8
33.2	22.5	17.1	10.8	4.8	15.6	23.3	28.7	35.6
18	9.5	6.7	3.4	1.6	4.4	10.5	14.8	20.7
6.9	2.5	1.3	0.3	0.3	0.4	3.1	6.2	10.1
2.8	0.7	0.3	0.1	0	0.1	1	2.2	4.7
1.1	0.2	0.1	0	0	0	0.3	1	2.6
0.2	0	0	0	0	0	0.1	0.4	1.1
0.1	0	0	0	0	0	0	0.1	0.4
0	0	0	0	0	0	0	0	0.1
0	0	0	0	0	0	0	0	0
0	0	0	0	0	0	0	0	0
0	0	0	0	0	0	0	0	0
0	0	0	0	0	0	0	0	0
0	0	0	0	0	0	0	0	0
0	0	0	0	0	0	0	0	0
71.1	79.8	84.2	98.6	98.5	83.8	78	72.3	69.1
82.4	91.7	96.6	105	107	96.9	89.8	83.6	80
57.4	69.2	75.1	85	89.8	77.4	67.2	59.8	52.6
4.87		4.54	4.34	4.3	4.4	4.66	4.79	
1.96	1.96	1.96	1.96	5.02	5.02	5.02	5.02	5.02
5	8	10	13	13	8	5	3	0
165	185	170	142	15	50	85	105	123
Ideal	Ideal	Ideal	Ideal	Too low	Low	Low	Ideal	Ideal

The data giving rise to Figures D2 and D3, are tabulated below, and are derived from the general data tabulated above. The relevant data have been rearranged into SMD versus Lift formats. (Fast : 50 m/s air speed; Slow : 20 m/s air speed).

Lift	100G	100G	10M90G	10M90G	Unleaded	Unleaded
	Fast	Fast	Fast	Fast	Fast	Fast
(mm)	SMD(μm)	'Conc'	SMD(μm)	'Conc'	SMD(μm)	'Conc'
15	90.14	0.015	81.22	0.05		
13					89.82	0.015
10	78.92	0.045				
8	74.3	0.065	73.03	0.06	77.35	0.05
5	61.99	0.095	65.81	0.09	67.15	0.085
3	59.06	0.115	59.5	0.113	59.78	0.105
0	52.3	0.135	52	0.134	52.57	0.123
Lift	100G	100G	10M90G		Unleaded	Unleaded
	Slow	Slow	Slow		Slow	Slow
(mm)	SMD(μm)	'Conc'	SMD(μm)		SMD(μm)	'Conc'
18	87.52	0.085	86.69			
15	85.27	0.12	85.39			
13	83.17	0.14	82.4		84.97	0.142
10	76.9	0.165	75.81		75.09	0.17
8	69.91	0.178	70.5		69.15	0.185
5	59.42	0.165	60.92		57.43	0.165
3	51.9	0.145	53.52			
0	43.59	0.11	44.01		43.24	0.103

APPENDIX E. STATISTICAL ANALYSIS

In order to correlate the influence of the group of control variables ('fixed' quantities) and the behaviour of the experimental observations (measured data), a multivariate analysis of variance was initiated. The analysis also evaluated the performance of the model in its ability to predict the experimental data.

To provide a framework for this investigation, the data were arranged into a convenient tabular format. Although data were collected spanning a vast range of control variable conditions, only certain representative sets were used for the analysis, since the tabulation of these data proved very laborious (mean and range data were measured manually, off reams of graphical printouts).

Each particular data set consisted of a group of five 'fixed' input variables (volume percentage methanol of the fuel, air velocity, inlet air temperature, fuel/air mass ratio and inlet fuel temperature) and a description of the behaviour of the observations (see Figure 21). This behaviour is reported as the mean and range of each measurement over a period of 150 seconds (sampling every five seconds making 30 individual data points from which the mean and range data was extracted). The means and ranges were estimated from the graphical histories of the observations, with the 150 second window chosen after it was apparent that steady state conditions existed. The selected physical probes consisted of four film measuring thermocouples (at 0.1, 0.2, 0.6 and 1.0 metres downstream of the fuel inlet), and three droplet temperature measurement probes (at 0.1, 0.2 and 0.6 metres downstream).

Input to and output from the statistical package

The commercially available statistical package BMDP was fed the data appearing in the tables below, together with a set of analysis instructions. The specific instructions used are included later in this Appendix. The output from these computer runs comprised over 100 pages of highly technical statistical data, and thus this output would be beyond the scope of this Appendix. The set of instructions giving rise to the BMDP runs are included in the Appendix, however, to provide the framework for verifying the claims of this thesis. These instructions, coupled with the data in the tables can be used to regenerate the full technical

findings of the statistical investigation.

Key to the data tables

The data used for the statistical analysis is tabulated below. Each set of initial conditions (control parameters) and measurements (output variables) is numbered, and these numbers correspond to those in Appendix D.

% - The percentage methanol in the base gasoline (0 = 100G, 10 = 10M90G blend, 20 = 20M80G blend).

v - The velocity of the air-stream through the 34 mm pipe. This parameter was chosen in preference to the air mass flow-rate for the following reasons: (i) This parameter was thought to be slightly more influential on/representative of the system, insofar as heat and mass transfer coefficients are influenced more by stream velocity than by mass flow-rates. In addition, the air density measurement is incorporated in the velocity term, and this term would otherwise have been ignored. (ii) Air velocity is almost completely interchangeable with the mass flow-rate because the air density changes almost insignificantly, so the choice of test parameter is immaterial.

tai - The initial air temperature (read immediately upstream of the fuel inlet point).

smc - The fuel/air equivalence ratio, where a fuel/air mass ratio of 1/14.7 [kg/kg] is considered a stoichiometric mix, giving rise to an 'smc' of 1 (an 'smc' of greater than 1 implies a rich mixture, therefore). (The use of the letters 'smc' for equivalence ratio may seem confusing, but this notation was preferred by Professor Dunne of the Statistical Sciences Department at the University of Cape Town, who was consulted for the statistical analysis).

tfi - The initial fuel temperature.

[0], [1], [3], [5] - Shorthand for the standard positions of the temperature measurements. These positions correspond to distances downstream of the fuel inlet point of 0.1m, 0.2m, 0.6m, and 1.0m respectively.

(As a technical point, the tables for the actual statistical runs had the film mean and range data appearing before the droplet data. They have been superimposed in this Appendix simply because they fit better on the pages).

D P MORAN						D	R	O	P	S	
Means and ranges for fuel data						Means			Ranges		
EXPERIMENTAL DATA						0.1	0.2	0.6	0.1	0.2	0.6
#	%m	v	tai	smc	tfi	[0]	[1]	[3]	[0]	[1]	[3]
501	0	11	63	1	27	22	28	27	2.5	1.9	1.1
503	0	20	62	1	28	23	29	29	1.3	1	1
505	0	30	61	1	29	15	23	27	0.6	0.8	0.6
510	0	45	61	1	31	12	17	24	1.3	1.8	1
512	0	53	61	1	31	11	15	23	1.2	1.2	1
514	0	56	80	1	32	18	23	32	1.4	1.9	1.1
517	0	52	61	1	38	14	18	24	1	0.7	0.9
531	0	12	83	1	28	38	43	38	2.8	2	1.5
534	0	22	82	1	29	12	17	23	0.3	0.2	0.3
536	0	32	81	1	31	25	34	38	0.8	0.5	0.7
538	0	47	81	1	32	20	26	33	0.8	1.8	1
540	0	55	82	1	33	20	24	32	0.6	0.8	0.7
550	0	11	63	1	23	17	23	24	1.8	1.4	0.6
553	0	20	61	1	23	20	25	27	0.5	0.5	0.4
555	0	29	60	1	23	15	22	25	0.4	0.3	0.5
559	0	53	61	0.8	20	12	17	23	0.3	0.2	0.3
601	10	11	60	1	18	13	17	19	2	2.2	2
603	10	19	60	1	18	13	20	21	1.3	1	0.7
605	10	30	60	1	19	4.3	14	19	0.6	0.8	0.5
611	10	54	62	1	22	2.8	1.7	8.5	0.3	0.4	0.4
701	10	12	80	1	19	16	24	25	1.5	2.5	1.5
705	10	32	80	1	22	9.7	19	27	0.6	0.6	0.9
713	10	55	81	1	24	5.5	9.3	20	1	1.5	2
752	20	11	59	1	14	5.3	9.8	9.8	1.4	1.5	1.5
754	20	20	61	1	14	4.8	11	13	0.5	0.7	0.5

756	20	30	59	1	15	1.5	5.1	9	0.5	1.3	2
758	20	41	60	1	16	0.5	2.5	6.4	0.4	0.5	0.8
760	20	52	60	1	17	0	1.2	3.9	0.6	0.7	0.7
801	20	11	59	1	24	9	13	13	1.3	1.3	1.7
803	20	20	61	1	24	7.4	13	14	0.4	0.8	0.6
804	20	29	61	1	24	5.4	9.6	14	0.4	0.7	0.5
807	20	40	58	1	24	4.1	6.5	11	1.2	1	1
1121	20	56	80	1.1	24	6.1	7.9	14	0.6	0.8	1
1004	0	17	49	0.6	20	21	24	23	1.2	0.7	0.5
1006	0	17	49	1.1	20	15	19	18	0.6	0.6	0.5
1008	0	29	53	0.7	20	16	24	26	0.4	0.6	0.5
1010	0	29	52	1	21	11	19	21	0.4	0.5	0.4
1012	0	40	52	0.7	21	10	18	23	0.6	0.5	1
1014	0	40	51	1.1	21	7.1	12	19	0.8	0.7	0.4
1016	0	52	51	0.8	21	6.6	12	20	0.4	0.6	0.4
1018	0	52	51	1.1	22	5.8	9.1	16	0	0.5	0.6
1020	0	52	53	1.2	22	6.5	8.8	15	0	0.6	0.4
1042	10	10	39	0.9	20	5	9.5	9.7	1.4	1	0.7
1044	10	17	49	0.6	20	11	17	20	0.4	0.5	0.5
1046	10	17	49	1.1	21	6.4	11	12	0.8	0.7	0.8
1048	10	29	53	0.7	21	6.7	15	20	0.5	0.6	0.6
1050	10	29	52	1	21	3.4	9.4	15	0.3	0.7	0.4
1072	20	11	40	1	19	0.5	7.5	7.3	3	3	2.5
1077	20	19	51	0.6	20	8.8	15	20	1.5	2.1	0.8
1079	20	19	51	1	20	4	8.4	10	0.9	0.2	0.5
1081	20	29	53	0.7	21	2.8	7.9	15	0.6	0.7	0.7
1083	20	29	53	1	21	1.9	5.7	11	0.4	0.3	0.4
1085	20	40	53	0.7	21	1.8	4.8	12	0.2	0.3	0.7
1087	20	40	53	1	22	1	3	8.2	0.4	0.5	0.6

1089	20	51	52	0.8	22	1	2.9	8.5	0.6	0.5	0.8
1091	20	51	52	1	23	0.6	1.8	6	0.2	0.2	0.5
1093	20	51	53	1.1	23	0.6	1.4	4.8	0.4	0.6	1
1102	20	12	91	1	21	18	25	23	3.5	2.5	2.2
1104	20	12	92	0.4	22	30	44	50	5.5	4	1
1107	20	21	80	0.7	22	14	24	32	1.1	1.4	1.1
1109	20	21	81	1	23	12	20	26	0.7	0.7	0.6
1111	20	30	73	0.7	23	8.6	16	27	0.5	0.6	0.9
1113	20	31	82	1	23	9.4	16	25	0.4	0.6	0.8
1115	20	43	79	0.7	23	8.9	15	25	0.4	0.7	0.8
1117	20	42	78	1	23	6.5	9.3	18	0.4	0.5	1
1119	20	55	80	0.8	24	7	10	20	0.4	0.6	0.5
1132	20	12	77	0.9	19	12	16	15	1.8	1.8	1.8
1134	20	20	70	0.9	20	7.9	15	20	0.5	0.8	0.7
1136	20	21	71	1	21	6.8	13	17	0.5	0.4	0.7
1138	20	30	69	0.7	21	6	12	22	0.4	0.4	1
1140	20	30	71	1	22	4.9	9.6	17	0.2	0.6	0.7
1142	20	41	68	0.9	22	3.8	6.3	15	0.5	0.5	0.7
1144	20	42	70	1	22	3.6	6.2	12	0.3	0.5	0.8
1146	20	53	68	0.8	23	3.2	5.5	13	0.3	0.4	0.5
1147	20	54	72	0.9	23	3.8	5.8	12	0.3	0.3	0.7
1162	20	12	82	1	17	12	17	17	1.3	1.2	1.8
1164	20	20	76	1	18	10	16	21	0.9	0.6	0.6
1166	20	31	79	1	19	8.6	14	21	0.6	0.7	1
1168	20	47	79	0.9	19	7.3	11	17	0.4	0.7	0.8
1170	20	47	81	1	20	6.3	9.5	15	0.7	0.9	1
1173	20	55	80	1	21	6.8	9.1	14	0.6	0.4	0.7
1175	20	55	80	1	22	7.1	9.4	14	0.3	0.5	1.1

	F I L M							
	Means				Ranges			
	0.1	0.2	0.6	1	0.1	0.2	0.6	1
#	[0]	[1]	[3]	[5]	[0]	[1]	[3]	[5]
501	9.5	10	14	15	0.6	0.5	0.7	0.5
503	7.2	8.4	12	14	0.7	0.5	0.5	0.6
505	8.2	7.8	12	15	0.6	0.5	0.5	0.5
510	11	11	15	18	0.5	0.5	0.3	0.2
512	11	12	17	21	0.8	0.6	0.7	1.5
514	17	16	25	31	0.8	1.2	0.4	1
517	11	8	16	22	0.3	0.9	1	1.1
531	12	14	19	21	0.5	0.3	0.3	0.2
534	6.7	6.9	13	17	0.3	0.3	0.3	0.3
536	14	12	18	23	0.4	0.4	0.4	0.5
538	12	11	20	25	0.3	0.4	0.2	0.4
540	15	13	22	29	0.3	0.2	0.5	0.8
550	11	11	14	16	0.3	0.3	0.3	0.3
553	6.4	6.8	11	13	0.2	0.2	0.3	0.2
555	7.8	6.2	9.7	13	0.2	0.3	0.5	0.4
559	6.7	6.9	13	17	0.3	0.3	0.3	0.3
601	2.5	2.3	5.1	6.7	0.6	0.9	0.7	1.5
603	-1	-1	2.9	3.7	0.3	0.4	0.1	0.2
605	-1	-2	1.9	4.3	0.4	0.3	0.4	0.4
611	0.7	-3	2.7	6.7	0.3	0.2	0.5	0.6
701	4.8	5.3	7.4	9.3	0.5	0.5	0.3	0.5
705	3.5	2.2	7.2	12	0.3	0.4	0.4	0.2
713	5.4	7.6	13	16	0.5	0.6	0.3	0.8
752	1.5	1.8	3.8	5.5	0.2	0.2	0.4	0.6
754	-2	-1	1.6	1.6	0.3	0.2	0.2	0.2

756	-2	-2	0.8	0.9	0.2	0.6	0.3	0.7
758	-1	0	0.8	0.9	0	0.4	0.4	0.4
760	0	0.2	1.6	1.1	0.2	0.4	0.2	0.4
801	3.9	4.4	6.4	8.4	0.3	0.4	0.2	0.3
803	1.5	2.2	5	5.2	0.3	0.3	0.2	0.3
804	1.6	1.9	5	5.7	0.2	0.3	0.4	0.4
807	2.2	3.4	4.7	5.3	0.3	0.2	0.6	0.8
1121	5	6.2	9.6	13	0.2	0.1	0.3	0.4
1004	3.3	5.8	12	15	0.4	0.5	0.9	0.7
1006	2.5	4.1	7.5	8.1	0.2	0.4	0.6	0.4
1008	6.3	6.7	12	17	0.3	0.3	0.3	0.4
1010	4.4	3.7	7.1	9.3	0.4	0.3	0.5	0.5
1012	7.7	9	11	15	0.4	0.3	0.5	0.4
1014	5.5	6.2	9.5	12	0.5	0.5	0.3	0.5
1016	9.2	9.8	15	18	0.5	0.6	0.4	0.3
1018	5.4	7.4	11	14	0.3	0.2	0.2	0.2
1020	5.6	6.8	10	12	0.4	0.2	0.2	0.2
1042	0.8	1.2	3.7	5.1	0.4	0.3	0.4	0.7
1044	-1	1	7.1	9.9	0.5	0.5	0.3	0.3
1046	0	-1	1.9	2	4.3	0.7	0.8	0.4
1048	0.3	0.4	5.3	9.4	0.3	0.3	0.3	0.3
1050	-2	-1	2.5	4.5	0.4	0.4	0.4	0.5
1072	-2	-1	1.2	1.5	0.6	0.4	0.3	0.4
1077	-2	0	4.8	5.7	0.4	0.2	0.4	0.4
1079	-2	-1	1.2	1.1	0.4	0.4	0.2	0.3
1081	-1	0	4	5.9	0.4	0.3	0.4	0.2
1083	-2	-2	1.7	2	0.3	0.3	0.2	0.4
1085	0.3	1.3	4.1	5.9	0.4	0.3	0.4	0.3
1087	-1	0.2	1.7	2.4	0.3	0.4	0.3	0.5

1089	1.4	2.9	4.9	7.1	0.5	0.5	0.3	0.8
1091	0	0.8	2.8	3.4	0.2	0.3	0.3	0.3
1093	-1	0	1.9	2	0.3	0.3	0.3	0.3
1102	6.3	7.6	10	11	0.5	0.3	0.6	0.4
1104	11	15	24	19	0.5	0.9	0.5	0.4
1107	4.7	6.6	13	15	0.6	0.4	0.3	0.6
1109	3.7	5	9.2	9.8	0.4	0.4	0.7	0.4
1111	4.9	5.9	12	16	0.3	0.2	0.2	0.6
1113	4.8	5.1	9.1	11	0.2	0.3	0.4	0.3
1115	7	8.9	14	18	0.2	0.2	0.4	0.4
1117	5.1	6.3	8.2	9.4	0.3	0.3	0.3	0.2
1119	9.2	11	15	23	0.5	0.2	0.3	0.4
1132	3.9	5.1	7.9	8.1	0.5	0.4	0.3	0.2
1134	1	2.4	6	6.5	0.2	0.3	0.2	0.2
1136	1.1	1.9	4.5	5	0.6	0.4	0.3	0.4
1138	2	2.5	6.4	9.3	0.2	0.4	0.3	0.5
1140	1.1	1.4	4.5	5.5	0.3	0.3	0.4	0.3
1142	1.6	2.9	5.9	7.5	0.3	0.2	0.3	0.4
1144	1.2	1.9	4.4	5.2	0.2	0.3	0.1	0.3
1146	2.4	3.9	8.4	15	0.1	0.2	0	0.4
1147	1.7	3.1	7	12	0	0.1	0	0.3
1162	5.9	7.1	9.9	10	0.3	0.4	0.3	0.6
1164	2.9	4	7.3	7.9	0.6	0.6	0.5	0.4
1166	3.9	4	7.9	9.6	0.3	0.3	0.5	0.3
1168	5.3	6.7	9.8	12	0.3	0.2	0.3	0.3
1170	4.2	5.9	7.9	9	0.3	0.4	0.3	0.3
1173	5.6	6.8	9.2	10	0.3	0.4	0.4	0.4
1175	5.6	6.9	9.7	11	0.3	0.2	0.2	0.5

COMPUTER MODEL PREDICTIONS							
	FILM				DROPLETS		
	0.1	0.2	0.6	1	0.1	0.2	0.6
#	[0]	[1]	[3]	[5]	[0]	[1]	[3]
501	3.91	15.06	20.95	21.36	14.54	21.41	27.13
503	2.64	12.72	19.79	20.57	12.22	17.81	25.37
505	1.92	11.00	18.53	19.48	10.37	15.54	23.22
510	1.52	9.48	17.40	18.53	9.11	13.69	21.50
512	1.60	9.52	17.53	18.70	8.81	13.21	21.08
514	7.96	19.72	27.78	28.69	17.19	22.97	31.54
517	3.26	11.31	18.71	19.77	10.38	14.77	22.22
531	11.30	25.00	30.19	30.22	24.92	32.36	36.41
534	9.70	22.92	29.34	29.67	21.56	28.44	35.17
536	9.05	21.91	28.92	29.44	19.49	26.01	33.68
538	8.61	20.80	28.41	29.18	18.06	24.08	32.44
540	8.68	20.49	28.48	29.36	18.14	23.99	32.43
550	3.23	14.79	20.79	21.19	13.87	20.92	26.85
553	0.87	10.53	18.05	18.92	10.34	15.84	23.78
555	0.25	9.27	17.26	18.29	8.47	13.61	21.82
559	0.60	10.92	19.27	20.36	6.92	11.49	20.36
601	-0.89	4.10	9.07	10.19	7.72	10.74	18.99
603	-1.33	3.04	7.98	9.09	5.90	9.10	14.54
605	-1.26	2.76	7.69	8.84	5.11	7.83	12.93
611	-0.62	2.63	7.36	8.46	4.82	7.00	12.08
701	4.63	11.17	18.88	21.13	15.40	19.43	31.63
705	4.38	10.32	17.67	19.98	12.07	15.45	22.50
713	4.37	9.48	16.11	18.08	11.19	14.08	20.63
752	-1.80	1.24	4.43	5.10	6.13	7.79	12.50
754	-1.50	1.27	4.52	5.27	5.00	7.43	10.53

756	-1.95	0.29	3.34	4.07	3.66	5.54	8.88
758	-1.66	0.31	3.33	4.05	3.47	5.05	8.68
760	-1.53	0.06	2.91	3.58	3.15	4.55	8.15
801	-0.90	2.17	5.34	6.05	6.74	8.39	13.33
803	-0.50	2.28	5.51	6.29	5.74	8.15	11.30
804	-0.68	1.75	4.86	5.61	4.84	6.79	10.12
807	-1.17	0.73	3.64	4.33	3.65	5.18	8.73
1121	2.13	13.55	18.03	18.27	4.88	10.00	19.35
1004	-4.02	2.10	9.31	10.33	4.48	8.93	16.43
1006	1.62	13.59	19.22	19.64	5.12	10.01	19.10
1008	-2.85	4.08	11.92	13.03	4.65	9.08	16.90
1010	-0.29	10.66	17.39	18.18	4.16	8.45	17.01
1012	-3.33	2.26	10.05	11.36	3.46	7.34	14.82
1014	-2.33	6.20	14.02	15.10	2.90	6.62	14.55
1016	-3.16	1.85	9.66	11.09	3.17	6.77	14.12
1018	-2.88	0.87	8.12	9.67	3.68	7.30	14.48
1020	-6.82	-3.26	0.41	1.08	-0.37	1.78	6.72
1042	-1.12	5.62	14.61	16.08	2.61	5.46	11.35
1044	-4.12	-1.30	2.59	3.39	2.44	4.88	9.24
1046	-1.51	4.44	11.17	13.37	2.84	5.54	10.73
1048	-3.24	-0.15	4.15	5.09	2.45	4.90	9.32
1050	-6.53	-4.91	-2.43	-1.87	-0.44	0.81	3.63
1072	-1.86	2.50	8.66	11.35	2.31	4.71	8.16
1077	-3.53	-1.40	1.40	2.03	2.05	4.17	6.82
1079	-2.04	1.82	6.10	7.65	2.25	4.17	7.72
1081	-2.84	-0.98	1.82	2.46	2.16	3.90	6.94
1083	-2.48	0.74	4.24	5.21	1.80	3.29	6.99
1085	-2.78	-1.25	1.45	2.09	1.69	3.07	6.38
1087	-2.85	-0.24	2.94	3.70	1.21	2.47	6.05

1089	-2.77	-1.47	1.18	1.80	1.27	2.48	5.80
1091	-2.27	-1.89	0.37	0.96	1.46	2.65	5.82
1093	6.75	11.48	18.41	21.23	16.68	19.13	33.04
1102	17.67	17.67	17.67	17.67	18.00	18.00	18.00
1104	5.45	10.86	22.80	26.41	11.66	14.83	20.59
1107	3.92	7.63	12.05	13.41	11.62	14.53	19.25
1109	3.58	8.47	17.03	20.95	8.63	11.11	15.57
1111	4.28	7.87	12.23	13.62	11.09	13.51	18.00
1113	4.83	9.77	18.31	22.46	9.89	12.03	17.04
1115	3.27	6.09	9.79	10.78	9.40	11.34	15.71
1117	4.28	8.39	13.80	15.99	9.50	11.40	16.26
1119	3.70	6.29	9.88	10.81	9.52	11.30	15.76
1132	3.94	8.55	15.62	18.51	12.67	14.90	25.64
1134	1.64	5.52	9.98	11.47	8.23	10.97	14.98
1136	1.48	4.66	8.30	9.24	8.53	11.20	14.94
1138	2.19	6.87	13.89	17.18	7.24	9.62	13.83
1140	1.60	4.69	8.34	9.32	7.81	10.04	13.83
1142	0.98	4.13	7.86	8.92	6.31	8.09	12.22
1144	1.48	4.20	7.67	8.56	7.11	8.89	12.97
1146	1.33	4.99	9.29	10.73	6.00	7.65	11.96
1147	1.87	4.82	8.52	9.52	7.10	8.77	13.04
1162	4.05	8.09	12.65	14.05	13.74	15.90	26.95
1164	2.43	5.78	9.63	10.65	9.94	12.74	16.89
1166	3.14	6.57	10.66	11.84	9.95	12.30	16.57
1168	3.41	6.96	11.27	12.62	9.29	11.23	15.90
1170	3.47	6.38	10.16	11.19	9.61	11.51	16.06
1173	3.48	6.39	10.18	11.21	9.29	11.09	15.65
1175	3.54	6.46	10.25	11.28	9.35	11.16	15.72

BM6P.OUT

BMDP6R - PARTIAL CORRELATION AND MULTIVARIATE REGRESSION

BMDP Statistical Software, Inc. | BMDP Statistical Software
1440 Sepulveda Blvd | Cork Technology Park, Model Farm Rd
Los Angeles, CA 90025 USA | Cork, Ireland
Phone (213) 479-7799 | Phone +353 21 542722
Fax (213) 312-0161 | Fax +353 21 542822
Telex 4972934 BMDP UI | Telex 75659 SSWL EI

Version: 1990 (VAX/VMS) DATE: 18-NOV-92 AT 09:33:11
Manual: BMDP Manual Vol. 1 and Vol. 2.
Digest: BMDP User's Digest.
Updates: State NEWS. in the PRINT paragraph for summary of new features.

PROGRAM INSTRUCTIONS

```
/problem title is 'Moran fm data'.
/input
file is 'sta:[dunne.consult.moran]mor.asc'.
variables are 20.
format is '(f5,f6,f6.2,f6.1,f6.2,f6.1,14f6.2)'.
reclen=121.
/variable names are
label,methp,veloc,tai,smc,tfi,fm0,fm1,fm3,fm5,fr0,fr1,fr3,fr5,
dm0,dm1,dm3,dr0,dr1,dr3,vel02.
use are 1 to 10,21.
blanks are missing.
add=1.
/transform vel02=veloc*veloc.
/regress dependent are fm0,fm1,fm3,fm5.
        independ are methp,veloc,tai,smc,tfi,vel02.
/print matrices are corr,part,covapart,creg,rreg,ttest,resi.
/end
```

PROGRAM INSTRUCTIONS

```
/problem title is 'Moran dm data'.
/input
file is 'sta:[dunne.consult.moran]mor.asc'.
variables are 20.
format is '(f5,f6,f6.2,f6.1,f6.2,f6.1,14f6.2)'.
reclen=121.
/variable names are
label,methp,veloc,tai,smc,tfi,fm0,fm1,fm3,fm5,fr0,fr1,fr3,fr5,
dm0,dm1,dm3,dr0,dr1,dr3,vel02.
use are 1 to 10,21.
blanks are missing.
add=1.
/transform vel02=veloc*veloc.
/regress dependent are dm0,dm1,dm3.
      independ are methp,veloc,tai,smc,tfi,vel02.
/print matrices are corr,part,covapart,creg,rreg,ttest,resi.
/end
```

PROGRAM INSTRUCTIONS

```
/problem title is 'Moran tfm data'.
/input
file is 'sta:[dunne.consult.moran]mor.asc'.
variables are 20.
format is '(f5,f6,f6.2,f6.1,f6.2,f6.1,14f6.2)'.
reclen=121.
/variable names are
label,methp,veloc,tai,smc,tfi,fm0,fm1,fm3,fm5,fr0,fr1,fr3,fr5,
dm0,dm1,dm3,dr0,dr1,dr3,vel02,tfm0,tfm1,tfm3,tfm5.
use are 1 to 10,21.
blanks are missing.
add=5.
/transform vel02=veloc*veloc.
tfm0=fm0/(fr0+0.0001).
tfm1=fm1/(fr1+0.0001).
tfm3=fm3/(fr3+0.0001).
tfm5=fm5/(fr5+0.0001).
/regress dependent are tfm0,tfm1,tfm3,tfm5.
      independ are methp,veloc,tai,smc,tfi,vel02.
/print matrices are corr,part,covapart,creg,rreg,ttest,resi.
/end
```

PROGRAM INSTRUCTIONS

```
/problem title is 'Moran tdm data'.
/input
file is 'sta:[dunne.consult.moran]mor.asc'.
variables are 20.
format is '(f5,f6,f6.2,f6.1,f6.2,f6.1,14f6.2)'.
reclen=121.
/variable names are
label,methp,veloc,tai,smc,tfi,fm0,fm1,fm3,fm5,fr0,fr1,fr3,fr5,
dm0,dm1,dm3,dr0,dr1,dr3,vel02,tdm0,tdm1,tdm3.
use are 1 to 10,21.
blanks are missing.
add=4.
/transform vel02=veloc*veloc.
tdm0=dm0/(dr0+0.0001).
tdm1=dm1/(dr1+0.0001).
tdm3=dm3/(dr3+0.0001).
/regress dependent are tdm0,tdm1,tdm3.
        independ are methp,veloc,tai,smc,tfi,vel02.
/print matrices are corr,part,covapart,creg,rreg,ttest,resi.
/end
```

BM6D.OUT

BMDP6D - BIVARIATE (SCATTER) PLOTS

BMDP Statistical Software, Inc. | BMDP Statistical Software
1440 Sepulveda Blvd | Cork Technology Park, Model Farm Rd
Los Angeles, CA 90025 USA | Cork, Ireland
Phone (213) 479-7799 | Phone +353 21 542722
Fax (213) 312-0161 | Fax +353 21 542822
Telex 4972934 BMDP UI | Telex 75659 SSWL EI

Version: 1990 (VAX/VMS) DATE: 18-NOV-92 AT 11:24:42
Manual: BMDP Manual Vol. 1 and Vol. 2.
Digest: BMDP User's Digest.
Updates: State NEWS. in the PRINT paragraph for summary of new features.

PROGRAM INSTRUCTIONS

```
/problem title is 'Moran fm vs mf data'.
/input
file is 'sta:[dunne.consult.moran]mor.asc'.
variables are 27.
format is '(f5,f6,f6.2,f6.1,f6.2,f6.1,21f6.2)'.
reclen=163.
/variable names are
label,methp,veloc,tai,smc,tfi,fm0,fm1,fm3,fm5,fr0,fr1,fr3,fr5,
dm0,dm1,dm3,dr0,dr1,dr3,
mf0,mf1,mf3,mf5,md0,md1,md3,vel02,tfm0,tfm1,tfm3,tfm5.
blanks are missing.
add=5.
grouping is methp.
/group codes(2) are 0,10,20.
names(2) are z,q,t.
/transform vel02=veloc*veloc.
/plot xvar are mf0,mf1,mf3,mf5,md0,md1,md3.
yvar are fm0,fm1,fm3,fm5,dm0,dm1,dm3.
pair.
statistics.
group is z.
group is q.
group is t.
groups are z,q,t.
/end
```

(The above run generated scatter plots, which are too voluminous for this Appendix, but the abbreviated fits to these plots are included for completeness.)

```
N =  25
R = .724                    mf0
P < .001
                          MEAN   S.D.
--REGRESSION LINE--  -RES.MS-   X 2.3996 4.5274
Y= 7.2207 +.58230*X   6.5990    Y 8.6180 3.6434

mf0     VERSUS fm0     ( 21 VS.  7 ) GROUP=z      , SYMBOL=z
```

```
N =  12
R = .737                    mf0
P = .006
                          MEAN   S.D.
--REGRESSION LINE--  -RES.MS-   X -.62750 3.5297
Y= 1.3220 +.51322*X   3.0333    Y 1.0000 2.4575

mf0     VERSUS fm0     ( 21 VS.  7 ) GROUP=q      , SYMBOL=q
```

```
N =  44
R = .865                    mf0
P < .001
                          MEAN   S.D.
--REGRESSION LINE--  -RES.MS-   X .87386 3.0260
Y= 1.4944 +.80610*X   2.0569    Y 2.1989 2.8212

mf0     VERSUS fm0     ( 21 VS.  7 ) GROUP=t      , SYMBOL=t
```

```
N =  81
R = .700                    mf0
P < .001
                          MEAN   S.D.
--REGRESSION LINE--  -RES.MS-   X 1.1223 3.7131
Y= 3.0823 +.81990*X   9.7427    Y 4.0025 4.3462

mf0     VERSUS fm0     ( 21 VS.  7 ) GROUP=z      , SYMBOL=z
                           GROUP=q      , SYMBOL=q
                           GROUP=t      , SYMBOL=t
```

```
N =  25
R = .644                    mf1
P < .001
                          MEAN   S.D.
--REGRESSION LINE--  -RES.MS-   X 12.024 6.9548
Y= 5.3451 +.28584*X   5.8241    Y 8.7820 3.0876

mf1     VERSUS fm1     ( 22 VS.  8 ) GROUP=z      , SYMBOL=z
```

```
N =  12
R = .675                    mf1
P = .016
                          MEAN    S.D.
--REGRESSION LINE--  -RES.MS-   X 4.0708  4.5378
Y=-1.0256 +.46791*X   5.9171    Y .87917  3.1444

mf1     VERSUS fm1     ( 22 VS.  8 )  GROUP=q      , SYMBOL=q
```

```
N =  44
R = .843                    mf1
P < .001
                          MEAN    S.D.
--REGRESSION LINE--  -RES.MS-   X 3.9757  3.8610
Y= .48561 +.67560*X   2.8304    Y 3.1716  3.0934

mf1     VERSUS fm1     ( 22 VS.  8 )  GROUP=t      , SYMBOL=t
```

```
N =  81
R = .806                    mf1
P < .001
                          MEAN    S.D.
--REGRESSION LINE--  -RES.MS-   X 6.4738  6.2674
Y= 1.0295 +.54591*X   6.3998    Y 4.5636  4.2457

mf1     VERSUS fm1     ( 22 VS.  8 )  GROUP=z      , SYMBOL=z
                           GROUP=q      , SYMBOL=q
                           GROUP=t      , SYMBOL=t
```

```
N =  25
R = .782                    mf3
P < .001
                          MEAN    S.D.
--REGRESSION LINE--  -RES.MS-   X 19.165  6.6462
Y= 4.1903 +.50591*X   7.4754    Y 13.886  4.2977

mf3     VERSUS fm3     ( 23 VS.  9 )  GROUP=z      , SYMBOL=z
```

```
N =  12
R = .770                    mf3
P = .003
                          MEAN    S.D.
--REGRESSION LINE--  -RES.MS-   X 9.8075  5.9965
Y= .97374 +.41265*X   4.6199    Y 5.0208  3.2129

mf3     VERSUS fm3     ( 23 VS.  9 )  GROUP=q      , SYMBOL=q
```

```
N =  44
R = .884                    mf3
P < .001
```

```
                          MEAN    S.D.
--REGRESSION LINE--  -RES.MS-   X  8.2314  5.4162
Y= 1.3173 +.59332*X   2.9615    Y  6.2011  3.6359

mf3     VERSUS fm3     ( 23 VS.  9 )  GROUP=t      , SYMBOL=t
```

```
N =  81
R = .893                    mf3
P < .001
                          MEAN    S.D.
--REGRESSION LINE--  -RES.MS-   X  11.839  7.6493
Y= 1.1034 +.61614*X   5.7013    Y  8.3981  5.2767

mf3     VERSUS fm3     ( 23 VS.  9 )  GROUP=z      , SYMBOL=z
                           GROUP=q      , SYMBOL=q
                           GROUP=t      , SYMBOL=t
```

```
N =  25
R = .786                    mf5
P < .001
                          MEAN    S.D.
--REGRESSION LINE--  -RES.MS-   X  20.016  6.3892
Y= 3.1424 +.69672*X   12.769    Y  17.088  5.6615

mf5     VERSUS fm5     ( 24 VS. 10 )  GROUP=z      , SYMBOL=z
```

```
N =  12
R = .812                    mf5
P = .001
                          MEAN    S.D.
--REGRESSION LINE--  -RES.MS-   X  11.232  6.5424
Y= 1.8159 +.50163*X   6.1029    Y  7.4500  4.0396

mf5     VERSUS fm5     ( 24 VS. 10 )  GROUP=q      , SYMBOL=q
```

```
N =  44
R = .790                    mf5
P < .001
                          MEAN    S.D.
--REGRESSION LINE--  -RES.MS-   X  9.5836  6.2307
Y= 1.6715 +.63200*X   9.5628    Y  7.7284  4.9846

mf5     VERSUS fm5     ( 24 VS. 10 )  GROUP=t      , SYMBOL=t
```

```
N =  81
R = .865                    mf5
P < .001
                          MEAN    S.D.
--REGRESSION LINE--  -RES.MS-   X  13.048  7.8273
Y= .96493 +.73661*X   11.291    Y  10.576  6.6628
```

```
mf5     VERSUS fm5      ( 24 VS. 10 )  GROUP=z      , SYMBOL=z
                                       GROUP=q      , SYMBOL=q
                                       GROUP=t      , SYMBOL=t
```

```
N =  25
R = .741                        md0
P < .001
                              MEAN    S.D.
--REGRESSION LINE--  -RES.MS-   X  10.436  6.4628
Y= 7.2468 +.81847*X   23.970    Y  15.788  7.1380

md0     VERSUS dm0      ( 25 VS. 15 )  GROUP=z      , SYMBOL=z
```

```
N =  12
R = .573                        md0
P = .052
                              MEAN    S.D.
--REGRESSION LINE--  -RES.MS-   X  6.0150  4.7158
Y= 4.8428 +.52974*X   14.056    Y  8.0292  4.3610

md0     VERSUS dm0      ( 25 VS. 15 )  GROUP=q      , SYMBOL=q
```

```
N =  44
R = .875                        md0
P < .001
                              MEAN    S.D.
--REGRESSION LINE--  -RES.MS-   X  6.7795  3.9337
Y=-.16231 +.89907*X   3.9154    Y  5.9330  4.0414

md0     VERSUS dm0      ( 25 VS. 15 )  GROUP=t      , SYMBOL=t
```

```
N =  81
R = .760                        md0
P < .001
                              MEAN    S.D.
--REGRESSION LINE--  -RES.MS-   X  7.7947  5.2084
Y= 1.5479 +.99263*X   19.830    Y  9.2852  6.8052

md0     VERSUS dm0      ( 25 VS. 15 )  GROUP=z      , SYMBOL=z
                                       GROUP=q      , SYMBOL=q
                                       GROUP=t      , SYMBOL=t
```

```
N =  25
R = .748                        md1
P < .001
                              MEAN    S.D.
--REGRESSION LINE--  -RES.MS-   X  15.626  7.4864
Y= 9.2956 +.76351*X   26.860    Y  21.226  7.6428
```

```
md1     VERSUS dm1      ( 26 VS. 16 )  GROUP=z      , SYMBOL=z
```

```
N =   12
R = .559                      md1
P = .059
                            MEAN    S.D.
--REGRESSION LINE--  -RES.MS-    X  8.8492  5.1764
Y= 8.1529 +.64803*X   27.183     Y  13.888  5.9970

md1     VERSUS dm1      ( 26 VS. 16 )  GROUP=q      , SYMBOL=q
```

```
N =   44
R = .812                      md1
P < .001
                            MEAN    S.D.
--REGRESSION LINE--  -RES.MS-    X  8.7689  4.2566
Y= .71390 +1.0818*X   11.194     Y  10.200  5.6690

md1     VERSUS dm1      ( 26 VS. 16 )  GROUP=t      , SYMBOL=t
```

```
N =   81
R = .805                      md1
P < .001
                            MEAN    S.D.
--REGRESSION LINE--  -RES.MS-    X  10.897  6.3517
Y= 3.0967 +1.0143*X   22.761     Y  14.149  7.9989

md1     VERSUS dm1      ( 26 VS. 16 )  GROUP=z      , SYMBOL=z
                           GROUP=q      , SYMBOL=q
                           GROUP=t      , SYMBOL=t
```

```
N =   25
R = .846                      md3
P < .001
                            MEAN    S.D.
--REGRESSION LINE--  -RES.MS-    X  23.270  7.0082
Y= 8.3212 +.71932*X   10.506     Y  25.060  5.9566

md3     VERSUS dm3      ( 27 VS. 17 )  GROUP=z      , SYMBOL=z
```

```
N =   12
R = .719                      md3
P = .008
                            MEAN    S.D.
--REGRESSION LINE--  -RES.MS-    X  15.055  7.1285
Y= 9.3865 +.57047*X   16.968     Y  17.975  5.6535

md3     VERSUS dm3      ( 27 VS. 17 )  GROUP=q      , SYMBOL=q
```

N = 44
R = .673 md3
P < .001

MEAN S.D.
--REGRESSION LINE-- -RES.MS- X 13.293 5.9726
Y= 5.6590 +.71303*X 22.479 Y 15.137 6.3319

md3 VERSUS dm3 (27 VS. 17) GROUP=t , SYMBOL=t

N = 81
R = .821 md3
P < .001

MEAN S.D.
--REGRESSION LINE-- -RES.MS- X 16.634 7.8212
Y= 5.5237 +.78736*X 18.592 Y 18.620 7.5021

md3 VERSUS dm3 (27 VS. 17) GROUP=z , SYMBOL=z
GROUP=q , SYMBOL=q
GROUP=t , SYMBOL=t

APPENDIX F. INLET TEMPERATURE AND OCTANE NUMBER

A tentative relationship connecting inlet temperature to ON was described in section 6.1. Figure 37 shows the logical connection between CR and temperature, and how changed inlet temperatures can be compensated for by altered compression ratios to result in unchanged final temperatures. The crucial assumption is made that this compensation for temperature results in top of compression conditions that for the purposes of this analysis can be considered identical to those before. The basis for comparison is temperature, and while it is conceded that knocking is a weak function of pressure, it is a much stronger function of temperature, and hence it is reasonable to use this parameter as the basis for the analysis.

A simple pressure-volume relationship is employed for this analysis. It is perhaps most instructive, at first, to think of two chemically identical fuels, one of which manifests more evaporative cooling than the other. The extra compression that is required to act on the cooler inlet mixture can be derived according to the following equation:

$$T_{comp} = Ti_0 \times CR_0^{\gamma-1} = Ti_C \times CR_C^{\gamma-1}$$

where T = mixture temperature (Ti = inlet temperature),

γ = Gamma = the coefficient of isentropic compression

subscripts: comp = at top of compression,

C = the cooler mixture,

0 = for the reference mixture

And $Ti_c = Ti_0$ - (Extra evaporative cooling)

So, given a reference inlet temperature and compression ratio, the influence of any evaporative cooling can be quantified in terms of a new CR = CR_C, and this would correspond to the extra compression arising from evaporative cooling effects.

$$CR_C = CR_0 \times \left[\frac{Ti_0}{Ti - Cooling}\right]^{\frac{1}{\gamma - 1}}$$

By default, CR_0 is taken to be 10:1.

The relative cooling can be estimated by the computer program (based on the experimental findings of this study). Finally, using the experimentally-based relationship between CR and ON (see Figure 38), any change in CR from the reference can be translated into an altered ON.

Several assumptions form the foundation for the logic behind this analysis, and these are discussed below.

Relative cooling and ON enhancement

This analysis is incapable of predicting absolute Octane Numbers. It is aimed, rather, at predicting relative RON alterations arising from relative temperature differences. It does, however, use the known RONs of some fuels as a pivot about which to focus the predictions due to cooling. The crux of the matter is this: if a fuel enters the cylinder at a slightly cooler temperature than before, this additional cooling will reduce its tendency to knock, and this will be interpreted as an increased RON, simply due to cooling differences. If two hypothetical fuels had identical chemical resistance to knocking, but one provided better cooling, it would have the better RON. It is the intention of this analysis to quantify the contribution of these thermal differences.

Gases only

From the outset of this project, it was intended to use only the gas temperature as the basis for this type of analysis. The analysis demands some indicative/representative 'mixture' temperature. While it would be simple to use some lumped temperature derived from a combination of gas, droplet and film temperatures (for example 80%, 15% and 5% respectively), using the gas temperature alone was considered to be the most appropriate choice, since it is the gases only to which the compression laws may be applied (also the lumping the temperatures makes almost no difference).

Liquid fuel entering the cylinder

If the liquid fuel in the cylinder (entering from the droplet and film streams) continued to cool the gas temperature during compression, this would affect the results of the analysis developed here. It is assumed that the gas in the cylinder is not affected by the liquid fuel.

This is a more reasonable assumption than it may initially appear to be, for the following reasons:

1. The liquid fuel entering the cylinder will rush through the valve, and consequently a large proportion of this mass will be have the inertia to land on the cylinder walls, and on the piston head itself. The residence time of this liquid fuel in the cylinder before it lands on a surface is likely to be very short indeed. It has been shown[6] that a large proportion of the heat of vaporization of the liquid fuel has to be provided by the hot cylinder walls (and piston crown). Thus it is expected that this remaining evaporation of the fuel (that did not occur in the intake manifold) is not likely to influence the gas temperatures significantly.
2. The small proportion of liquid fuel entering the cylinder that may avoid landing on a hot surface is also unlikely to be of importance because (i) this liquid fuel will comprise mainly the heaviest fractions of the fuel that did not manage to evaporate in the intake manifold (because they evaporate less readily), (ii) the time available during compression is also very limited, and the heat transfer rates from gas to droplet are not likely to be high enough so as to be important, (iii) this in-cylinder residence time will be very small compared with the time the liquid has spent in the manifold (less than 2.5% at most), and so the evaporation occurring here is not likely to be significant when compared with that occurring in the manifold.

Spreadsheet setup

A spreadsheet was used to house the data imported as output from the computer model, and the provide a means to manipulate these data. The spreadsheet setup used to perform the analysis described above, is outlined briefly below.

The raw data occupy columns A, B, C and D, for distance (m), gas temperature (°C), droplet temperature (°C), and film temperature (°C) respectively. Specific blocks are occupied by the data for gasoline (B5..D210), 10%-methanol blend* (B212..D417), 20%-methanol blend* (B419..D624), 40%-methanol blend* (B626..D831), 60%-methanol blend* (B833..D1038), 90%-methanol blend* (B1040..D1245). The calculation cells reference these data cells.

* stoichiometric mixtures are used as per the assumptions in section 6.2. (These blends are abbreviated into gasoline, 10m, 20m, 40m, 60m and 90m).

Pav - Proportion of the gas temperature to be used as the mixture temperature (exclusively the gas temperature) (av = air and vapour mix i.e. the gas). Similarly, Pd and Pf represent the droplet and film temperature contributions (which are both zero).

Def RON - The default RON. Since only relative RON change is computed, the default RON is simply an additive adjustment to reach the base RON value.

Tgasoline - The temperature (air and vapour) of gasoline. The principle applies to composites, for example T10m is the gas temperature for the 10%-methanol blend.

RON(gasoline) - the predicted relative RON of gasoline. Since the datum fuel in this case is gasoline itself, the relative RON for gasoline does not change. The nomenclature applies to composite labels, as above (for example RON(10m) is the predicted RON of 10%-methanol blend relative to the RON of pure gasoline).

Example of the spreadsheet formula cells are provided below.

```
E1: 'Pav
F1: 1
G1: '(gamma-1)
H1: 0.35
E2: 'Pd
F2: 0
G2: 'Def RON
H2: 96
E3: 'Pf
F3: 0
E4: 'X metres
F4: 'Tgasoline
G4: 'RON(gasoline)
H4: 'T10%M
I4: 'RON(10%M)
J4: 'T20%M
K4: 'RON(20%M)
L4: 'T40%M
M4: 'RON(40%M)
N4: 'T60%M
O4: 'RON(60%M)
P4: 'T90%M
Q4: 'RON(90%M)
F5: +$F$1*(B5+273)+$F$2*(C5+273)+$F$3*(D5+273)
G5: (10*($F5/F5)^(1/$H$1)-10)*5+$H$2
H5: +$F$1*(B212+273)+$F$2*(C212+273)+$F$3*(D212+273)
I5: (10*($F5/H5)^(1/$H$1)-10)*5+$H$2
J5: +$F$1*(B419+273)+$F$2*(C419+273)+$F$3*(D419+273)
K5: (10*($F5/J5)^(1/$H$1)-10)*5+$H$2
L5: +$F$1*(B626+273)+$F$2*(C626+273)+$F$3*(D626+273)
M5: (10*($F5/L5)^(1/$H$1)-10)*5+$H$2
```

N5: +$F$1*(B833+273)+$F$2*(C833+273)+$F$3*(D833+273)
O5: (10*($F5/N5)^(1/$H$1)-10)*5+$H$2
P5: +$F$1*(B1040+273)+$F$2*(C1040+273)+$F$3*(D1040+273)
Q5: (10*($F5/P5)^(1/$H$1)-10)*5+$H$2
R5: +$F$1*(B1247+273)+$F$2*(C1247+273)+$F$3*(D1247+273)
S5: (10*($F5/R5)^(1/$H$1)-10)*5+$H$2
E6: 1E-05
F6: +$F$1*(B6+273)+$F$2*(C6+273)+$F$3*(D6+273)
G6: (10*($F6/F6)^(1/$H$1)-10)*5+$H$2
H6: +$F$1*(B213+273)+$F$2*(C213+273)+$F$3*(D213+273)
I6: (10*($F6/H6)^(1/$H$1)-10)*5+$H$2
J6: +$F$1*(B420+273)+$F$2*(C420+273)+$F$3*(D420+273)
K6: (10*($F6/J6)^(1/$H$1)-10)*5+$H$2
L6: +$F$1*(B627+273)+$F$2*(C627+273)+$F$3*(D627+273)
M6: (10*($F6/L6)^(1/$H$1)-10)*5+$H$2
N6: +$F$1*(B834+273)+$F$2*(C834+273)+$F$3*(D834+273)
O6: (10*($F6/N6)^(1/$H$1)-10)*5+$H$2
P6: +$F$1*(B1041+273)+$F$2*(C1041+273)+$F$3*(D1041+273)
Q6: (10*($F6/P6)^(1/$H$1)-10)*5+$H$2

An example of this spreadsheet is shown in the tables below. The full set of data that give rise to Figures 39 and 40 is not shown since the principle is clear, and reprinting the full set would be unnecessary.

Pav	1	(gamma-1)	0.35
Pd	0	Def RON	96
Pf	0		

X metres	Tgasoline	RON(gasoline)	T10%M	RON(10%M)	T20%M	RON(20%M)
0	323	96	323	96	323	96
0.00001	322.9981	96	322.9981	96	322.998	96.00004
0.000023	322.9958	96	322.9957	96.00004	322.9956	96.00009
0.00004	322.9928	96	322.9927	96.00004	322.9925	96.00013
0.000062	322.9888	96	322.9887	96.00004	322.9884	96.00018
0.00009	322.9837	96	322.9835	96.00009	322.9831	96.00027
0.000128	322.9771	96	322.9767	96.00018	322.9762	96.0004
0.000176	322.9684	96	322.968	96.00018	322.9672	96.00053
0.000239	322.9571	96	322.9565	96.00027	322.9554	96.00075
0.00032	322.9423	96	322.9415	96.00035	322.9401	96.00097
0.000426	322.9231	96	322.922	96.00049	322.9201	96.00133
0.000564	322.8979	96	322.8964	96.00066	322.8939	96.00177
0.000743	322.8649	96	322.863	96.00084	322.8595	96.00239
0.000976	322.8216	96	322.819	96.00115	322.8144	96.00319
0.001279	322.7648	96	322.7611	96.00164	322.755	96.00434
0.001673	322.6898	96	322.6848	96.00221	322.6765	96.00589
0.002185	322.5907	96	322.5836	96.00314	322.5725	96.00806
0.00285	322.4593	96	322.4492	96.00447	322.434	96.01121
0.003715	322.2846	96	322.27	96.00647	322.249	96.01578
0.00484	322.0515	96	322.0299	96.00958	322.0006	96.02259
0.006302	321.7401	96	321.7075	96.01448	321.6659	96.03296
0.008202	321.3541	96	321.3061	96.02134	321.2482	96.04711
0.010673	320.8239	96	320.7507	96.03261	320.6674	96.06975
0.013885	320.1037	96	319.9891	96.05118	319.8663	96.1061
0.01806	319.1967	96	319.0196	96.07935	318.8401	96.15994
0.023488	318.3557	96	318.1175	96.10704	317.8853	96.21169
0.028916	317.5454	96	317.2352	96.13982	316.9444	96.27137
0.034344	316.7738	96	316.3805	96.17779	316.0257	96.33892
0.039772	316.0462	96	315.5584	96.22115	315.1346	96.41436
0.0452	315.3644	96	314.7711	96.26974	314.2736	96.49744

T40%M	RON(40%M)	T60%M	RON(60%M)	T90%M	RON(90%M)
323	96	323	96	323	96
322.9979	96.00009	322.9977	96.00018	322.9975	96.00027
322.9953	96.00022	322.995	96.00035	322.9945	96.00057
322.992	96.00035	322.9914	96.00062	322.9905	96.00102
322.9876	96.00053	322.9868	96.00088	322.9854	96.0015
322.982	96.00075	322.9807	96.00133	322.9787	96.00221
322.9746	96.00111	322.9729	96.00186	322.9701	96.0031
322.965	96.0015	322.9626	96.00257	322.9587	96.00429
322.9525	96.00203	322.9492	96.00349	322.944	96.0058
322.9362	96.0027	322.9318	96.00465	322.9247	96.00779
322.9149	96.00363	322.9089	96.00628	322.8996	96.0104
322.887	96.00482	322.8791	96.00832	322.8666	96.01385
322.8504	96.00642	322.8399	96.01106	322.8235	96.01832
322.8023	96.00854	322.7885	96.01465	322.7668	96.02426
322.739	96.01142	322.7207	96.01952	322.6922	96.03215
322.6552	96.01532	322.6311	96.026	322.5935	96.04266
322.5441	96.02064	322.5122	96.03478	322.4626	96.05677
322.396	96.02805	322.3536	96.04686	322.2881	96.07592
322.1976	96.03858	322.1411	96.06366	322.0543	96.10222
321.9307	96.05362	321.8548	96.08736	321.7394	96.1387
321.5698	96.07569	321.4673	96.12133	321.3129	96.19017
321.1184	96.10493	320.9823	96.16565	320.7907	96.25131
320.4873	96.15019	320.3024	96.23294	320.0548	96.34406
319.6109	96.22058	319.3553	96.33551	319.0233	96.48532
318.4808	96.32179	318.1305	96.48027	317.6325	96.70673
317.4326	96.41655	316.9988	96.61393	316.3618	96.90565
316.3923	96.52241	315.8723	96.76041	315.1042	97.11473
315.3692	96.6389	314.7616	96.91868	313.8688	97.3336
314.3698	96.76557	313.6739	97.08803	312.662	97.56185
313.3974	96.90186	312.6134	97.26744	311.4874	97.79873